Mathematical Modeling for Mechanical Analysis of Composite Structures

A Thesis

submitted in partial fulfillment of the requirements for the award of the degree of

Doctor of Philosophy

in

Department of Mathematics

by

Mohit Dhuria

Reg no: 901811018

under the supervision of

Dr. Kavita

Associate Professor (Department of Mathematics)

Dr. Neeraj Grover

Associate Professor (Department of Mechanical Engineering)

THAPAR INSTITUTE OF ENGINEERING AND TECHNOLOGY
PATIALA-147004, PUNJAB, INDIA
February, 2024

DEDICATED

TO

THE ALMIGHTY

AND

MY PARENTS

Certificate

I hereby certify that the work, which is being presented in the thesis, entitled **Mathematical Modeling for Mechanical Analysis of Composite Structures**, in partial fulfillment of the requirements for the award of the degree of **Doctor of Philosophy** and submitted to the institution is an authentic record of my own work carried out during the period **February 2019** to **February 2024** under the supervision of **Dr. Kavita**, Associate Professor, Department of Mathematics, and **Dr. Neeraj Grover**, Associate Professor, Department of Mechanical Engineering, Thapar Institute of Engineering and Technology, Patiala.

Date:

Mohit Dhuria.

(Mohit Dhuria)
Candidate

It is certified that the above statement made by the candidate is correct to the best of our knowledge.

Date: 28/2/24

Dr. Kavita
Supervisor

Dr. Neeraj Grover
Supervisor

Acknowledgements

First and foremost, I would like to thank God. He has given me strength and encouragement throughout all the challenging moments of completing this thesis. I am truly grateful for his unconditional and endless love, mercy, and grace.

Thank you so much to everyone who has helped me along my student journey. So many people have been so kind. There are far too many to name but there are some people who I would like to especially thank.

I am extremely grateful to my supervisors **Dr. Kavita**, Associate Professor, School of Mathematics, and **Dr. Neeraj Grover**, Associate Professor, Department of Mechanical Engineering Thapar Institute of Engineering and Technology, Patiala for their valuable guidance, consistent encouragement, understanding, unwavering support and patience throughout my research work. Their valuable insights and feedback have greatly influenced the development of this work, and making it possible. It has been a great honour to work under their guidance.

I take this opportunity to express my deep sense of gratitude and respectful regards to Dr. Mahesh Kumar Sharma, Professor and Head, Department of Mathematics for providing all the necessary facilities in the department. I am thankful to all the members of the doctoral committee Dr. Sapna Sharma, Dr. Paramjeet Singh, and Dr. Gagandeep Bhardwaj for their valuable comments and suggestions. Also, thanks to Prof. Jitendra Kumar (IIT, Ropar) for accepting to be the external examiners in my SRF assessment committee. My sincere thanks to Dr. Satish Kumar Sharma for his encouragement in starting my P.hd journay and help at various times during the period. I would like to express my gratitude to Dr. Harish Garg for his motivation towards research and future direction. I am highly thankful to all other faculty members of the School of Mathematics and non-teaching staff members for providing me guidance and the necessary facilities for carrying out my research work.

This journey would not have been possible without the constant support from my friends. First of all, I would like to thank my best friend Pankaj Makkar, and Pardeep Bawa, Priya Ahuja for his consistent support throughout these years and his selfless help every time. I would also like to especially thank my batch mates Ravinder Sharma, and Uma Bharti and others lab mates Shweta, Meenu, Daljeet, Nishtha, Shivani, Khusboo, Kallal Pal for being a great bunch of people in and out of the lab. Also, I would like to special thanks to my

hostel mates Amandeep Sidhu, Vivek Dhingra, Athar Ahmed for having great time with me and always support to me. I am thankful to Dr. Yadwinder Singh Joshan, Mr. Manu Dev Sharma, for stimulating discussions, and motivation throughout the journey.

I would want to express my sincere gratitude to my parents whose unwavering support, faith and patience have been instrumental in making this achievement possible. Special thanks to my sister Shilpa for always being so supportive to me. I would like to express my deepest gratitude to my wife, Pooja, whose unwavering support, and understanding sustained me throughout the arduous process of completing this thesis. I am profoundly grateful for her sacrifices and the countless hours she spent by my side, offering invaluable insights.

I gratefully acknowledge the Council of Scientific & Industrial Research (CSIR) for given financial support (File No: 09/677(0035)/2019-EMR-1) during this journey.

Mohit Dhuria

Abstract

The usage of composite materials in the structural analysis have increased extensively in recant decades across various engineering applications. The functionally graded materials (FGM) are advanced composite materials which are significantly used for fabrication and have improved the performance of structural components due to their unique combination of properties. The advancements in material technologies in last few years have played a crucial role in the development of modeling and analysis techniques of composite structures. Therefore, it is essential to mathematically model these structures. The mathematical modeling consists of converting any physical phenomenon into mathematical problem. Composite plates are the most significant structural elements that have been studied by many researchers in the past. The analysis of composite plates have been carried out in terms of three mechanical responses: static, buckling and free vibration. Different solution methodologies have been adopted to derive the governing mathematical system and predict the accurate mechanical response of composites plates. In this light, the current work focuses on different modeling and solution techniques to study the structural behavior of composite structures.

The thesis aims to propose a new higher order hyperbolic shear deformation theory for mechanical analysis of cross-ply and angle-ply multi-layered plates. Analytical solutions to the static and buckling responses of symmetric and anti-symmetric laminates are presented. The theory incorporate secant hyperbolic function in terms of thickness variable in the displacement field. Also the developed theory assumes non-linear distribution of displacements and ensures that the top and lower surfaces of the plates have zero transverse shear stresses. The equilibrium equations are derived by implementing the principle of virtual work (PVW). The consideration of stiffness characteristics is essential in the analysis of cross-ply and angle-ply laminates when solving the governing equations. The Navier solution are applied to solve the governing equations of plate satisfying the simply supported boundary conditions. The results for non-dimensional deflections, and stresses of composite laminates under the effect of sinusoidal and uniform distributed load are thus obtained. The uni-axial and bi-axial loads are incorporated to evaluate critical buckling loads. The validity of present formulation is demonstrated by comparing our results with some of the available results in literature. Also some new results are generated for future references and applications in structural analysis.

The functionally graded materials (FGM) are advanced composite materials which are significantly used for fabrication and have improved the performance of structural components

due to their unique combination of properties. During the manufacturing process, porosities may exist within the material, and hence it is necessary to assess the porosity effect while modeling the FGM. Thus, the effect of porosity distribution on static and buckling response of a functionally graded (FG) porous plate with all its edges simply supported is investigated. The plate's displacement field is approximated based on an inverse hyperbolic shear deformation theory (IHSDT) involving five variables. The material properties of porous FG plate are assumed with an additional term of porosity and power-law is adopted for smooth variation in the direction of thickness. In this study, five types of porosity distribution functions are considered. The analytical solutions for non-dimensional deflections and critical buckling loads of FG plate are thus obtained. To validate the accuracy of present findings, the results are compared with available results in the literature, and good agreement is achieved. Moreover, the novel results are presented to study the influence of various parameters such as porosity parameter, the power-law exponent, side-thickness ratio etc. on the dimensionless deflections, stresses, and critical buckling loads. The contribution of this study is seen in its utilisation across diverse industries.

The Navier's technique provides analytical solutions and is applicable for analysis of plates with simply supported edges. Most of the problems with general boundary conditions are solved via numerical technique. The numerical solutions have gained popularity in last few decades due to its applicability in complex geometries problems. This study aims to investigate the static deformation characteristics and stress analysis of laminated and functionally graded porous plates for various combination of boundary conditions in the framework of finite element method. The variation of properties in FG material is supposed to be along the thickness direction according to the power-law (P-FGM) and sigmoid-law (S-FGM). A novel secant hyperbolic higher order shear deformation theory is utilized to approximate the displacement field of FG plate containing five unknown variables. Furthermore, three different kinds of porosity distributions are assumed in terms of thickness parameter to model the porous plate. A suitable C^0 continuous isoparametric eight noded FE with 7 degrees of freedom (DOF) per node combined with biquadratic serendipity shape functions is employed to examine the desired mechanical responses of FG plates. The numerical assessments of bending deflections and buckling loads for laminated and funcionally graded(P-FGM and S-FGM) porous plate are presented. Moreover, the influences of parameters like span-thickness ratio, boundary conditions, material exponent, etc. on the dimensionless deflection, and buckling load are discussed in detail. To demonstrate the accuracy of proposed theory, the comparison study is made between present and previously published results in literature and well agreement is achieved. Additionally, several numerical illustrations with new generated results are provided to serve as benchmarks for further study of porous FG plates.

List of Publications

1. **M. Dhuria**, N. Grover, and K. Goyal."Influence of porosity distribution on static and buckling responses of porous functionally graded plates." *Structures, 34:1458-1474, Elsevier, 2021.* https://doi.org/10.1016/j.istruc.2021.08.050. (**SCI, Impact factor: 4.01**).

2. **M. Dhuria**, N. Grover, and K. Goyal. "A new shear deformation theory in axiomatic framework for structural analysis of cross-ply and angle-ply laminated composite plates". *Journal Of Applied Mechanics*, 90(5):051004, 2023. https://doi.org/10.1115/1.4056647. (**SCI, Impact factor: 2.794**).

3. **M. Dhuria**, N. Grover and K. Goyal. "Review of solution methodologies for structural analysis of composites". *European Journal of Mechanics-A/Solids*, 105157, 2023. https://doi.org/10.1016/j.euromechsol.2023.105157. (**SCI, Impact factor: 4.1**).

4. **M. Dhuria**, K. Goyal and N. Grover. "Finite element modeling for deflection, buckling and stress analysis of sigmoid functionally graded (S-FGM) porous plates". (**Communicated**).

Table of Contents

List of Figures

List of Tables

List of Abbreviations/Notations

FGM	Functionally graded material
ESL	Equivalent Single Layer
CPT	Classical plate theory
FSDT	First shear deformation theory
HSDT	Higher shear deformation theory
ZZ	Zig-zag
LW	Layerwise
CNT	Carbon nanotube
SSL	Sinusoidal Load
UDL	Uniform Distributed Load
FEM	Finite Element Method
IHSDT	Inverse Hyperbolic Shear Deformation Theory
SSSS	Simply Supported Edges
CCCC	Clamped Edges
a, b	Dimension of Plate
h	Plate Thickness
x_1, x_2, x_3	Cartesian Coordinates
$f(x_3)$	Shear Strain Shape Function
u, v, w	Displacements in x_1, x_2, x_3 direction
u_0, v_0	Mid-plane displacements along x_1, x_2 direction.
w_0	Transverse displacement in x_3 direction at mid-plane
Θ_{x_1}, Θ_{x_2}	Shear rotations about x_2, and x_1 axis respectively
$\{\sigma\}$	Stress vector
$\{\epsilon\}$	Strain vector
$[\bar{Q}]$	Reduced transformed stiffness matrix
N_{11}, N_{22}, N_{12}	Stress Resultants
M_{11}, M_{22}, M_{12}	In-plane Moment Resultants
P_{11}, P_{22}, P_{12}	Higher order moments
P_{11}, P_{22}, P_{12}	Higher order moments
Q_{13}, Q_{23}	Transverse Shear Stress Resultants
K_{13}, K_{23}	Transverse Moment Resultants
$\left[\bar{\mathbb{K}}^{\mathbb{C}}\right]$	Stiffness Matrix for Cross-ply plate
$\left[\bar{\mathbb{K}}^{\mathbb{A}}\right]$	Stiffness Matrix for Angle-ply plate
N_0	Buckling Load Parameter

$\{\triangle\}$	Field Variables Vector
$[G]$	Geometric Stiffness Matrix
E	Young's Modulus
ν	Poisson's ratio
ϕ_{x_1}, ϕ_{x_2}	Artificial Degree of Freedom
ξ, η	Natural Coordinates
$[\mathbf{H}]$	Transformation Matrix
$\{\bar{\epsilon}\}$	Generalized Strain
U_l	Total Linear Strain Energy
U_{nl}	Total Non-Linear Strain Energy
W	Total Work Done
$[\mathbf{K}]$	Global Stiffness Matrix
$[K_G]$	Global Geometric Stiffness Matrix
$\{\mathbf{F}\}$	Force Vector Due to External Loading
λ	Buckling Parameter
E_1, E_2	Elastic Modulus in Longitudinal and Transverse Direction
G_{12}	In-Plane Shear Modulus
G_{13}, G_{23}	Transverse Shear Modulus
k	Power-law Index
e	Porosity Parameter
$\Phi(x_3)$	Porosity Distribution Function

Chapter 1

Introduction

1.1 Composite Material

The majority of man made materials developed for structural applications such as concrete, metals and ceramics have uniform properties throughout the material. Typically such structural materials exhibit strong mechanical properties to resist the maximum stress. It is however well known that maximal stress occurs most often in a small portion of the structural element. Therefore, the structural safety is ensured through this approach but it is inefficient in the use of material resources, as it results in some of the structural elements receiving a higher volume of resources than it is necessary. The advancements in material technologies in the last few decades and their usage in engineering applications have led to significant advances in the modeling and analysis of composite structures. The utilisation of composite materials in the designs of structural components has gained significant growth in recent decades across various engineering fields. The composite material refers to the material which has strong reinforcements as fibers surrounded by a matrix material. The matrix which is continuous provides support to hold the fibres together at proper orientation and reinforcement (discontinuous) provides strength to the composites. Matrix transfers the loads acting on the composite to the reinforcement. These advanced materials are significantly used for fabrication and have improved structural system performance due to their higher specific strength, stiffness-weight ratios, impact resistance, specific Young's modulus, design flexibility, etc. Due to these attributes, these potential materials find enormous applications related to aerospace industry, civil and automobile engineering, aeronautical and sports industries, marine structures, thermal conductivity, etc.

Classification of Composites

The composite material are classified based on reinforcements in three different categories listed below:

- Particulate Composite

The content of this chapter has been published in The European Physical Journal B, 93: 1-10, (2020).

- Fiber reinforced Composites
- Laminated Composite

Where the laminated composite material is mainly used in the structural industry as well as in many engineering applications. Laminated composites are composed of layers of different materials and bonded with each others in a specific sequence and orientation. In industry and emerging fields of technology, laminated composite plates are extensively used. The performance and reliability of such structures depend strongly on the modeling, analysis, and design methodologies adopted. The increased use of such advance structures has contributed to the development of modern and efficient analytical and approximate tools which are capable for the study and accurate prediction of the mechanical behavior of such multi-layer structures. For efficient use of laminated composite plates, a thorough understanding of their dynamic and structural behavior, also an effective knowledge of bending characteristics, stress distribution, and buckling loads subjected to different conditions is needed.

1.1.1 Functionally Graded Material

Along with above mentioned composite materials, the functionally graded material (FGM) is an advance composite material widely utilised in several structural systems during the last few years. In mid-1980s, the scientists of Japan firstly introduced the FGMs, which are amalgamation of two distinct materials ceramics and metal [1]. These advanced materials are inhomogeneous composites used in many engineering industries whose material properties are varied smoothly in the specified direction. The gradual variation in properties allows for tailored performance characteristics such as ability to control deformation, high thermal resistance, heat conductivity, etc. Therefore, these materials have wide range of applications in aerospace industry, aircraft, biomedical implants, nuclear reactors and civil engineering [2]. The material properties of functionally graded (FG) structures are mainly described by using power-law, exponential-law and sigmoid-law distributions along thickness direction. The other advantage of FGM is that it eliminates the delamination between the interfaces associated with laminated composite. These advantages have drawn the attention of numerous researchers to study the structural behavior of FG structures [3–5].

1.1.2 Porous Material

Recent advancements in FGM include the incorporation of micro-voids or porosity. During preparation of functionally graded structures, voids may occur in the materials when the sintering technique is used [6]. This is because of the substantial disparity in solidification temperature between the material constituents. Porous materials are a type of

low weight materials that can have their mechanical characteristics continuously varied in certain directions. Consequently, these materials have received considerable interest from the researchers ever since their initial proposition by German scientist Terzaghi in 1923. The FG porous materials have been applied in various systems because of their high tensile strength, better stiffness, light weights and good conductivity etc. Therefore, it is essential to consider the porosity effect when modeling the FG structures. Usually, the distribution of porosity in porous plates is analysed in the direction of their thickness. Wattanasakulpong *et al.* [7] discussed the effect of considering porosity in FGM beams to study the vibration behavior.

1.2 Mathematical Modeling

The most important things the researchers do is to model physical phenomena. Practically, every phenomenon in nature, whether aerospace, biological and mechanical can be described in terms of algebraic, differential or integral equations with the help of law of physics or other fields. In mathematical modeling, it is required to accurately model the physical system in terms of mathematical parameters and then implement the governing principles of the physical system to yield the system of differential or integral equations [8]. The next step is to get the mathematical solution of this governing system of equations.

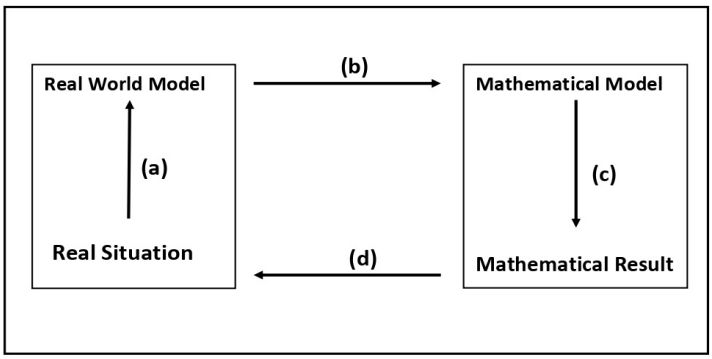

The obtained solution is then interpreted in terms of the physical parameters or response. Some Real world situations requiring mathematical modeling are given in Fig. (1.1)

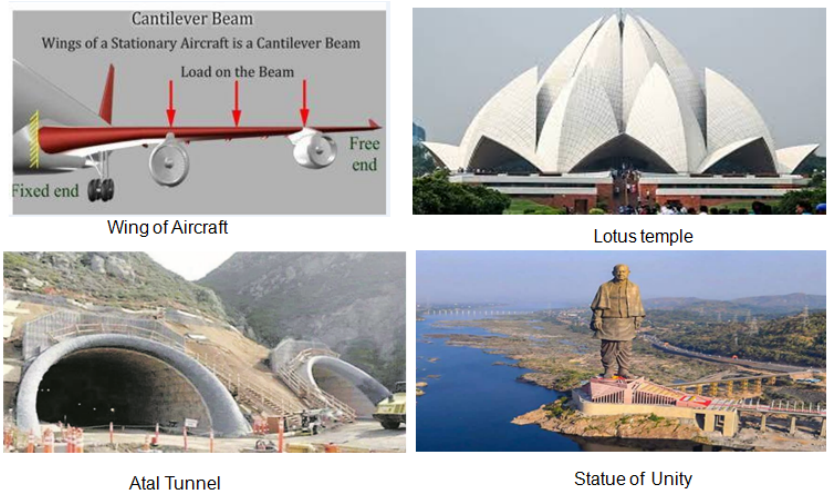

Figure 1.1: Structures requiring mathematical modeling

Mathematical model:
Consider a **Real world model** of cantilever beam as shown below:
Where one end is fixed at A, on other end, there is load applied (P) at point B. Let the deflection between loaded beam and unloaded beam is δ measure from point B.

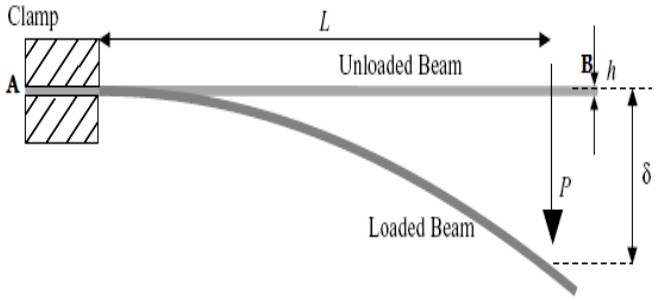

- Let L be length of cantilever beam and x be distance covered from point B towards A. That is, at point B, x=0 and at A, x=L.

- Therefore, the differential equation of above real world model is given as:

$$EI\frac{d^2y}{dx^2} = M \qquad \textit{(Beam deflection equation)} \tag{1.1}$$

Where E is young's modulus, I is moment of inertia. Using $M = px$ in equation (1.1), we

have

$$EI\frac{d^2y}{dx^2} = px, \quad 0 \leq x \leq L \tag{1.2}$$

$$\text{On Integrating twice,} \quad EIy = \frac{px^3}{6} + C_1x + C_2 \tag{1.3}$$

Boundary conditions: (i) $y = 0$, at x=L (ii) $\frac{dy}{dx} = 0$, at x=L

$$0 = \frac{pL^3}{6} + C_1L + C_2, \quad \text{using (i)} \tag{1.4}$$

$$0 = \frac{pL^2}{2} + C_1, \quad \text{using (ii)} \tag{1.5}$$

Solving (1.4) and (1.5), we get, $C_1 = -\frac{pL^2}{2}$ and $C_2 = \frac{pL^3}{3}$.

Mathematical result:

Putting values of C_1 and C_2 in equation (1.3), we get,

$$y = \frac{1}{EI}\left[\frac{px^3}{6} - \frac{pL^2}{2}x + \frac{pL^3}{3}\right] \tag{1.6}$$

Thus, equation (1.6) represent deflection of beam at a x distance from B. Where $0 \leq x \leq L$

Interpretation of the solution in the terms of physical parameter or real situation :

Since maximum deflection is at point B, where $x = 0$.

Hence, $y_B = \delta = \frac{PL^3}{3EI}$ is maximum deflection of beam at B.

Modeling of Composite Structures

The growing utilisation of composites for the structural applications particularly in the form of multilayered structures, FGM porous plates, and carbon nanotubes (CNTs) reinforced composites, has prompted the development of new analytical and numerical tools which are suitable to effectively analyse and accurate prediction of the mechanical behavior of these structures. The complicating effects of these composite structures have been mathematically addressed in a variety of ways. The accuracy of any mathematical model depends primarily on two factors: how any physical system is converted into a mathematical one and the methodology employed to solve the resulting mathematical problem. In order to mathematical model the composite structures, the 3D elasticity equations are implemented to model these structures in a three-dimensional manner. Incorporating the equilibrium equations, strain-displacement relationship, and constitutive relations (Generalised Hooke's

law) into the principle of virtual work yields the governing equations of the plate. The elasticity solution is found by solving these governing equations exactly. Some of the significant studies on 3D modeling of composite structures were performed by Pagano [9], Pagano and Hatfield [10], Noor [11, 12], Srinivas and Rao [13], and Demasi [14]. Nonetheless, it is important to note that the application of 3D solutions is restricted to simple geometry and specific boundary conditions. In addition, the exorbitant computational cost of 3D modeling reduces its applicability for practical problems. The fact that, in plate structures, one dimension is significantly smaller relative to the other two dimensions provides the facility to implement a 2D approach instead of a 3D. Hence the use of two-dimensional models is favoured for the purpose of modeling and analysing composite structures. Further, these approaches can be classified as models of a continuum, asymptotic, and axiomatic form [15]. The axiomatic type approaches can further be classified as displacement based, stress based or mixed formulation depending upon the choice of the approximation. The displacement-based axiomatic approaches are equivalent single layer (ESL), zig-zag (ZZ), and layerwise theories (LW) which depends upon the variable description chosen. The classification of these plate theories is depicted in Fig. (1.2).

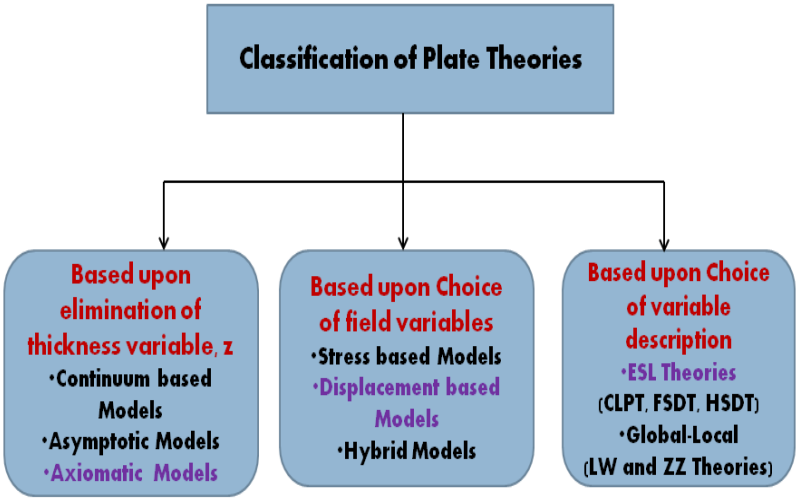

Figure 1.2: Classification of Plate Theories

1.3 Solution Methodologies

In addition to the advancement of plate theories, significant developments has been made towards the solution techniques. The choice of solution approach to derive the governing mathematical system for practical applications is an important feature for accurate analysis. The closed-form solutions are the most accurate and different analytical techniques are em-

ployed for structural responses of laminated plates. Different solutions techniques have been adopted by researchers to evaluate the bending, stability and free vibration behavior of composite structures. A solution that satisfies the governing differential equations at all points of the given domain and satisfies the associated boundary conditions of the problem is called an analytic solution. There are various methods for finding the analytical solution of differential equations, called *analytical methods*. The set of functions including t^n, exp(t), sin(t), log(t), etc. manipulation of these functions according to the laws of mathematics is used to find behaviors in closed form. Navier's and Levy's methods are mainly analytical approach used to examine laminated composite plates. These approaches are generally applied to specific boundary constraints, lamination sequences, loading conditions, etc. The presence of these constraints renders analytical solutions less suitable for practical problems that involve curved geometries and various boundary conditions. Consequently, analytical solutions are mostly employed for validation purposes. Therefore, in most practical problems, the solution approach involves the application of numerical/approximate computational methods for solving the governing equations of system [16]. With the development of computational technologies, various numerical solutions came into existence for the structural analysis of composites. The finite element method (FEM) are widely used for analysing the plate and shell structures. In addition to finite element method, various numerical solutions such as Rayleigh-Ritz, meshfree, wavelets-based, and differential quadrature methods have been developed in the past.

1.4 Objectives of the Ph.D. Thesis

The purpose of this study is to investigate appropriate solution approaches and their extensions for solving problems related to mechanical responses of composite structures. The complete objectives of the work are outlined as follows.

1. Development of shear deformation theory for the modeling of composite structures.
2. Development of numerical techniques and their comparison with the analytical solutions.
3. Application of the developed methodology to predict the mechanical responses of the composite structures.

1.5 Organization of the Thesis

The thesis' primary contribution is the modification, and development in modeling and analysis techniques of composite structures. The applications of developed plate theories and

solution methodologies in analyzing laminated and FGM composites have been discussed. The affects of porosity in computing the mechanical responses of the structures have also been examined. In addition, the thesis consist of seven chapters and is organized based on the following concepts as

Chapter 1 provides an overview and introduction to the structures composed of composite materials such as laminated composite plates, FGM porous square/rectangular plates, and CNT reinforced plate/shell. Different shear deformation theories have been discussed in this chapter to model the composite and advanced composite structures. Further, in solution methodologies, the various analytical, semi-analytical, and numerical techniques to assess the free vibration, bending, and buckling response of composite structures have been briefly introduced.

Chapter 2 presented the literature review on the modeling techniques to analyse the mechanical behavior of composite structures. In order to analyze these structures, it becomes mandatory to develop appropriate mathematical models to govern the physical system. The effects of shear deformation are significant in composite structures due to the high ratio of elastic modulus to shear modulus. Therefore, different shear deformation theories in framework of equivalent single layer theories have been discussed in details in the present chapter. Also, the theories incorporating the interlaminar continuity in framework of LW and ZZ theories has been introduced. Moreover, it is necessary to employ a compendious solution technique to assure its suitability to various geometries, boundaries, and loading conditions. Thus, the literature review concerning about the static, buckling and free vibration response of composite plate, beam and shell structures employing various analytical and numerical methods has presented in detailed. The analytical approaches are reviewed in the framework of Navier technique, Levy Method, and Symplectic superposition method while the numerical approaches are reviewed in the framework of Rayleigh-Ritz method, finite element method (FEM), meshfree methods, wavelets-based methods and differential quadrature method. Then the gaps and motivation associated with this work has been identified.

In the **Chapter 3**, the mathematical formulation for modeling the laminated and FG composite plate is provided in details. The displacement field of plate is assumed in terms of non-polynomial shear deformation theory. The governing equations are derived based on principle of virtual work incorporating strain-displacement, stress-strain relations. The Navier's method is most efficient in finding the analytical solutions to differential equations with particular boundary conditions. Further, the system of equations to examine the static and buckling responses are derived for cross-ply as well as angle-ply plates. The finite element methodology also presented in this chapter along with detailed formulation to derive

the numerical solution of composite plates subjected to various boundary conditions.

In the **Chapter 4**, the new hyperbolic shear deformation theory proposed in **Chapter 3** is implemented to examine the mechanical response of laminated composite plates. The analytical solutions are presented for simply supported cross-ply and angle-ply plates. The problem is solved by Navier's approach and matlab code is implemented to find the solution. The non-dimensional results for deflection and stresses are validated with pre-existing data. Also the new results are presented for multilayered plates subjected to uniform distributed (UDL) and sinusoidal loads (SSL). The dimensionless buckling loads are obtained for symmetric plates under in-plane uni- and bi-axial compressive force. The influence of different parameters such as aspect ratio, lamination sequence, etc. on the static and buckling response of plate are evaluated.

Chapter 5 deals with application of IHSDT to predict the structural response of FG plate with porosity. The impact of porosity distributions on bending and buckling behavior of porous plate is investigated. Five different kinds of porosity distributions are taken for analysis. The analytical solutions are obtained for dimensionless deflections, and buckling loads using Navier's methodology. To show the applicability and accuracy of this approach, the obtained results are validated with the existing literature and are found to agree well. The results due to new secant hyperbolic theory are also validated with IHSDT. The non-dimensional stresses are also plotted in this chapter for FG plate under transverse loading. The effects of parameters such as side-thickness ratio, power-law index, porosity content, and aspect ratio on the desired responses are also evaluated. At the end of the each chapter, the conclusion of the outcomes is presented.

Chapter 6 provides the analysis of laminated and FGM porous plate in framework of finite element (FE) formulation. An eight noded continuous isoparametric FE with 7 degrees of freedom per node is taken to divide the plate domain. The mathematical formulation for finite element modeling discussed **Chapter 3** is implemented providing the displacement field involves higher order theory based on secant hyperbolic function. The numerical findings of bending deflections and buckling loads for FG porous plate subjected to different boundary conditions are presented. The material properties of FGM vary according to power-law and sigmoid-law distributions. The comparison study demonstrates that the proposed theory is well accurate for analysis of laminated, P-FGM and S-FGM plates and revealed good agreement with available results in literature.

Chapter 7 of the thesis provides a summary of the findings discussed in the earlier chapters. The major outcomes of the thesis revolve around finding the modeling and analysis techniques of investigating laminated and FGM composite structures. Additionally, we detail several intriguing potential extensions of the proposed models for future research

problems.

The literature review discussed in next chapter help us to choose the suitable modeling and solution technique to accurately predict the response of plate structure and identified the gaps in the research.

Chapter 2

Literature Review

The composite structures have been investigated through various approaches in the past. But the focus is made on 2D displacement based approaches. In general, the mechanical responses of composite structures are obtained in the form of displacements at any general point within the domain of the structure. Thus, the first step in two dimensional approaches is to mathematically define the displacements at any arbitrary point within the domain in terms of mid-plane parameters. The two dimensional displacement based approaches are classified as:

(a) Equivalent single-layer (ESL) theories
(b) Layerwise Theories
(c) Zig zag Theories

2.1 *Equivalent Single Layer Theories*

In this approach, a single displacement field is axiomatically prescribed for all the layers of the structure. In these theories, the field variables depends solely upon the displacement field and remains independent of the number of layers. The orthotropic/anisotropic plates were modeled and analyzed using conventional plate theories particularly developed for homogeneous plates. Love [17] presented the theories for isotropic plates and their refinements. These theories are classified as Love first (LFAT) and second approximation theory (LSAT). The assumption in LFAT is that the normal to the reference plane remain normal in the deformed state and do not change in length (Kirchoff's assumption). The refinements in LFAT were obtaining by relaxing the assumptions of normality in LFAT and the theories were termed as LSAT. However, Koiter [18] took into account the energy considerations and suggested a recommendation popularly known as *Koiter's Recommendation* which states that: "a refinement of Love's first approximation theory is indeed meaningless, in general, unless the effects of transverse shear and normal stresses are taken into account at the same

The content of this chapter has been published in European Journal of Mechanics-A/Solids, 105157, 2023.

time." The implementation of LFAT to multilayered composite plate is termed as classical plate theory (CPT). It should be noted that the implication of CPT for modeling thick and moderately thick plates leads to inadequate results since it does not consider shear deformation effects which are more pronounced for such cases. The limitations of CPT led to the development of alternative approaches that consider the transverse shear effects. Therefore, the first shear deformation theory (FSDT) provided by Reissner [19, 20] is consistent theory to include the shear deformation effect. The basic assumption made by Reissner gives a consistent representation of stress distribution across the thickness, which results in a through-thickness linear variation of in-plane displacements and constant normal deflection across the plate thickness. The primary assumption in the formulation of FSDT is that the transverse lines to the reference plane remains straight in deformed state. However, it is no longer perpendicular to the reference surface. Mindlin [21] obtained the governing equations using the direct method without imposing the assumptions of corresponding stress distributions. In Mindlin's derivation, it is necessary to introduce a correction factor in the shear stress resultants to meet the plate boundary conditions on the bottom and top surface. Yang et al. [22] generalized the Reissner-Mindlin thick plate theory for arbitrary laminated anisotropic plates and isotropic plates. The FSDT cannot accurately predict the mechanical response because the shear correction factor (SCF) depends upon the lamination sequence, loading, and boundary conditions as discussed by Pai [23]. The requirement of SCF and constant shear stress throughout the plate's thickness makes the FSDT less reliable. Therefore, the research continued with the removal of the assumption of planer cross-section i.e, an initial planer cross-section is allowed to deform in a generic shape after deformation. There are various higher shear deformation theories (HSDTs) that possess the non-linear representation of the deformation. These theories also omit the transverse shear stress conditions on the plate surfaces without any need of SCF [24, 25]. The advancement of HSDTs can be seen in terms of polynomial (PSDTs) and non-polynomial shear deformation theories (NPSDTs). In the framework of PSDTs, the displacements are expanded by employing Taylor's series coefficients of thickness coordinate and higher-order terms. Hildebrand *et al.* [26] firstly introduced the Taylor's series approach to improve plate and shell theories. The significant development in PSDTs are due to Levinson [27], Reddy [28], Kant *et al.* [29], Maiti and Sinha [30], Khdeir and Reddy [31], Kant and Swaminathan [32, 33], Swaminathan and Patil [34], Ferreira *et al.* [35]. In framework of NPSDTs, a shear strain function is taken to define the shear deformation. The several strain shape functions such as trigonometric (Touratier [36]; Soldatos [37]; Grover *et al.* [38]; Singh and Singh [39]), exponential (Aydogdu [40];), hyperbolic (Mahi and Tounsi [41]), inverse trigonometric [42], inverse hyperbolic [43], etc. have been utilized for accurate representation of the shear stress distribution. The notable review articles on this topic are due to Mallikarjuna and Kant [44],

Reddy and Robbins [45], Ghugal and Shimpi [46], Carrera and Brischetto [47], and Jha and Kant [48]. Overall, the development of theories has been a significant point of interest of the research community involved in composite plates modeling and analysis.

2.1.1 *Layerwise and Zigzag Theories*

In addition to shear deformation effects, the interlaminar continuity has played a significant role in the modeling of multilayered composites. The various approaches in the framework of LW and ZZ theories and their requirements are outlined in the review articles presented by Carrera [49] and Carrera and Brischetto [47]. The significant development towards layerwise approaches are presented by Ambartsumyan [50], Srinivas [51], Reddy [52], Toledano and Murakami [53], Cho *et al.* [54], Ferreira *et al.* [55], Cetkovic and Vuksanovic [56], and Thai *et al.* [57]. The layerwise theories discussed above are excellent in terms of accuracy for multilayered composite plates. However; In LW theories, the field variables depend on the number of layers which makes computationally very expensive especially when multilayered structures are the subject of concern. In order to maintain control over the field variables while satisfying the continuity requirement of displacements and stresses, zig-zag theories were developed. The significant work on Zig-zag theories is presented by Ren [58], Di Sciuva [59], Cho and Parameter [60], Chakrabarti *et al.* [61]. Although ESL theories are not very precise in predicting inter-laminar behaviour of layered structures, due to their lower computational cost and ease of execution, they are commonly used to evaluate the response of structures. Additionally, it should be emphasized that the ZZ theories are derived from ESL theories by boosting all displacements with a zigzag function such as Murakami's zigzag function, Heaviside function. Whereas each layer is modeled using ESL theory in LW theories as if it is a plate. It should be noted that for ESL theory serve as a basis for both LW and ZZ theories. From the reviewed literature in above section, the displacement fields of various ESL theories given by different researchers are listed in Table 2.1

2.2 Mechanical Response

When there is a load acting on structure components, the structure tends to deform. The structural response depends upon the loading conditions, material and geometric properties. In general following three linear mechanical responses are significant, *Bending*, *Buckling* and *Free vibrations*. Therefore, these mechanical analysis of composite plates have received widespread attention in recent years. The various analytical and numerical methods based on plates theories have been developed by the researchers for analysis of shear deformable structures.

Table 2.1: Displacement field of various ESL theories having different shear strain functions.

Model	Displacement field	No. of unknowns
Mindlin [21]	$u = u_0 - z\phi_1, \quad v = v_0 - z\phi_2, \quad w = w_0$	05
Ambartsumian [62]	$u = u_0 - z\frac{\partial w}{\partial x} + \left[\frac{z}{2}\left(\frac{h^2}{4} - \frac{z^2}{3}\right)\right]\phi_1$	05
	$v = v_0 - z\frac{\partial w}{\partial y} + \left[\frac{z}{2}\left(\frac{h^2}{4} - \frac{z^2}{3}\right)\right]\phi_2$	
	$w = w_0$	
Panc [63]	$u = u_0 - z\frac{\partial w}{\partial x} + \left[\frac{5}{4}z\left(1 - \frac{4z^2}{3h^2}\right)\right]\phi_1$	05
	$v = v_0 - z\frac{\partial w}{\partial y} + \left[\frac{5}{4}z\left(1 - \frac{4z^2}{3h^2}\right)\right]\phi_2$	
	$w = w_0$	
Reddy [28]	$u = u_0 + z\left[\phi_1 - \frac{4}{3}(\frac{z}{h})^2\left(\phi_1 + \frac{\partial w}{\partial x}\right)\right]$	05
	$v = v_0 + z\left[\phi_2 - \frac{4}{3}(\frac{z}{h})^2\left(\phi_2 + \frac{\partial w}{\partial y}\right)\right]$	
	$w = w_0$	
Pandya and Kant [64]	$u = u_0 + z\theta_x + z^2u_0^* + z^3\theta_x^*$	9
	$v = v_0 + z\theta_y + z^2v_0^* + z^3\theta_y^*$	
	$w = w_0$	
Touratier [36]	$u = u_0 - z\frac{\partial w}{\partial x} + \frac{h}{\pi}\sin(\frac{\pi z}{h})\phi_1$	5
	$v = v_0 - z\frac{\partial w}{\partial y} + \frac{h}{\pi}\sin(\frac{\pi z}{h})\phi_2$	
	$w = w_0$	
Soldatos [37]	$u = u_0 - z\frac{\partial w}{\partial x} + \left[z\cosh(\frac{1}{2}) - h\sinh(\frac{z}{h})\right]\phi_1$	05
	$v = v_0 - z\frac{\partial w}{\partial y} + \left[z\cosh(\frac{1}{2}) - h\sinh(\frac{z}{h})\right]\phi_2$	
	$w = w_0$	
Shimpi *et al.* [65]	$u = u_0 - z\frac{\partial w}{\partial x} + \sin(\frac{\pi z}{h})\phi_1$	06
	$v = v_0 - z\frac{\partial w}{\partial y} + \sin(\frac{\pi z}{h})\phi_2$	
	$w = w_0 + \cos(\frac{\pi z}{h})\xi$	
Ferreira *et al.* [55]	$u = u_0 - z\frac{\partial w}{\partial x} + \sin(\frac{\pi z}{h})\phi_1$	05
	$v = v_0 - z\frac{\partial w}{\partial y} + \sin(\frac{\pi z}{h})\phi_2$	
	$w = w_0$	

Table 2.1: Continued.

Model	Displacement field	No. of unknowns
Karama *et al.* [66]	$u = u_0 - z\frac{\partial w}{\partial x} + ze^{-2(\frac{z}{h})^2}\phi_1$ $v = v_0 - z\frac{\partial w}{\partial y} + ze^{-2(\frac{z}{h})^2}\phi_2$ $w = w_0$	05
Aydogdu [40]	$u = u_0 - z\frac{\partial w}{\partial x} + z\alpha^{-2(z/h)^2/ln(\alpha)}\phi_1$ $v = v_0 - z\frac{\partial w}{\partial y} + z\alpha^{-2(z/h)^2/ln(\alpha)}\phi_2$ $w = w_0$	05
Mieche *et al.* [67]	$u = u_0 - z\frac{\partial w_b}{\partial x} - \left[\frac{\frac{h}{\pi}\sinh(\frac{\pi z}{h})-z}{\cosh(\pi/2)-1}\right]\frac{\partial w_s}{\partial x}$ $v = v_0 - z\frac{\partial w_s}{\partial y} - \left[\frac{\frac{h}{\pi}\sinh(\frac{\pi z}{h})-z}{\cosh(\pi/2)-1}\right]\frac{\partial w_s}{\partial y}$ $w = w_b + w_s$	04
Mantari *et al.* [68]	$u = u_0 - z\frac{\partial w}{\partial x} + \left[\sin(\frac{\pi z}{h})e^{\frac{1}{2}\cos(\frac{\pi z}{h})} + \frac{m\pi z}{h}\right]\phi_1$ $v = v_0 - z\frac{\partial w}{\partial y} + \left[\sin(\frac{\pi z}{h})e^{\frac{1}{2}\cos(\frac{\pi z}{h})} + \frac{m\pi z}{h}\right]\phi_2$ $w = w_0$	05
Mantari *et al.* [69]	$u = u_0 - z\frac{\partial w}{\partial x} + \left[\tan(mz) - \sec^2(\frac{mh}{2})\right]\phi_1$ $v = v_0 - z\frac{\partial w}{\partial y} + \left[\tan(mz) - \sec^2(\frac{mh}{2})\right]\phi_2$ $w = w_0$	05
Neves *et al.* [70]	$u = u_0 + zu_1 + \sinh(\frac{\pi z}{h})u_z$ $v = v_0 + zv_1 + \sinh(\frac{\pi z}{h})v_z$ $w = w_0 + zw_1 + z^2w_2$	9
Thai *et al.* [71]	$u = u_0 - \left(z - \frac{4z^3}{3h^2}\right)\beta_x - \frac{4z^3}{3h^2}\phi_x$ $v = v_0 - \left(z - \frac{4z^3}{3h^2}\right)\beta_y - \frac{4z^3}{3h^2}\phi_y$ $w = w_0$	07
Thai and Vo [72]	$u = u_0 - z\frac{\partial w_b}{\partial x} - \left[z - \frac{h}{\pi}\sinh(\frac{\pi z}{h})\right]\frac{\partial w_s}{\partial x}$ $v = v_0 - z\frac{\partial w_s}{\partial y} - \left[z - \frac{h}{\pi}\sinh(\frac{\pi z}{h})\right]\frac{\partial w_s}{\partial y}$ $w = w_b + w_s$	04
Grover [43]	$u = u_0 - z\frac{\partial w}{\partial x} - \left[\sinh^{-1}(\frac{rz}{h}) - z\frac{2r}{h\sqrt{(r^2+4)}}\right]\phi_1$ $v = v_0 - z\frac{\partial w}{\partial y} - \left[\sinh^{-1}(\frac{rz}{h}) - z\frac{2r}{h\sqrt{(r^2+4)}}\right]\phi_2$ $w = w_0$	05
Zenkour [73]	$u = u_0 - z\frac{\partial w}{\partial x} - \left[h\sinh(\frac{z}{h}) - \frac{4}{3}\frac{z^3}{h^2}\cosh(\frac{1}{2})\right]\frac{\partial \phi_1}{\partial x}$ $v = v_0 - z\frac{\partial w}{\partial y} - \left[h\sinh(\frac{z}{h}) - \frac{4}{3}\frac{z^3}{h^2}\cosh(\frac{1}{2})\right]\frac{\partial \phi_1}{\partial y}$ $w = w_0 + \frac{1}{12}\left[\cosh(\frac{z}{h}) - \frac{4z^2}{h^2}\cosh(\frac{1}{2})\right]\phi_1$	04

2.3 Analytical Methods

These series-based solutions have been well summarised in [74] based on Navier's and Levy's methods. In the Navier method, the field variables of the governing differential equation are expressed in the series of double trigonometric functions. The series solution is chosen in such a way that it satisfies the prescribed boundary conditions as a priori. The series solution in Navier form is well established for simply supported end conditions. It should be noted that the Navier solution is limited to specific boundary conditions (simply supported), however, it provides the series solution and is free from any computational error. Moreover, the trigonometric series of the Navier solution also depends upon the lamination sequence specifically categorized for cross-ply and angle-ply laminates. The assumed series solution is then substituted into the differential equations to yield the algebraic system of equations. As discussed so far, Navier's solution is simple and provides mathematical advantages by simplifies the solution to algebraic equations and can handle any type of load acting on lateral sides of the plate. However, its applicability is restricted solely to boundary conditions that are simply supported. So Nadai-Levy in 1899 developed the Levy-type solution to solve the differential equations of rectangular plates having simply supported two opposite edges and the other two edges with arbitrary boundary conditions, it may be subjected to clamped, free or a combined all edges. The method reduces the partial differential equations to ordinary ones. Reddy *et al.* [75] developed Levy type solutions for bending analysis of laminated rectangular Plates in framework of first-order transverse shear deformation theory. In analytical approaches, the investigations focus on analysing the buckling, static bending, and free vibration behavior of composite structures by Navier's and Levy's approach. Kant *et al.* [76] adopted the Navier's method to find the natural frequencies of composite beams based on higher-order refined theory. The theory assumed cubic in-plane and transverse displacements and involves eight field variables. Matsunaga [77] analyzed the natural frequencies and buckling stresses of multilayered cross-ply plates in framework of global higher order theory. A set of governing equations of a two-dimensional plate theory is derived using Hamilton's principle. Kant and Swaminathan [32] obtained the analytical solutions of simply supported laminated plates for vibration characteristics. They implemented a 12 variables theory incorporating cubic in-plane displacements and then reduced it to a nine variable displacement field by assuming the negligible transverse normal strain. The eigenvalue problem was formulated in closed form by expanding these nine field variables in double trigonometric series using Navier's technique. Matsunaga [78] considered angle-ply rectangular composite plates to evaluate the buckling loads and natural frequencies using two-dimensional higher order plate theory. The results for bending deformations of simply supported composite plates are presented by Kant and Swaminathan [33] using

HSDT. Swaminathan and Patil [34] applied the Navier method to find theoretical solutions for bending analysis of angle-ply composite plates. Akavci [79] implemented displacement-based new HSDT to predict the buckling loads and natural frequencies for symmetric and anti-symmetric thick elastic rectangular plates. Analytical solutions related to critical buckling for laminated plates were obtained using Navier's method. Aydogu [40] employed a new shear deformation theory in modification of model given by Karama *et al.* [80] to assess the static and dynamic behavior of composite structures. Using the Navier's approach, the free vibration and buckling response of composite plates have been evaluated by various researchers using different plate theories in following papers [81–85]. After analyzing previous work by researchers, Grover *et al.* [43] discussed the static response of laminated composite cross-ply plates. A new shear deformation theory which involves an inverse hyperbolic shape function in displacement field was introduced. The theory accounts for the non-linear distribution of the transverse strains and is well accurate for further analysis of composite plate in terms of structural behavior. Ghugal and Sayyad [86] presented the trigonometric shear deformation theory to investigate the static response of a symmetric and anti-symmetric laminated square plates. Adim *et al.* [87] obtained the analytical solution for the bending analysis and vibration characteristics of cross- and angle-ply laminated plates using simple refined higher-order theory involving four variables. The generalized differential equations were obtained with help of the Hamilton's principle. Lam *et al.* [88] carried out the bending, buckling, free vibrations of rectangular uniform loaded Levy-plates based on two-parameter elastic foundations. The canonical exact solutions for assumed plates with all six combinations of boundary conditions are obtained using Green's function. Xiang and Wei [89] presented Levy solution with the state-space approach to attain the vibration frequencies of simply supported Mindlin plates involving free and clamped boundary conditions. Xiang *et al.* [90] presented the Levy method to examine the behavior of free vibrations for multi-span rectangular plates with internal line supports. The plate with simply supported conditions on the two opposite edges and combination of simply supported, or clamped boundaries on other remaining two edges is considered. The analytical solutions for different mechanical responses (free vibrations, Hashemi *et al.* [91], Baferani *et al.* [92], Farsangi and Saidi [93]) and buckling behavior (Bodaghi and Saidi [94], Mohammadi *et al.* [95], Hu *et.al* [96]) were predicted for functionally graded thin or thick plates with arbitrary boundary conditions along edges in framework of levy method. Also, the analytical solutions in terms of a static response of laminated structures have been investigated in following research [84, 97] and static behavior of composite FG plates were examined by researchers [98–100]. Zenkour and Aljadani [101] applied the refined 3D-quasi theory for buckling of FG porous plates by employing the three porosity distribution models. The theory assumes the effect of thickness stretching in the displacement field. The analytical solutions discussed so far, Navier's and

Levy's, are restricted to certain boundary conditions. Numerous other analytical methodologies have been devised in the literature to overcome this limitation. Li *et al.* [102] proposed a symplectic superposition method (SSM) to analyse the flexural behaviour of rectangular thick plates. They derived the governing equations that describe the flexural behaviour of a thick plate within the framework of Hamiltonian space. The separation of variables technique is used to solve the governing equation, resulting in the acquisition of the eigenvalue problem. The general solution of the problem is obtained by employing the characteristic equation form. To obtain the specific solution for the prescribed boundary conditions, the deriving expressions for the boundary conditions are employed which yields a set of linear simultaneous equations. Further, the attainment of a non-trivial solution necessitates the determinant of the coefficient matrix of the simultaneous equation to be zero. This yields transcendental equations of non-zero eigenvalues. The symplectic solutions of three types of problems are obtained, considering the following cases of plates: plates with opposite two edges as simply supported, plates with other opposite edges as slidingly clamped and plates with an edge slidingly clamped and its opposite edge simply supported.

2.4 Numerical Methods

The advances in computational technology over the last few decades have enabled the implementation of efficient numerical techniques for solving the governing mathematical system related to composite structures. As the analytical and semi-analytical methods are limited to a restricted class of problems, most of the problems of the general category are solved using different numerical techniques.

Rayleigh Ritz Method:

In 1908, Ritz [103] introduced a method for determining the natural frequencies and mode shapes of continuum systems such as strings, plates, beams, etc. This method is further used by Rayleigh in his research hence is called the Rayleigh-Ritz method. This is a numerical method for finding the approximate solution of eigenvalue equations that are not amenable to analytical solutions. For the free vibration eigenvalue problem and static equilibrium, the multiple admissible displacement functions (satisfying the geometric boundary conditions of the problem) having undetermined coefficients are assumed. By minimising an energy functional that incorporates both potential and kinetic energies, one can determine the frequencies and mode shapes associated with the system.It is an integral approach method and is useful for solving structural analysis problems.

Solution procedure of Rayleigh method

- Assume a approximate function by linear combinations of certain linear independent functions as

$$v(x) = c_1 g_1(x) + c_2 g_2(x) + c_3 g_3(x) + ... + c_n g_n(x)$$

where $c_i's$ are unknowns and $g_i(x)'s$ are known functions, for example, algebraic polynomials or trigonometric functions. The deflection curve $v(x)$ is chosen such that it must satisfies displacement boundary conditions.

- The potential energy is obtained as function of coefficients as

$$I(c_1, c_2, ...c_n) = \text{U(potential energy) +V(kinetic energy)}$$

- Apply the principle of minimum potential energy to determine unknown coefficients, that is the functional I is minimized by simply taking the partial derivatives

$$\frac{\partial I}{\partial c_i} = 0 \quad \text{for all i's.}$$

Finite Element Method:

The use of the finite element method for structural applications is versatile. A finite element method (FEM) is a numerical approach to a class of problems governed by partial elliptical differential equations to obtain an approximate solution. The FEM transforms the elliptic partial differential equation into a series of algebraic equations which are easy to solve. The detailed discussion about FEM for different problems is provided by J.N. Reddy [104]. Zhang and Yang [105] presented the recent development of the FE technique for analysis of composite plates. The FEM approach have also been extensively developed and employed for the nonlinear analysis of structures subjected to various geometry and loading conditions.

The FEM involves the following steps:

1. ***Integral Form***: Firstly, the governing differential equation of problem is transformed into an integral form. There are two techniques to obtain this form, (i) Variational Technique and (ii) Weighted Residual Technique. The calculus of variation is applied in the variational technique for attaining the integral form to the corresponding differential equation. The integral form for structural dynamics problems turns out to be the expression for the overall potential energy of the system. Then this integral must be minimized to get the problem solved. The integral form is constructed as a weighted integral of the governed differential equation in the weighted residual technique, where the given weight functions are arbitrary except that they satisfy certain boundary conditions. In order to get a solution to the problem, the integral form is then set equal to zero. The weight function is then called a virtual displacement for

structural analysis problems and the integral form then becomes the representation of the structure's virtual work.

2. ***Finite element discretization***. In this second step, the problem domain is divided into several subdomains, called finite elements. This is named discretization of domain. For one-dimensional (1-D) problems, the elements are line segments with only length and no geometrical structure. The components used are triangles, rectangles, and quadrilaterals with angled/smooth borders for two-dimensional (2D) problems, and with straight or curved surfaces for three-dimensional problems, tetrahedron and parallelepiped. Domain division into elements is called mesh. The elements are connected with each other at points called *nodes*.

3. ***Element equations***. In this step, over each element an appropriate approximation for the primary variable of the problem is chosen as linear combinations of approximation functions (shape functions) and undetermined coefficients (nodal values). Usually, polynomials are chosen as the approximation functions and they are derived using interpolation theory, so-called interpolation functions. In addition, in the integral form, the primary variable approximation is then replaced. The algebraic equations for the unknown nodal values of the primary variable are minimized for the variational type integral form and it is set to zero in the weighted-integral sense to obtain the algebraic equations. In each cases, the algebraic relations among the unknown coefficients are obtained element-wise and then assembled for the whole domain using continuity over each element to get the solution .

Meshless Method:

The meshless methods have also been adopted in the last two decades to find the approximate solution of an elliptical boundary value problem for the structural analysis of composites. Meshless methods have several advantages, including their ability to be applied to complex geometries, moving discontinuities such as crack propagation, and the capability to couple with other numerical methods. In the framework of meshless methods, the approximate solution is assumed employing various methods such as kernel approximations (reproducing kernel particle (RKP) [106]), element-free Galerkin (EFG) [107], mesh-less Galerkin using radial basis function (RBF) [108], mesh-less local Petrov-Galerkin (MLPG) [109], the collocation technique employing RBF and the modified smoothed particle hydrodynamics.
The basic framework of the meshless methods is outlined as follows: A linear elliptical boundary value problem defined in domain Ω is as follows:

$$\mathrm{S}u(y) = g(y), \quad y \in \Omega$$

$$\mathrm{R}u(y) = f(y), \quad y \in \partial\Omega$$

Where S and R are linear differential operators, and g and f are smooth functions. A collection of nodes (n) is constructed within the domain.
In kernel approximations, the solution $u^k(y)$ is approximated as follows:

$$u^k(y) = \int_{\Omega} w(y-x,k)u(x)d\Omega_x$$

Where *w(y-x,k)* is the kernel or weight function and k is the measure of size of the support. The kernel is required to satisfy the conditions such as non-negativity, normality, monotonically decreasing [110]. The commonly used weight functions are the exponential, the cubic spline and the quartic spline.
The EFG method depends on moving least square (MLS) approximations in which the function *u(y)* is expressed as

$$u^k(y,\bar{y}) = \sum_{i=1}^{n} p_i(\bar{y})a_i(y)$$

Where $p_i(\bar{y})$ are the monomial basis functions of order m, and $a_i(y)$ are the coefficients to be determined by performing minimization of difference between local approximation and nodal values. With the determination of these coefficients, the MLS approximation is obtained as follows

$$u^k(y) = \sum_{i=1}^{n} \Psi_i(y)u_i$$

Where $\Psi_i(y)$ is the shape function and n is the number of local nodes.
The mesh-free collocation methods with finite point multiquadric for the analysis of composite and functionally graded plates is presented by Ferreira *et al.* [111]. The multiquadric method is based on the selection of points on $\partial\Omega$ and in the interior of domain Ω.
The solution $u^k(y)$ for the boundary value problem is approximated as

$$u^k(y) = \sum_{i=1}^{n} a_i g\left(||y - y^{(i)}||, c\right)$$

Where a_i are the constants to be determined, and norm is the Euclidean distance between points y and y^i and c is a constant. There are various form of function $g\left(||y - y^{(i)}||, c\right)$ such as mutiquadric, inverse multiquadric, Gaussian, Thin Plate spline, etc. The substitution of the assumed solution alongwith the prescribed boundary conditions into the defined boundary value problem at appropriate points yield a system of algebraic equations which are employed to find the constant coefficients (a_i).

Differential Quadrature Method:

The Differential Quadrature (DQ) Method is also numerical approach was presented by

Bellman and Casti [112] in 1971 and has been used recently by Bert and Malik [113], Chen *et al.* [114] in the solid mechanics solution problems. Wu and Liu [115] proposed differential quadrature method to solve initial and boundary-value problems. The proposed method can be used to solve single-span Bernoulli beam's buckling equation and the dynamic equation having one degree of freedom.

The mechanical responses of composite structures examined via discussed numerical methods are given in literature as follows. Chen *et al.* [116] developed two triangular elements for dynamical behavior of plates/shells structures based on the integral finite element approach. They proposed an element with 12 nodes having 42 degrees of freedom (DOF) and also a 6 noded element with 33 DOF to discretize a plate domain. Ribeiro [117] studied the natural frequencies for moderately thick isotropic laminated plates using p-version hierarchical finite element method with geometrical non-linearity. The harmonic balance method was used to derive the frequency-domain equations of motion, which were further solved by a predictor-corrector method. Hu *et al.* [118] adopted the procedure of Rayleigh-Ritz to study the vibration characteristics of angle-ply composite laminated plates. A set of orthogonal polynomials generated by the Gram–Schmidt process was assumed to be displacement functions with three linear and two angular displacement components. Chakrabarti and Sheikh [119, 120] carried out bending and dynamic response of composite and sandwich plates. They developed a C^1 continuous six-noded triangular element for derivation of governing equation. Liew *et al.* [121] presented moving least squares DQ method to studied the free vibration behavior of symmetrically laminated plates. The first shear deformation theory is used to obtained the governing equations of plate. Malekzadeh and Karam [122] studied the free vibrations of rectangular plate of non-uniform thickness on elastic foundations in framework of differential quadrature method. Gupta *et al.* [123] studied the elastic foundation effect to buckling loads and natural frequency of circular polar plates with elastically restrained edge using Ritz method. Fazzolari *et al.* [124] reported numerical results of the free-vibrations and critical buckling loads of anisotropic multi-layered composite plates by employing the method of Rayleigh-Ritz approximation and Carrera Unified Formulation. Also, the mechanical responses of anisotropic laminated rectangular plates have been evaluated using different plate theories in framework of hierarchical Ritz formulation [125, 126]. The free vibrations and buckling response are evaluated by Oyekoya *et al.* [127] for FG composite plates using the finite element technique. In the present model, Mindlin-type formulation assuming average transverse shear distribution based on Lagrangian interpolation and Reissner-type element formulation based on the Hermitian interpolation was proposed. Ferreira *et al.* [128] studied the collocation method of higher order for analysis of isotropic laminated composite plates. The results for bending and free vibration analysis are evaluated based on Deslaurier–Dubuc interpolating wavelets. Talha and Singh [129] used

polynomial based HSDT to examined the bending and free vibration analysis of FGM plate. Castro *et al.* [130] employed a wavelet collocation method based on Deslaurier-Dubuc interpolating functions to examine the static deformation of sandwich plates. Hao *et al.* [131] presented the non-linear vibrations of FGM plates having different boundary conditions along adjacent edges. Zhang [132] proposed the modified couple stress theory for examined the static, free vibrations and stability behavior of non-classical Mindlin plate. The numerical solutions are evaluated by using finite element formulations. Mantari and Soares [133] presented a FE approach based on a generalized LW higher order plate theory to analyze static response of symmetric composite plates. A C^0 Lagrangian iso-parametric four-noded quadrilateral element was assumed to discretize a plate domain. Further, the higher order ZZ theory have been employed by Chakrabarti *et al.* [134] to find the buckling behavior and by Chalak *et al.* [135] to examine the bending and free vibration analysis of soft core sandwich structures using refined C^0 finite element method. However, implementation of ZZ theory in finite element formulation makes it difficult as C^1 continuity is required for transverse displacement at each node. Therefore, Pandey and Pradyumna [136] employed a new higher-order LW theory for the bending characteristics and natural frequencies of laminated composite plates using C^0-continuous finite element procedure. An eight-noded isoparametric element with 13 DOF is proposed for discretization of the plate. Ferreira *et al.* [137] predicted the static deformations and the free vibration behavior of thick cross-ply laminated plates. They used the generalized differential quadrature (DQ) technique to solve the governing equations. Liu *et al.* [138] adopted the DQ based finite element method to analyze free vibration responses of isotropic laminated composite plates subjected to arbitrary boundary conditions. Some studies related to different mechanical responses of composite structures in framework of differential quadrature method are reported in [121, 122, 139].
In order to find the approximate solution of an elliptical boundary value problem for the structural analysis of composite plates, the meshless methods have been adopted in the last two decades. The meshless methods possess advantages such as applicability to complex geometries, moving discontinuities such as crack propagation, and the capability to couple with other numerical/approximate methods. A continuous moving least square approximation is presented by Belytschko *et al.* [140] in order to develop a common framework for MLS approximations and kernel approximations. A mesh-free approach was developed by Liu and Chen [141] to study the deflection and free vibrations of thin rectangular plates with regular irregular node distribution. They employed moving least-squares (MLS) interpolation to approximate shape function. Ferreira *et al.* [142] considered the laminated composite moderately thick plates and examined the free vibration behavior. The FSDT and multiquadric radial basis function (RBF) was employed to derive the equations of motion and describes a problem of eigenvalue which can be solved by different algorithms. Further,

Ferreira *et al.* [143] used a LW deformation theory to evaluate deflections and natural frequencies of composite laminated plates. The multiquadric RBF meshless method is applied to discretize the domain of plate with uniform and sinusoidal distributed force. Vaghefi *et al.* [144] purposed meshless local Petrov-Galerkin method to obtain complete 3D elastostatics solutions of FG thick plates with different boundary conditions. Bui *et al.* [145] further studied the vibration behavior of multi-layered plates by employing an efficient meshfree method. Rodrigues *et al.* [146] presented meshless local RBF based differential quadrature collocation method to obtain the static, free vibrations and buckling response of square laminated plates. Carrera's unified formulation was applied to obtain equations of motions and the loading conditions for a plate. Some other significant meshless methods are smoothed particle hydrodynamics (SPH) method [147], hp-clouds [148] and and radial point interpolation method (RPIM) [149]. Sator *et al.* [150] analyze the bending of thin and or thick elastic FG plates by using the Kirchhoff Love theory, FSDT and HSDT. They employed meshless technique with the moving least square approximation for governing field variables. Do and Lee [151] employed the modified mesh-free RPIM for the nonlinear bending analyses of simply supported FGM plates. The shape functions are constructed by the new radial basis function without any fitting parameters to approximate the displacement fields. An improved meshless technique of moving kriging in proposed by Do and Lee [152] to investigate the stability behavior of composite FGM plates. The nth-order shear deformation theory was implemented for the formulation of discrete system equations of the thermal buckling problem. Huang [153] *et al.* proposed meshfree isogeometric collocation technique to study the mechanical behavior of laminated plates. The FSDT is applied to govern the deformation of plate under different boundary constraints. Chaabani *et al.* [154] present a higher order continuation based FE approach to predict the buckling characteristics of porous FG plates under various loading conditions.

2.5 Discussion and Literature Gap

This chapter provides a state-of-art literature review of modeling techniques and solution methodologies for structural analysis of composites. Such a review is inherently incomplete, considering the scope of the subject is as extensive as that of a complete book. An overview of mathematical formulation for the numerical methods is also presented. The comprehensive overview of the primary advantages and drawbacks of each approaches are enumerated ahead. The plates with general boundary conditions along the edges cannot be analyzed properly by using analytical methods. As Navier's method is only applicable to predict mechanical response of structures with simply supported boundary conditions. Therefore, numerous approximate and semi-analytical methods were explored to investigate the struc-

tural response subjected to various boundary conditions. Rayleigh-Ritz method, finite element method (FEM), meshfree methods, differential quadrature method and wavelets-based method are efficient numerical tools for solving PDEs problems which could not be solved analytically. The FEM is most useful numerical tool for solving problems with complex geometries, loadings and material properties. The FE method has demonstrated remarkable efficacy in conducting both static and dynamic analyses of plates. However, the FEM requires a mesh to provide connectivity between elements in order to form the finite element equations. Also in this method, the function remains continuous over the meshes while partial derivatives are not continuous. Recently, in the field of computational mechanics, there has been development of a numerical technique known as the mesh-free method which does not necessitate the use of a mesh for the interpolation of displacement fields. The meshless nature and straightforward implementation of this approach make it a viable substitute for finite elements in the study of structures with arbitrary shapes.
Apart from FEM and meshless techniques, various numerical approaches have also been explored in literature. The available analytical tools for a specific class of boundary value problems provide a strong basis for comparing with exact solution and various numerical techniques. Moreover, the applications of developed methodologies to investigate the composite/advance composite structures have been discussed. The observations drawn from the aforementioned literature review are as follows:

- The polynomial and non-polynomial shear deformation theories have been applied to model and study the laminated and functionally graded composite plates. The use of non-polynomial higher order theory is very limited in analyzing FG plate with porosity.

- However it is evident from literature review, the porous FG plate is not previously modeled in framework of NPSDT incorporating inverse hyperbolic function.

- There has been limited literature towards the development of mathematical models/solution methodologies for the response of composite structures.

- The research related to static and buckling response of angle-ply laminated plates based on non-polynomial higher order plate theory is somehow limited.

- During the manufacturing of FGM, porosity or voids may occur in the materials, which may behave differently depends upon type of distributions. Therefore, effects of porosity needs to be considered while analyzing FGM structures.

2.6 Summary

In this chapter, the study has been conducted on several modeling techniques, structural analysis, porosity effect and solution methodologies in the analysis of composite structures. The literature review related to different plate theories and solutions techniques to solve the governing equations are presented in detailed. An overview of mathematical formulation for the numerical methods is also presented. On the basis of the review presented for different mechanical responses, some observations are identified. By analysing literature and considering the motivation behind the study, the relevant research gaps are identified. Based on these research gaps, objectives for the current study are established.

Chapter 3

MATHEMATICAL FORMULATION

Introduction

In the chapter 2, the literature review of modeling approaches, and solution methodologies for structural behavior of laminated and FG composite structures has been done. Based on the discussion and observations made in chapter 2, this chapter provides the modeling and mathematical formulation of laminated and FG plate in detailed within the context of non-polynomial shear deformation theory. The basic assumptions taken for the modeling and analysis of multi-layered and functionally graded composite plates are also introduced. The strain-displacement relationship, and constitutive relations are introduced to describe the kinematics of the structure, and the behaviour of deformation. The derivation of the governing differential equation using the principle of virtual displacements is briefly explained in this chapter. The system of governing equations are further transformed in terms of primary field variables. Then these differential equations are solved analytically by employing Navier Solution technique along with associated boundary conditions. Further, the porous FG plate is modeled mathematically in the framework of inverse hyperbolic shear deformation theory (IHSDT) wherein the material follows the linear elastic behavior. The volume fraction of FG materials is defined by some rule of mixture and different porosity distributions are considered for analysis of structural behavior. This chapter also includes a detailed presentation of the finite element method for deriving the numerical solution of composite plates under different boundary conditions. The mathematical system involves simultaneous equations is then obtain for analysis of mechanical behavior (bending, buckling and vibration response).

The chapter is divided into five sections: The mathematical formulation for displacement field of laminated plate is presented in section 3.1. The analytical formulation of governing differential equations of plate are discussed in Section 3.2. The section 3.3 carried out the Navier's methodology to solve the governed system of equations to predict the mechanical response characteristics and section 3.4 presents the modeling of functionally graded plate. In section 3.5, the modeling of plate in the framework of finite element methodology is

The content of this chapter has been published in Journal Of Applied Mechanics, 90(5):051004, 2023.

presented. The summary and scope of this chapter is concluded in section 3.6.

3.1 Mathematical Formulation

Assumption: The following assumptions are led to the mathematical development in this work:

1. For laminated and FG plates, the reference plane used to determine displacements and rotations is assumed to be the centre plane (at x_3=0).
2. The composition of FG material varies gradually from one end to the other and assumed to follow a certain mathematical rule to define the material property.
3. The material is assumed to follow linear elastic behavior
4. The structural kinematics relies on the premise that deformations and rotations are small.
5. The displacement field of proposed theory involves five primary field variables.
6. The in-plane displacements varies non-linearly and transverse displacement is supposed to be constant through the thickness of composite plate.

3.1.1 Displacement Field

In the present work, a rectangular laminated plate having dimensions a, b, and h and composed of N orthotropic layers is modeled mathematically in the framework of a new displacement-based hyperbolic shear deformation theory. The geometry of considered plate in the Cartesian co-ordinate ($x_1 - x_2 - x_3$) is depicted in Fig. (3.1) The axiomatic formulation based displacement field with non-polynomial function of thickness as shear strain function is as follows.

$$u(x_1, x_2, x_3) = u_0(x_1, x_2) - x_3 \frac{\partial w_0}{\partial x_1} + f(x_3) \cdot \Theta_{x_1}(x_1, x_2)$$

$$v(x_1, x_2, x_3) = v_0(x_1, x_2) - x_3 \frac{\partial w_0}{\partial x_2} + f(x_3) \cdot \Theta_{x_2}(x_1, x_2)$$

$$w(x_1, x_2, x_3) = w_0(x_1, x_2) \tag{3.1}$$

where (u, v, w) are the displacements at any point in the x_1, x_2, and x_3 directions, respectively. u_0, v_0 are the in-plane deformations of mid-plane ($x_3 = 0$) along x_1 and x_2 co-ordinates respectively and w_0 is the transverse displacement at a point on the mid-plane. The parameters Θ_{x_1} and Θ_{x_2} are the shear rotations about x_2 and x_1 axis of plate respectively.

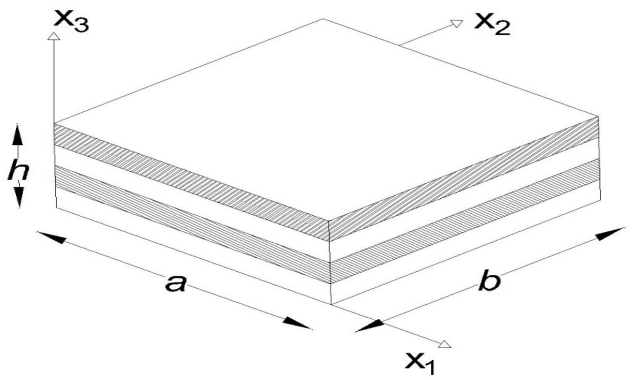

Figure 3.1: Geometry of Laminated plate

The coefficient $f(x_3)$ of shear rotations represent the strain shape function, which determines the variations of transverse shear strains through the plate thickness. The function f is expressed as $f(x_3) = g(x_3) + \Omega x_3$, where $g(x_3) = x_3\ \text{sech}\left(\frac{rx_3}{h}\right)$ and Ω = -sech(*r/2*)(1-(*r/2*)tanh(*r/2*)). The value of parameter Ω determined by satisfying the condition of zero transverse shear stress as a priori on the top and bottom surfaces of plate i.e at $z = \pm h/2$. An optimized value of r is selected as 2.5 and the evaluation of parameter r is achieved through post-processing after comparison the results of the present theory with the elasticity solution for a variety of examples. In order to represent the transverse shear stress distribution, the different shape functions given by authors are listed in Table 3.1.

3.1.2 Structural Kinematics

Under the assumption of small elastic deformations, the strains associated with displacements given in Eqs.(3.2) are expressed linearly in terms of variables $(u_0, v_0, w_0, \Theta_{x_1}, \Theta_{x_2})$ and are as follows [155]

$$\epsilon_{11} = \frac{\partial u}{\partial x_1} = \frac{\partial u_0}{\partial x_1} - x_3\frac{\partial^2 w_0}{\partial x_1^2} + (g(x_3)+\Omega x_3)\frac{\partial \Theta_{x_1}}{\partial x_1}, \quad \epsilon_{22} = \frac{\partial v}{\partial x_2} = \frac{\partial v_0}{\partial x_2} - x_3\frac{\partial^2 w_0}{\partial x_2^2} + (g(x_3)+\Omega x_3)\frac{\partial \Theta_{x_2}}{\partial x_2}$$

$$\gamma_{12} = \left(\frac{\partial u}{\partial x_2} + \frac{\partial v}{\partial x_1}\right) = \left(\frac{\partial u_0}{\partial x_2} + \frac{\partial v_0}{\partial x_1}\right) - 2x_3\frac{\partial^2 w_0}{\partial x_1 \partial x_2} + (g(x_3)+\Omega x_3)\left(\frac{\partial \Theta_{x_1}}{\partial x_2} + \frac{\partial \Theta_{x_2}}{\partial x_1}\right) \quad (3.2)$$

$$\gamma_{23} = \frac{\partial v}{\partial x_3} + \frac{\partial w}{\partial x_2} = f'(x_3)\Theta_{x_2} = (g'(x_3)+\Omega)\Theta_{x_2}, \quad \gamma_{13} = \frac{\partial u}{\partial x_3} + \frac{\partial w}{\partial x_1} = f'(x_3)\Theta_{x_1} = (g'(x_3)+\Omega)\Theta_{x_1}$$

Where prime ($'$) in $f'(x_3)$ denotes the derivative of function f with respect to x_3. The parameters $\epsilon_{ii}(i = 1, 2)$ are direct strains in x_1, and x_2 directions. Where γ_{13} and γ_{23}

represent the transverse shear strains while γ_{12} denotes the in-plane shear strain. The γ_{13} and γ_{23} are found to be clearly dependent on shear rotations and $f'(x_3)$.

Table 3.1: Different shear strain shape functions.

Model	$g(x_3)$	Ω
Reddy [28]	$\left(x_3 - \frac{4x_3^3}{3h^2}\right)$	0
Touratier [36]	$\frac{h}{\pi}\sin(\frac{\pi x_3}{h})$	0
Soldatos [37]	$h\sinh(\frac{x_3}{h})$	$\cosh(\frac{1}{2})$
Karama *et al.* [66]	$x_3 e^{-2(x_3/h)^2}$	0
Aydogdu [40]	$x_3\alpha^{-2(x_3/h)^2/ln(\alpha)}, \alpha > 0$	0
Mieche [156]	$0.6626\frac{h}{\pi}\sinh\frac{\pi x_3}{h}$	-0.6626
Mantari [68]	$\sin\left(\frac{\pi x_3}{h}\right) e^{\frac{1}{2}cos\left(\frac{\pi x_3}{h}\right)}$	$\frac{\pi}{2h}$
Mantari [69]	$\tan(mx_3)$	$-m\sec^2(\frac{mh}{2})$
Grover *et al.* [43]	$\sinh^{-1}(\frac{rx_3}{h})$	$\frac{-2r}{h\sqrt{(r^2+4)}}$; r=3
Present	$x_3\ \mathrm{sech}(\frac{rx_3}{h})$	0.0320; r=2.5

3.1.3 Constitutive Relations

Since the laminated plate is made of orthotropic layers, thus the stress-strain relations for each layer k of the composites having any fiber orientation are defined as follows [38]

$$\begin{bmatrix}\sigma_{11}\\ \sigma_{22}\\ \tau_{12}\\ \tau_{23}\\ \tau_{13}\end{bmatrix}_{(k)} = \begin{bmatrix}\bar{Q}_{11} & \bar{Q}_{12} & \bar{Q}_{16} & 0 & 0\\ \bar{Q}_{12} & \bar{Q}_{22} & \bar{Q}_{26} & 0 & 0\\ \bar{Q}_{16} & \bar{Q}_{26} & \bar{Q}_{66} & 0 & 0\\ 0 & 0 & 0 & \bar{Q}_{44} & \bar{Q}_{45}\\ 0 & 0 & 0 & \bar{Q}_{45} & \bar{Q}_{55}\end{bmatrix}_{(k)} \begin{bmatrix}\epsilon_{11}\\ \epsilon_{22}\\ \gamma_{12}\\ \gamma_{23}\\ \gamma_{13}\end{bmatrix}_{(k)} \quad \text{or,} \quad [\sigma]_{5\times1} = \left[\bar{Q}\right][\epsilon]_{5\times1} \tag{3.3}$$

The $\left[\bar{Q}\right]$ is reduced transformed stiffness matrix depending upon the material properties (Young's modulus, shear modulus, Poisson's ratio) [87]. Where $[\sigma]$=$[\sigma_{11}\ \sigma_{22}\ \tau_{12}\ \tau_{23}\ \tau_{13}]^T$ and $[\epsilon]$= $[\epsilon_{11}\ \epsilon_{22}\ \gamma_{12}\ \gamma_{23}\ \gamma_{13}]^T$ are the stress and strain vectors, respectively. The relationship between coefficients of the reduced transformed stiffness matrix and fiber angle are given

as

$$\bar{Q}_{11} = Q_{11}\cos^4\theta + 2(Q_{11} + 2Q_{66})\sin^2\theta\cos^2\theta + Q_{22}\sin^4\theta$$

$$\bar{Q}_{12} = (Q_{11} + Q_{22} - 4Q_{66})\sin^2\theta\cos^2\theta + Q_{12}(\sin^4\theta + \cos^4\theta)$$

$$\bar{Q}_{22} = Q_{11}\sin^4\theta + 2(Q_{12} + 2Q_{66})\sin^2\theta\cos^2\theta + Q_{22}\cos^4\theta$$

$$\bar{Q}_{16} = (Q_{11} - Q_{12} - 2Q_{66})\sin\theta\cos^3\theta + (Q_{12} - Q_{22} + 2Q_{66})\sin^3\theta\cos\theta$$

$$\bar{Q}_{26} = (Q_{11} - Q_{12} - 2Q_{66})\sin^3\theta\cos\theta + (Q_{12} - Q_{22} + 2Q_{66})\sin\theta\cos^3\theta \tag{3.4}$$

$$\bar{Q}_{66} = (Q_{11+}Q_{22} - 2Q_{12} - 2Q_{66})\sin^{2\theta\cos^2\theta + Q_{66}(\sin^4\theta + \cos^4\theta)}$$

$$\bar{Q}_{44} = Q_{44}\cos^2\theta + Q_{55}\sin^2\theta$$

$$\bar{Q}_{45} = (Q_{55} - Q_{44})\cos\theta\sin\theta$$

$$\bar{Q}_{55} = Q_{55}\cos^2\theta + Q_{44}\sin^2\theta$$

$$\text{Where} \quad Q_{11} = \frac{E_1}{1-\nu_{12}\nu_{21}}, \quad Q_{22} = \frac{E_2}{1-\nu_{12}\nu_{21}}, \quad Q_{12} = \frac{\nu_{12}E_2}{1-\nu_{12}\nu_{21}}, \quad Q_{21} = \frac{\nu_{21}E_1}{1-\nu_{12}\nu_{21}}$$

$$Q_{44} = G_{23}, \quad Q_{55} = G_{13}, \quad Q_{66} = G_{12}, \quad \nu_{21} = \frac{\nu_{12}E_2}{E_1}$$

Where E is young's modulus and ν is poisson's ratio.

3.2 Analytical Formulation

The derivation of governing differential equations and analytical solution approach to solve these equations is presented in this section. The system of equations is then attained in algebraic way to obtain the structural response of composite plates.

3.2.1 Equations of Motion

The governing equations of the plate are generated by implementing the principle of virtual work as follows

$$\int_0^T (\delta U - \delta W)dt = 0 \tag{3.5}$$

where expression for variation of strain energy, δU, virtual work done δW as a result of applied forces are

$$\delta U = \int_{\Omega} \left\{ \int_{-\frac{h}{2}}^{\frac{h}{2}} [\sigma_{11}\delta\epsilon_{11} + \sigma_{22}\delta\epsilon_{22} + \tau_{12}\delta\gamma_{12} + \tau_{23}\delta\gamma_{23} + \tau_{13}\delta\gamma_{13}] dx_3 \right\} dx_1 dx_2 \tag{3.6}$$

$$\delta W = -\left[\int_{\Omega_s} \left(\bar{q}\delta w_0 + \hat{N}_{11} \frac{\delta w_0}{\delta x_1} \frac{\partial \delta w_0}{\delta x_1} + \hat{N}_{22} \frac{\delta w_0}{\delta x_2} \frac{\partial \delta w_0}{\delta x_2} \right) dx_1 dx_2 \right] \tag{3.7}$$

where, $\bar{q}$ and $\hat{N}_{11}$, $\hat{N}_{22}$ are transverse, axial compressive forces in x_1 and x_2 directions. Here, $\hat{N}_{11} = -N_0$, and $\hat{N}_{22} = -K_m N_0$. Where K_m corresponds to the load index and N_0 to buckling load.

The expression of virtual strains from the Eqs.(3.2) is adopted to compute the strain energy δU and then the value of δU and δW is substituted in the equation of virtual work Eq. (3.5). Using the fundamental lemma of variation, the virtual terms are then solved. To satisfy Eq. (3.5) independently, it should be emphasized that all variations are arbitrary, and thus taking the coefficients of δu_0, δv_0, δw_0, $\delta\Theta_{x_1}$, and $\delta\Theta_{x_2}$ equal to zero. Hence, the system of differential equations is obtained as indicated in Eqs. (3.8).

$$\begin{gathered}
\frac{\partial N_{11}}{\partial x_1} + \frac{\partial N_{12}}{\partial x_2} = 0, \quad \text{and} \quad \frac{\partial N_{22}}{\partial x_2} + \frac{\partial N_{12}}{\partial x_1} = 0 \\
\frac{\partial^2 M_{11}}{\partial {x_1}^2} + \frac{\partial^2 M_{22}}{\partial {x_2}^2} + 2\frac{\partial^2 M_{12}}{\partial x_1 \partial x_2} + \bar{q} + \hat{N}_{11}\frac{\partial^2 w_0}{\partial {x_1}^2} + \hat{N}_{22}\frac{\partial^2 w_0}{\partial {x_2}^2} = 0 \\
\frac{\partial P_{11}}{\partial x_1} + \Omega\frac{\partial M_{11}}{\partial x_1} + \frac{\partial P_{12}}{\partial x_2} + \Omega\frac{\partial M_{12}}{\partial x_2} - \Omega Q_{13} - K_{13} = 0 \\
\frac{\partial P_{22}}{\partial x_2} + \Omega\frac{\partial M_{22}}{\partial x_2} + \frac{\partial P_{12}}{\partial x_1} + \Omega\frac{\partial M_{12}}{\partial x_1} - \Omega Q_{23} - K_{23} = 0
\end{gathered} \tag{3.8}$$

The terms N, M are stress resultants and (P, Q, K) denotes the higher-order moments which are defined as follows

$$\begin{bmatrix} N_{11} & M_{11} & P_{11} \\ N_{22} & M_{22} & P_{22} \\ N_{12} & M_{12} & P_{12} \end{bmatrix} = \int_{-\frac{h}{2}}^{\frac{h}{2}} \begin{bmatrix} \sigma_{11} \\ \sigma_{22} \\ \tau_{12} \end{bmatrix} \begin{bmatrix} 1 & x_3 & g(x_3) \end{bmatrix} dx_3 \tag{3.9}$$

$$\begin{bmatrix} Q_{23} & K_{23} \\ Q_{13} & K_{13} \end{bmatrix} = \int_{-\frac{h}{2}}^{\frac{h}{2}} \begin{bmatrix} \tau_{23} \\ \tau_{13} \end{bmatrix} \begin{bmatrix} 1 & g'(x_3) \end{bmatrix} dx_3 \tag{3.10}$$

To transform the governing equations Eqs.(3.8) in terms of primary deformations using the integral relations established in Eq. (3.11) and Eq. (3.12), we need to perform the necessary

substitutions.

$$\left[A_{ij} \quad B_{ij} \quad D_{ij} \quad E_{ij} \quad F_{ij} \quad H_{ij}\right] = \int_{-\frac{h}{2}}^{\frac{h}{2}} \left[\bar{Q}_{ij}\right] \left[1 \quad x_3 \quad x_3^2 \quad g(x_3) \quad x_3.g(x_3) \quad (g(x_3))^2\right] dx_3 \quad (3.11)$$

for i, $j = 1$, 2, 4, 5, 6.

$$\left[K_{ij} \quad L_{ij}\right] = \int_{-\frac{h}{2}}^{\frac{h}{2}} \left[\bar{Q}_{ij}\right] \left[g'(x_3) \quad (g'(x_3))^2\right] dx_3 \quad \text{for} \quad i, j = 4, 5. \quad (3.12)$$

After substituting equations Eqs.((3.9)-(3.12)) in (3.8), the governing equations of motion in general form can be written in terms of generalized displacements as follows

$$[\mathcal{K}]\{\Delta\} = \{\mathcal{F}\} \quad (3.13)$$

where $\mathcal{K}$ is an symmetric matrix of partial derivative with respect to x_1 and x_2, Δ denotes the vector of generalized displacement and $\mathcal{F}$ is load vector, respectively. Further, the most general form of system of governing equations as given in (3.13) is reliable for any lamination sequence. However, the governing equations for cross-ply and angle-ply laminates are derived in the form of primary displacements and are discussed in the further sections.

Governing equations for cross-ply laminates:

For cross-ply laminated plates, the characteristics of stiffness are given as

$$\begin{aligned} &A_{16} = A_{26} = B_{16} = B_{26} = D_{16} = D_{26} = 0 \\ &E_{16} = E_{26} = F_{16} = F_{26} = H_{16} = H_{26} = 0 \\ &A_{45} = K_{45} = L_{45} = 0 \end{aligned} \quad (3.14)$$

The above characteristics are substituted into Eq. (3.13) and thus, the governing equations for considered laminates in explicit form of generalized displacements are expressed as follows

$$A_{11}\left(\frac{\partial^2 u_0}{\partial {x_1}^2}\right) + B_{11}\left(\Omega\frac{\partial^2 \Theta_{x_1}}{\partial {x_1}^2} - \frac{\partial^3 w_0}{\partial x_1^3}\right) + E_{11}\left(\frac{\partial^2 \Theta_{x_1}}{\partial {x_1}^2}\right) + A_{12}\left(\frac{\partial^2 v_0}{\partial x_1 \partial x_2}\right) + B_{12}\left(\Omega\frac{\partial^2 \Theta_{x_2}}{\partial x_1 \partial x_2}\right) -$$
$$B_{12}\left(\frac{\partial^3 w_0}{\partial x_1 \partial x_2^2}\right) + E_{12}\left(\frac{\partial^2 \Theta_{x_2}}{\partial x_1 \partial x_2}\right) + A_{66}\left(\frac{\partial^2 u_0}{\partial {x_2}^2} + \frac{\partial^2 v_0}{\partial x_1 \partial x_2}\right) + B_{66}\left(\Omega\left(\frac{\partial^2 \Theta_{x_1}}{\partial {x_2}^2} + \frac{\partial^2 \Theta_{x_2}}{\partial x_1 \partial x_2}\right)\right) -$$
$$B_{66}\left(2\frac{\partial^3 w_0}{\partial x_1 \partial {x_2}^2}\right) + E_{66}\left(\frac{\partial^2 \Theta_{x_1}}{\partial {x_2}^2} + \frac{\partial^2 \Theta_{x_2}}{\partial x_1 \partial x_2}\right) = 0$$

$$A_{12}\left(\frac{\partial^2 u_0}{\partial x_1 \partial x_2}\right)+B_{12}\left(\Omega\frac{\partial^2 \Theta_{x_1}}{\partial x_1 \partial x_2}-\frac{\partial^3 w_0}{\partial x_1^2 \partial x_2}\right)+E_{12}\left(\frac{\partial^2 \Theta_{x_1}}{\partial x_1 \partial x_2}\right)+A_{22}\left(\frac{\partial^2 v_0}{\partial {x_2}^2}\right)+B_{22}\left(\Omega\frac{\partial^2 \Theta_{x_2}}{\partial {x_2}^2}\right)$$
$$-B_{22}\left(\frac{\partial^3 w_0}{\partial {x_2}^3}\right)+E_{22}\left(\frac{\partial^2 \Theta_{x_2}}{\partial {x_2}^2}\right)+A_{66}\left(\frac{\partial^2 u_0}{\partial x_2 \partial x_1}+\frac{\partial^2 v_0}{\partial {x_1}^2}\right)+B_{66}\left(\Omega\left(\frac{\partial^2 \Theta_{x_1}}{\partial x_1 \partial x_2}+\frac{\partial^2 \Theta_{x_2}}{\partial {x_1}^2}\right)\right)$$
$$-B_{66}\left(2\frac{\partial^3 w_0}{\partial {x_1}^2 \partial x_2}\right)+E_{66}\left(\frac{\partial^2 \Theta_{x_1}}{\partial x_1 \partial x_2}+\frac{\partial^2 \Theta_{x_2}}{\partial {x_1}^2}\right)=0$$

$$B_{11}\left(\frac{\partial^3 u_0}{\partial {x_1}^3}\right)+D_{11}\left(\Omega\frac{\partial^3 \Theta_{x_1}}{\partial {x_1}^3}-\frac{\partial^4 w_0}{\partial {x_1}^4}\right)+F_{11}\left(\frac{\partial^3 \Theta_{x_1}}{\partial {x_1}^3}\right)+B_{12}\left(\frac{\partial^3 v_0}{\partial {x_1}^2 \partial x_2}+\frac{\partial^3 u_0}{\partial x_1 \partial {x_2}^2}\right)+B_{22}\left(\frac{\partial^3 v_0}{\partial {x_2}^3}\right)$$
$$+D_{12}\left(\Omega\left(\frac{\partial^3 \Theta_{x_2}}{\partial {x_1}^2 \partial x_2}+\frac{\partial^3 \Theta_{x_1}}{\partial x_1 \partial {x_2}^2}\right)-2\frac{\partial^4 w_0}{\partial {x_1}^2 \partial {x_2}^2}\right)+F_{12}\left(\frac{\partial^3 \Theta_{x_2}}{\partial {x_1}^2 \partial x_2}+\frac{\partial^3 \Theta_{x_1}}{\partial x_1 \partial {x_2}^2}\right)+D_{22}\left(\Omega\frac{\partial^3 \Theta_{x_2}}{\partial {x_2}^3}\right)$$
$$-D_{22}\left(\frac{\partial^4 w_0}{\partial {x_2}^4}\right)+F_{22}\left(\frac{\partial^3 \Theta_{x_2}}{\partial {x_2}^3}\right)+2B_{66}\left(\frac{\partial^3 u_0}{\partial x_1 \partial {x_2}^2}+\frac{\partial^3 v_0}{\partial {x_1}^2 \partial x_2}\right)+2D_{66}\left(\Omega\left(\frac{\partial^3 \Theta_{x_1}}{\partial x_1 \partial {x_2}^2}+\frac{\partial^3 \Theta_{x_2}}{\partial {x_1}^2 \partial x_2}\right)\right)$$
$$-2D_{66}\left(2\frac{\partial^4 w_0}{\partial {x_1}^2 \partial {x_2}^2}\right)+2F_{66}\left(\frac{\partial^3 \Theta_{x_1}}{\partial x_1 \partial {x_2}^2}+\frac{\partial^3 \Theta_{x_2}}{\partial {x_1}^2 \partial x_2}\right)+\bar{q}+\hat{N}_{11}\frac{\partial^2 w_0}{\partial {x_1}^2}+\hat{N}_{22}\frac{\partial^2 w_0}{\partial {x_2}^2}=0$$

$$(\Omega B_{11}+E_{11})\left(\frac{\partial^2 u_0}{\partial {x_1}^2}\right)+(\Omega D_{11}+F_{11})\left(\Omega\frac{\partial^2 \Theta_{x_1}}{\partial {x_1}^2}-\frac{\partial^3 w_0}{\partial {x_1}^3}\right)+(\Omega F_{11}+H_{11})\left(\frac{\partial^2 \Theta_{x_1}}{\partial {x_1}^2}\right)+(\Omega B_{12}+E_{12})$$
$$\left(\frac{\partial^2 v_0}{\partial x_1 \partial x_2}\right)+(\Omega D_{12}+F_{12})\left(\Omega\frac{\partial^2 \Theta_{x_2}}{\partial x_1 \partial x_2}-\frac{\partial^3 w_0}{\partial x_1 \partial {x_2}^2}\right)+(\Omega F_{12}+H_{12})\left(\frac{\partial^2 \Theta_{x_2}}{\partial x_1 \partial x_2}\right)$$
$$+(\Omega B_{66}+E_{66})\left(\frac{\partial^2 u_0}{\partial {x_2}^2}+\frac{\partial^2 v_0}{\partial x_1 \partial x_2}\right)+(\Omega D_{66}+F_{66})\left(\Omega\left(\frac{\partial^2 \Theta_{x_1}}{\partial {x_2}^2}+\frac{\partial^2 \Theta_{x_2}}{\partial x_1 \partial x_2}\right)-2\frac{\partial^3 w_0}{\partial x_1 \partial {x_2}^2}\right)$$
$$+(\Omega F_{66}+H_{66})\left(\frac{\partial^2 \Theta_{x_1}}{\partial {x_2}^2}+\frac{\partial^2 \Theta_{x_2}}{\partial x_1 \partial x_2}\right)-\left[\Omega^2 A_{55}+2\Omega K_{55}+L_{55}\right]\Theta_{x_1}=0$$

$$(\Omega B_{12}+E_{12})\left(\frac{\partial^2 u_0}{\partial x_1 \partial x_2}\right)+(\Omega D_{12}+F_{12})\left(\Omega\frac{\partial^2 \Theta_{x_1}}{\partial x_1 \partial x_2}-\frac{\partial^3 w_0}{\partial {x_1}^2 \partial x_2}\right)+(\Omega F_{12}+H_{12})\left(\frac{\partial^2 \Theta_{x_1}}{\partial x_1 \partial x_2}\right)+$$
$$(\Omega B_{22}+E_{22})\left(\frac{\partial^2 v_0}{\partial {x_2}^2}\right)+(\Omega D_{22}+F_{22})\left(\Omega\frac{\partial^2 \Theta_{x_2}}{\partial {x_2}^2}-\frac{\partial^3 w_0}{\partial y^3}\right)+(\Omega F_{22}+H_{22})\left(\frac{\partial^2 \Theta_{x_2}}{\partial {x_2}^2}\right)+$$
$$(\Omega B_{66}+E_{66})\left(\frac{\partial^2 u_0}{\partial x_1 \partial x_2}+\frac{\partial^2 v_0}{\partial {x_1}^2}\right)+(\Omega D_{66}+F_{66})\left(\Omega\left(\frac{\partial^2 \Theta_{x_1}}{\partial x_1 \partial x_2}+\frac{\partial^2 \Theta_{x_2}}{\partial {x_1}^2}\right)-2\frac{\partial^3 w_0}{\partial {x_1}^2 \partial x_2}\right)+$$
$$(\Omega F_{66}+H_{66})\left(\frac{\partial^2 \Theta_{x_1}}{\partial x_1 \partial x_2}+\frac{\partial^2 \Theta_{x_2}}{\partial {x_1}^2}\right)-\left[\Omega^2 A_{44}+2\Omega K_{44}+L_{44}\right]\Theta_{x_2}=0 \qquad (3.15)$$

Governing equations for angle-ply plates:

The following stiffness characteristics for angle-ply laminated plates are identically zero

$$\begin{aligned} &A_{16} = A_{26} = D_{16} = D_{26} = 0 \\ &B_{11} = B_{22} = B_{12} = B_{66} = 0 \\ &E_{11} = E_{22} = E_{12} = E_{66} = 0 \\ &F_{16} = F_{26} = H_{16} = H_{26} = 0 \\ &A_{45} = K_{45} = L_{45} = H_{45} = 0 \end{aligned} \tag{3.16}$$

After substituting these characteristics into Eq. (3.13), the following governing equations (Eq. (3.17)) in explicit form for the angle-ply laminates are generated

$$\begin{aligned} &A_{11}\left(\frac{\partial^2 u_0}{\partial {x_1}^2}\right) + A_{12}\left(\frac{\partial^2 v_0}{\partial x_1 \partial x_2}\right) + B_{26}\left(\Omega\frac{\partial^2 \Theta_{x_2}}{\partial {x_2}^2} - \frac{\partial^3 w_0}{\partial x_2^3}\right) + E_{26}\left(\frac{\partial^2 \Theta_{x_2}}{\partial {x_2}^2}\right) + A_{66}\left(\frac{\partial^2 u_0}{\partial {x_2}^2} + \frac{\partial^2 v_0}{\partial x_1 \partial x_2}\right) \\ &+ B_{16}\left(\Omega\left(2\frac{\partial^2 \Theta_{x_1}}{\partial x_1 \partial x_2} + \frac{\partial^2 \Theta_{x_2}}{\partial {x_1}^2}\right) - 3\frac{\partial^3 w_0}{\partial {x_1}^2 \partial x_2}\right) + E_{16}\left(2\frac{\partial^2 \Theta_{x_1}}{\partial x_1 \partial x_2} + \frac{\partial^2 \Theta_{x_2}}{\partial {x_1}^2}\right) = 0 \end{aligned}$$

$$\begin{aligned} &A_{12}\left(\frac{\partial^2 u_0}{\partial x_1 \partial x_2}\right) + A_{22}\left(\frac{\partial^2 v_0}{\partial {x_2}^2}\right) + E_{26}\left(2\frac{\partial^2 \Theta_{x_2}}{\partial x_1 \partial x_2} + \frac{\partial^2 \Theta_{x_1}}{\partial {x_2}^2}\right) + B_{16}\left(\Omega\frac{\partial^2 \Theta_{x_2}}{\partial {x_1}^2} - \frac{\partial^3 w_0}{\partial {x_1}^3}\right) \\ &+ E_{16}\left(\frac{\partial^2 \Theta_{x_2}}{\partial {x_1}^2}\right) + A_{66}\left(\frac{\partial^2 u_0}{\partial x_2 \partial x_1} + \frac{\partial^2 v_0}{\partial {x_1}^2}\right) + B_{26}\left(\Omega\left(2\frac{\partial^2 \Theta_{x_1}}{\partial {x_2}^2} + 2\frac{\partial^2 \Theta_{x_2}}{\partial x_1 \partial x_2}\right) - 3\frac{\partial^3 w_0}{\partial x_1 \partial {x_2}^2}\right) = 0 \end{aligned}$$

$$\begin{aligned} &D_{11}\left(\Omega\frac{\partial^3 \Theta_{x_1}}{\partial {x_1}^3} - \frac{\partial^4 w_0}{\partial {x_1}^4}\right) + F_{11}\left(\frac{\partial^3 \Theta_{x_1}}{\partial {x_1}^3}\right) + B_{16}\left(3\frac{\partial^3 u_0}{\partial {x_1}^2 \partial x_2} + \frac{\partial^3 v_0}{\partial {x_1}^3}\right) + B_{22}\left(\frac{\partial^3 v_0}{\partial {x_2}^3}\right) + D_{12} \\ &\left(\Omega\left(\frac{\partial^3 \Theta_{x_2}}{\partial {x_1}^2 \partial x_2} + \frac{\partial^3 \Theta_{x_1}}{\partial x_1 \partial {x_2}^2}\right) - 2\frac{\partial^4 w_0}{\partial {x_1}^2 \partial {x_2}^2}\right) + F_{12}\left(\frac{\partial^3 \Theta_{x_2}}{\partial {x_1}^2 \partial x_2} + \frac{\partial^3 \Theta_{x_1}}{\partial x_1 \partial {x_2}^2}\right) + D_{22}\left(\Omega\frac{\partial^3 \Theta_{x_2}}{\partial {x_2}^3} - \frac{\partial^4 w_0}{\partial {x_2}^4}\right) \\ &+ F_{22}\left(\frac{\partial^3 \Theta_{x_2}}{\partial {x_2}^3}\right) + B_{26}\left(\frac{\partial^3 u_0}{\partial {x_2}^3} + 3\frac{\partial^3 v_0}{\partial x_1 \partial {x_2}^2}\right) + 2D_{66}\left(\Omega\left(\frac{\partial^3 \Theta_{x_1}}{\partial x_1 \partial {x_2}^2} + \frac{\partial^3 \Theta_{x_2}}{\partial {x_1}^2 \partial x_2}\right) - 2\frac{\partial^4 w_0}{\partial {x_1}^2 \partial {x_2}^2}\right) \\ &+ 2F_{66}\left(\frac{\partial^3 \Theta_{x_1}}{\partial x_1 \partial {x_2}^2} + \frac{\partial^3 \Theta_{x_2}}{\partial {x_1}^2 \partial x_2}\right) + \bar{q} + \hat{N}_{11}\frac{\partial^2 w_0}{\partial {x_1}^2} + \hat{N}_{22}\frac{\partial^2 w_0}{\partial {x_2}^2} = 0 \end{aligned}$$

$$(\Omega D_{11}+F_{11})\left(\Omega\frac{\partial^2\Theta_{x_1}}{\partial {x_1}^2}-\frac{\partial^3 w_0}{\partial {x_1}^3}\right)+(\Omega F_{11}+H_{11})\left(\frac{\partial^2\Theta_{x_1}}{\partial {x_1}^2}\right)+(\Omega B_{26}+E_{26})\left(\frac{\partial^2 v_0}{\partial {x_2}^2}\right)+(\Omega D_{12}+F_{12})$$
$$\left(\Omega\frac{\partial^2\Theta_{x_2}}{\partial x_1\partial x_2}-\frac{\partial^3 w_0}{\partial x_1\partial {x_2}^2}\right)+(\Omega F_{12}+H_{12})\left(\frac{\partial^2\Theta_{x_2}}{\partial x_1\partial x_2}\right)+(\Omega B_{16}+E_{16})\left(2\frac{\partial^2 u_0}{\partial x_1\partial x_2}+\frac{\partial^2 v_0}{\partial {x_1}^2}\right)$$
$$+(\Omega D_{66}+F_{66})\left(\Omega\left(\frac{\partial^2\Theta_{x_1}}{\partial {x_2}^2}+\frac{\partial^2\Theta_{x_2}}{\partial x_1\partial x_2}\right)-2\frac{\partial^3 w_0}{\partial x_1\partial {x_2}^2}\right)+(\Omega F_{66}+H_{66})\left(\frac{\partial^2\Theta_{x_1}}{\partial {x_2}^2}+\frac{\partial^2\Theta_{x_2}}{\partial x_1\partial x_2}\right)$$
$$-\left[\Omega^2 A_{55}+2\Omega K_{55}+L_{55}\right]\Theta_{x_1}=0$$

$$(\Omega D_{12}+F_{12})\left(\Omega\frac{\partial^2\Theta_{x_1}}{\partial x_1\partial x_2}-\frac{\partial^3 w_0}{\partial {x_1}^2\partial x_2}\right)+(\Omega F_{12}+H_{12})\left(\frac{\partial^2\Theta_{x_1}}{\partial x_1\partial x_2}\right)+(\Omega B_{16}+E_{16})\left(\frac{\partial^2 u_0}{\partial {x_1}^2}\right)$$
$$+(\Omega D_{22}+F_{22})\left(\Omega\frac{\partial^2\Theta_{x_2}}{\partial {x_2}^2}-\frac{\partial^3 w_0}{\partial y^3}\right)+(\Omega F_{22}+H_{22})\left(\frac{\partial^2\Theta_{x_2}}{\partial {x_2}^2}\right)+(\Omega B_{26}+E_{26})\left(\frac{\partial^2 u_0}{\partial x_1^2}+2\frac{\partial^2 v_0}{\partial x_1\partial x_2}\right)$$
$$+(\Omega D_{66}+F_{66})\left(\Omega\left(\frac{\partial^2\Theta_{x_1}}{\partial x_1\partial x_2}+\frac{\partial^2\Theta_{x_2}}{\partial {x_1}^2}\right)-2\frac{\partial^3 w_0}{\partial {x_1}^2\partial x_2}\right)+(\Omega F_{66}+H_{66})\left(\frac{\partial^2\Theta_{x_1}}{\partial x_1\partial x_2}+\frac{\partial^2\Theta_{x_2}}{\partial {x_1}^2}\right)$$
$$-\left[\Omega^2 A_{44}+2\Omega K_{44}+L_{44}\right]\Theta_{x_2}=0 \tag{3.17}$$

3.3 Solution Methodology

Navier Solution: In order to predict the accurate response of structure and applicability of the new higher order theory for laminated plates, it is necessary to solve the governing equations in exact manner. The above coupled partial differential equations for cross-ply Eq. (3.15) and angle-ply Eq. (3.17) plates are solved by implementing Navier solution to yield the static and buckling responses. However, the Navier type solution is restricted to Simply supported laminated plates. The SS1 boundary conditions are imposed for cross-ply laminated plate are mentioned in Eq. (3.18) [43]

$$v_0=w_0=\Theta_{x_2}=N_{11}=M_{11}=0 \quad at \quad x_1=0,a$$

$$u_0=w_0=\Theta_{x_1}=N_{22}=M_{22}=0 \quad at \quad x_2=0,b \tag{3.18}$$

For angle-ply plate, SS2 boundary conditions are given in Eq. (3.19) as

$$v_0=w_0=\Theta_{x_1}=N_{22}=M_{22}=0 \quad at \quad x_2=0,b$$

$$u_0=w_0=\Theta_{x_2}=N_{11}=M_{11}=0 \quad at \quad x_1=0,a \tag{3.19}$$

The suitable series solution of Navier in terms of mid-plane field variables for cross-ply plates is assumed to satisfy the boundary conditions Eq. (3.18) and is given as follows

$$\begin{aligned}
u_0 &= \sum_{m=1}^{\infty}\sum_{n=1}^{\infty} \mathbb{U}_{mn} cos(\beta x_1) sin(\gamma x_2) \\
v_0 &= \sum_{m=1}^{\infty}\sum_{n=1}^{\infty} \mathbb{V}_{mn} sin(\beta x_1) cos(\gamma x_2) \\
w_0 &= \sum_{m=1}^{\infty}\sum_{n=1}^{\infty} \mathbb{W}_{mn} sin(\beta x_1) sin(\gamma x_2) \\
\Theta_{x_1} &= \sum_{m=1}^{\infty}\sum_{n=1}^{\infty} \mathbb{X}_{mn} cos(\beta x_1) sin(\gamma x_2) \\
\Theta_{x_2} &= \sum_{m=1}^{\infty}\sum_{n=1}^{\infty} \mathbb{Y}_{mn} sin(\beta x_1) cos(\gamma x_2)
\end{aligned} \tag{3.20}$$

Where, $\beta = \frac{m\pi}{a}$, $\gamma = \frac{n\pi}{b}$. Here, the coefficients $\mathbb{U}_{mn}, \mathbb{V}_{mn}, \mathbb{W}_{mn}, \mathbb{X}_{mn}$, and $\mathbb{Y}_{mn}$ are the arbitrary coefficients to be determined.

The Navier solutions in terms of primary field variables are presented for angle-ply plate and satisfying SS2 conditions Eq. (3.19) are expressed as follows [157]

$$\begin{aligned}
u_0 &= \sum_{m=1}^{\infty}\sum_{n=1}^{\infty} \mathbb{U}_{mn} sin(\beta x_1) cos(\gamma x_2) \\
v_0 &= \sum_{m=1}^{\infty}\sum_{n=1}^{\infty} \mathbb{V}_{mn} cos(\beta x_1) sin(\gamma x_2) \\
w_0 &= \sum_{m=1}^{\infty}\sum_{n=1}^{\infty} \mathbb{W}_{mn} sin(\beta x_1) sin(\gamma x_2) \\
\Theta_{x_1} &= \sum_{m=1}^{\infty}\sum_{n=1}^{\infty} \mathbb{X}_{mn} cos(\beta x_1) sin(\gamma x_2) \\
\Theta_{x_2} &= \sum_{m=1}^{\infty}\sum_{n=1}^{\infty} \mathbb{Y}_{mn} sin(\beta x_1) cos(\gamma x_2)
\end{aligned} \tag{3.21}$$

Substituting the above series solutions (3.20) into differential equations given by (3.15) and solutions given by (3.21) into equations (3.17) yields the system of equation involving parameters ($\mathbb{U}_{mn}, \mathbb{V}_{mn}, \mathbb{W}_{mn}, \mathbb{X}_{mn}$, and $\mathbb{Y}_{mn}$) which is solved by any appropriate technique. Where the integers m, n are depending on the transverse loading type. The desired mechanical response is evaluated after solving these equations. In the similar fashion, the loading is

assumed in consistency with the transverse deformation, i.e.

$$\bar{q} = \sum_{m=1}^{\infty}\sum_{n=1}^{\infty} \bar{Q}_{mn} sin(\beta x_1) sin(\gamma x_2) \tag{3.22}$$

where $\bar{Q}_{mn} = \bar{q_0}$ for sinusoidal load (SSL) (m=n=1) and $\bar{Q}_{mn} = \frac{16\bar{q_0}}{\pi^2 mn}$ (m, n= 1,3,5,,.....13) for the uniformly distributed load (UDL). The substitution of assumed solution and loadings in the governing differential equations yields the general system of algebraic equation as shown in Eq. (3.23).

$$\left[\bar{K} - N_0 G\right] \{\triangle\} = \{\bar{q}\} \tag{3.23}$$

where $\{\triangle\} = \{\mathbb{U}_{mn}, \mathbb{V}_{mn}, \mathbb{W}_{mn}, \mathbb{X}_{mn}, \mathbb{Y}_{mn}\}^T$ is a vector of unknown field variables and $\{\bar{q}\} = \left\{0 \;\; 0 \;\; \bar{Q}_{mn} \;\; 0 \;\; 0\right\}^T$ is the load vector. Where, $\left[\bar{K}\right]$ is the stiffness matrix.

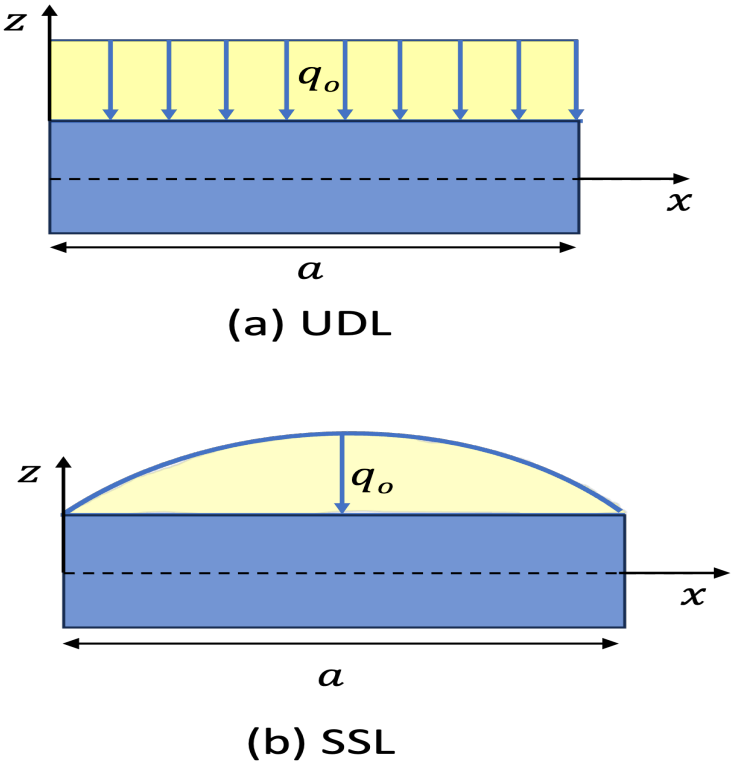

Figure 3.2: The sinusoidal and uniform distributed load

3.3.1 Static Analysis of Cross-ply and Angle-ply Plates

Cross-ply: In order to study the static response of cross ply laminated plate, the plate is assumed in the transverse direction and load is expressed in the Fourier expansion as given in

Eq. (3.22) The in-plane loads ($\hat{N}_{11}, \hat{N}_{22}$) are made equal to zero and hence, after substitution of solution from Eq. (3.20) and loadings from Eq. (3.22), the system of equations take the form as

$$\left[\bar{\mathbb{K}}^{\mathbb{C}}\right]\{\triangle\} = \{\bar{q}\} \tag{3.24}$$

The stiffness matrix $\left[\bar{\mathbb{K}}^{\mathbb{C}}\right]$ is defined in Appendix A.

Angle-ply: For bending behavior of laminated angle-ply plates, the assumed plate is having the SS2 boundary conditions. Hence, after substitution of assumed solution from Eq. (3.21) in the system of equations (3.17), the following matrix form is obtained

$$\left[\bar{\mathbb{K}}^{\mathbb{A}}\right]\{\triangle\} = \{\bar{q}\} \tag{3.25}$$

The stiffness matrix $\left[\bar{\mathbb{K}}^{\mathbb{A}}\right]$ is defined in Appendix B.The system of equations (3.24) and (3.25) are solved for the parameters appearing in $\{\triangle\}$ using the matrix inversion method. These parameters are then used in the presumed solutions (3.20) and (3.21) to compute the in-plane displacements and rotations.

3.3.2 Buckling Analysis of Laminates

In the proposed theory, to examine the buckling response, the assumed plate is subjected to in-plane compressive loads (uni-axial and bi-axial). The others loading terms ($\bar{q}$) appearing in Eq. (3.15) are taken as zero. Therefore, the following mathematical system is obtained for cross-ply laminated plate

$$\left[\bar{\mathbb{K}}^{C} - N_0 G\right]\{\triangle\} = 0 \tag{3.26}$$

The corresponding system for angle-ply plate is given as

$$\left[\bar{\mathbb{K}}^{\mathbb{A}} - N_0 G\right]\{\triangle\} = 0 \tag{3.27}$$

where $[G]$ is the geometric matrix due to axial load. The N_0 is buckling load parameter. Therefore, the above system becomes an eigenvalue problem. The buckling loads are represented by the eigenvalues, and minimum eigenvalue is analogous to the critical buckling load.

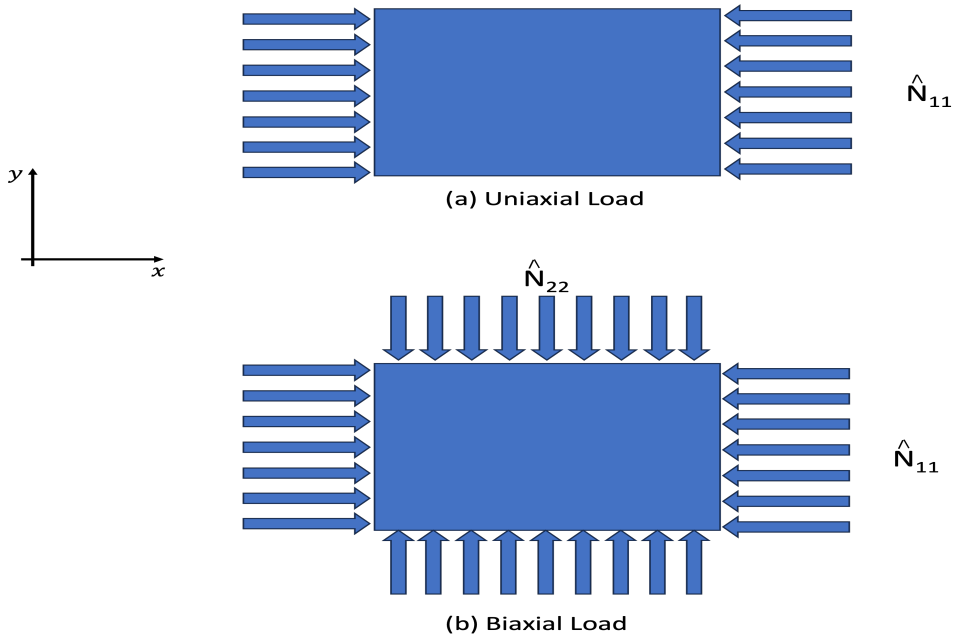

Figure 3.3: The Geometry of uniaxial and bi-axial buckling load

3.4 Modeling of Functionally Graded Plate

In this section, the mathematically modeling of functionally graded plate based upon IHSDT is presented wherein the gradient of the material properties is adopted using the power-law [158] and is given as follows

$$E(x_3) = E_b + (E_t - E_b)\left(\frac{2x_3 + h}{2h}\right)^k \tag{3.28}$$

Where E denotes Young's modulus, k is the power-law or volume fraction index. The material degenerates into an isotropic one for k=0. The subscripts b refer to the bottom and t represent top surfaces of the plate, respectively.

Displacement field: The displacement components at point (x_1, x_2, x_3) in terms of the shear strain function (inverse hyperbolic function of thickness coordinate [43]) are given as follows:

$$u(x_1, x_2, x_3) = u_0(x_1, x_2) - x_3\frac{\partial w_0}{\partial x_1} + \left(\sinh^{-1}\left(\tfrac{rx_3}{h}\right) - x_3\frac{2r}{h\sqrt{r^2+4}}\right)\cdot\Theta_{x_1}(x_1, x_2)$$

$$v(x_1, x_2, x_3) = v_0(x_1, x_2) - x_3\frac{\partial w_0}{\partial x_2} + \left(\sinh^{-1}\left(\tfrac{rx_3}{h}\right) - x_3\frac{2r}{h\sqrt{r^2+4}}\right)\cdot\Theta_{x_2}(x_1, x_2)$$

$$w(x_1, x_2, x_3) = w_0(x_1, x_2) \tag{3.29}$$

The value of parameter r is fixed as 3.0. The strain-displacement relations expressed as

given in Eq. (3.2). The material is assumed to follow the linear elastic behavior and under these assumptions, the stress-strain relations are defined using Hooke's laws as follows [159]:

$$\begin{bmatrix} \sigma_{11} \\ \sigma_{22} \\ \tau_{12} \\ \tau_{23} \\ \tau_{13} \end{bmatrix} = \begin{bmatrix} \bar{Q}_{11} & \bar{Q}_{12} & 0 & 0 & 0 \\ \bar{Q}_{12} & \bar{Q}_{22} & 0 & 0 & 0 \\ 0 & 0 & \bar{Q}_{66} & 0 & 0 \\ 0 & 0 & 0 & \bar{Q}_{44} & o \\ 0 & 0 & 0 & 0 & \bar{Q}_{55} \end{bmatrix} \begin{bmatrix} \epsilon_{11} \\ \epsilon_{22} \\ \gamma_{12} \\ \gamma_{23} \\ \gamma_{13} \end{bmatrix} \quad \text{or,} \quad [\sigma]_{5\times1} = \left[\bar{Q}\right]_{5\times5} [\epsilon]_{5\times1} \tag{3.30}$$

$$\text{Where} \quad \bar{Q}_{11} = \bar{Q}_{22} = \frac{E(x_3)}{1-\nu_o^2}, \quad \bar{Q}_{12} = \frac{\nu_o E(x_3)}{1-\nu_o^2}, \quad \bar{Q}_{44} = \bar{Q}_{55} = \bar{Q}_{66} = \frac{E(x_3)}{2(1+\nu_o)}$$

Where E is Young's modulus and ν_0 is the Poisson's ratio which is assumed to be constant through the thickness of the plate.

Algebraic system: The formulation derived in sections (3.2) and (3.3) is employed to obtain the governing differential equations based on SS1 boundary conditions (3.18) and algebraic system to examine the structural response of FG plates is given as follows:

$$\left[\bar{K} - N_0 G\right] \{\triangle\} = \{\bar{q}\} \tag{3.31}$$

The stiffness matrix $\left[\bar{K}\right]$ is defined in Appendix C.

3.5 Finite Element Formulation

The formulation and solution methodology described in the previous sections are limited to composite plates with simply supported boundary conditions. The Navier's approach is renowned for its ability to analyze the behaviour of simply supported plates. The plates with curved geometries and various boundary conditions along the edges cannot be analyzed properly by using analytical methods. Thus, the finite element method (FEM) is proposed to find the numerical solutions and overcome the limitations of existing method. FEM provides a versatile platform to simulate and analyze the response of composite plates under different loading scenarios. Consequently, in this section, the finite element formulation in framework of higher order theory is presented to derive the governing equations of composite plate and hence predict the response of structure under various boundary conditions.

3.5.1 Displacement Field

The displacement field given in Eqs. (3.1) requires condition of C^1 continuity in modeling the plate in framework of FEM because of the presence of first derivatives in the list of primary variables in the displacement field. However, difficulties related to C^1 continuous FE increase the computational expense. To reduce the continuity in the FE formulation and make the computation less expensive, auxiliary variables are introduced. Specifically, these variables correspond to the first-order derivatives of the transverse displacement appearing in the in-plane displacement terms. By treating these derivatives as separate independent degrees of freedom, $\phi_{x_1} = \frac{\partial w_0}{\partial x_1}$, and $\phi_{x_2} = \frac{\partial w_0}{\partial x_2}$, the displacement field is modified so as to ensure the C^0 continuity requirement and given in Eqs. (3.32).

$$u(x_1, x_2, x_3) = u_0(x_1, x_2) - x_3\phi_{x_1} + f(x_3)\Theta_{x_1}(x_1, x_2)$$

$$v(x_1, x_2, x_3) = v_0(x_1, x_2) - x_3\phi_{x_2} + f(x_3)\Theta_{x_2}(x_1, x_2)$$

$$w(x_1, x_2, x_3) = w_0(x_1, x_2) \tag{3.32}$$

3.5.2 Strain-displacement Relations

Under the assumption of small elastic deformations and moderate rotations, relationships between strain and displacements due to von-karman non-linear strains are given as [160]

$$\{\epsilon\} = \{\epsilon_l\} + \{\epsilon_{nl}\} \tag{3.33}$$

$$\{\epsilon\}_{5\times1} = [\epsilon_{11} \;\; \epsilon_{22} \;\; \gamma_{12} \;\; \gamma_{23} \;\; \gamma_{13}]^T$$

$$\{\epsilon_l\} = \left[\frac{\partial u}{\partial x_1} \;\; \frac{\partial v}{\partial x_2} \;\; \frac{\partial u}{\partial x_2} + \frac{\partial v}{\partial x_1} \;\; \frac{\partial v}{\partial x_3} + \frac{\partial w}{\partial x_2} \;\; \frac{\partial u}{\partial x_3} + \frac{\partial w}{\partial x_1}\right]^T$$

$$\{\epsilon_{nl}\} = \left[\frac{1}{2}\left(\frac{\partial w}{\partial x_1}\right)^2 \;\; \frac{1}{2}\left(\frac{\partial w}{\partial x_2}\right)^2 \;\; \frac{1}{2}\left(\frac{\partial w}{\partial x_1}\right)\left(\frac{\partial w}{\partial x_2}\right) \;\; 0 \;\; 0\right]^T$$

It should be noted that for static analysis, linear strains are considered to derive the elastic stiffness matrix while non-linear strains are assumed in buckling analysis to get the geometric stiffness matrix.

Proposed Element :
In the present finite element formulation, a C^0-continuous iso-parametric serendipity element with eight nodes at each element is chosen to discretize the plate geometry. The element assumed is biquadratic quadrilateral. Each node in the element has seven degrees of freedom, corresponding to the number of field variables required to meet the C^0 criteria. The shape functions at node i for an eight noded serendipity element are as follows [160]

$$N_i = \begin{cases} \frac{1}{4}(1+\xi\xi_i)(1+\eta\eta_i)(\xi\xi_i+\eta\eta_i-1) & \text{for } i\text{= 1, 2, 3, 4} \\ \frac{1}{2}(1-\xi^2)(1+\eta\eta_i) & \text{for } i\text{= 5, 7} \\ \frac{1}{2}(1-\eta^2)(1+\xi\xi_i) & \text{for } i\text{= 6, 8} \end{cases}$$

Due to the isoparametric serendipity element, the field variables and geometry are specified by the same shape function. Consequently, the general displacement vector and element geometry of the model at any point are represented in terms of shape functions in the following manner:

$$g = \sum_{i=1}^{n} N_i g_i, \quad q = \sum_{i=1}^{n} N_i q_i \tag{3.34}$$

Where g is the generalized geometrical co-ordinate, g_i is the value of variable corresponding to node i and N_i is the shape function at ith node, q_i is the value of field variable at node i for generalized variable q.

3.5.3 Derivation of Strain Energy and work Done

Linear strain energy: The strain-displacement relationships due to linear strain given in Eqs.(3.2) are employed and moreover, the strain components given in vector $\{\epsilon\}$ can be written in terms of generalized strains as follows [160]

$$\{\epsilon\} = [H]_{5\times 13}\,\{\bar{\epsilon}\}_{13\times 1} \tag{3.35}$$

where $\{\epsilon\}$= $[\epsilon_{11}\ \epsilon_{22}\ \gamma_{12}\ \gamma_{23}\ \gamma_{31}]^T$ is the strain vector. The elements of the matrix [H] are dependent on the variable x_3, unit step functions and parameter Ω, given as follows.

$$[H] = \begin{bmatrix} 1 & 0 & 0 & x_3 & 0 & 0 & g(x_3) & 0 & 0 & 0 & 0 & 0 & 0 \\ 0 & 1 & 0 & 0 & x_3 & 0 & 0 & g(x_3) & 0 & 0 & 0 & 0 & 0 \\ 0 & 0 & 1 & 0 & 0 & x_3 & 0 & 0 & g(x_3) & 0 & 0 & 0 & 0 \\ 0 & 0 & 0 & 0 & 0 & 0 & 0 & 0 & 0 & 1 & 0 & g'(x_3) & 0 \\ 0 & 0 & 0 & 0 & 0 & 0 & 0 & 0 & 0 & 0 & 1 & 0 & g'(x_3) \end{bmatrix} \tag{3.36}$$

Again, the generalized strain vector $\{\bar{\epsilon}\}_{13\times 1}$ consist of functions of unknown variables as follows

$\{\bar{\epsilon}\} = \{\epsilon_1^0,\quad \epsilon_2^0,\quad \epsilon_6^0,\quad k_1^0,\quad k_2^0,\quad k_6^0,\quad k_1^1,\quad k_2^1,\quad k_6^1,\quad \epsilon_4^0,\quad \epsilon_5^0,\quad k_4^2,\quad k_5^2\}^T$

where $\epsilon_1^0 = \frac{\partial u_0}{\partial x_1}$, $\epsilon_2^0 = \frac{\partial v_0}{\partial x_2}$, $\epsilon_6^0 = \frac{\partial u_0}{\partial x_2} + \frac{\partial v_0}{\partial x_1}$, $k_1^0 = \Omega\frac{\partial \Theta_{x_1}}{\partial x_1} - \frac{\partial \phi_{x_1}}{\partial x_1}$, $k_2^0 = \Omega\frac{\partial \Theta_{x_2}}{\partial x_2} - \frac{\partial \phi_{x_2}}{\partial x_2}$

$$k_6^0 = \Omega\left(\frac{\partial\Theta_{x_1}}{\partial x_2} + \frac{\partial\Theta_{x_2}}{\partial x_1}\right) - \left(\frac{\partial\phi_{x_1}}{\partial x_2} + \frac{\partial\phi_{x_2}}{\partial x_1}\right), \quad k_1^1 = \frac{\partial\Theta_{x_1}}{\partial x_1}, \quad k_2^1 = \frac{\partial\Theta_{x_2}}{\partial x_2}, \quad k_6^1 = \left(\frac{\partial\Theta_{x_1}}{\partial x_2} + \frac{\partial\Theta_{x_2}}{\partial x_1}\right),$$

$$\epsilon_4^0 = \frac{\partial w_0}{\partial x_2} + \Omega\Theta_{x_2} - \phi_{x_2}, \quad \epsilon_5^0 = \frac{\partial w_0}{\partial x_1} + \Omega\Theta_{x_1} - \phi_{x_1}, \quad k_4^2 = \Theta_{x_2}, \quad k_5^2 = \Theta_{x_1}$$

It should be noted that the generalised strains are derivative terms of field variables and hence an operator matrix [L] is used to establish the relationship between generalized strains and the field variables $\{q\}$. Therefore, the strain vector $\{\bar{\epsilon}\}$ in Eq. (3.35) can be presented in terms of field variables appearing in vector $\{q\}$ as follows

$$\{\bar{\epsilon}\}_{13\times1} = [L]_{13\times7}\,\{q\}_{7\times1} \tag{3.37}$$

where $\{q\}_{7\times1} = [u_0, v_0, w_0, \Theta_{x_1}, \Theta_{x_2}, \phi_{x_1}, \phi_{x_2}]^T$

The strain-displacement relations for the kth element can be derived by substituting Eq. (3.34) into Eq. (3.37), resulting in the following expressions:

$$\{\bar{\epsilon}\}_k = [B]_k\,\{q_i\}_k \tag{3.38}$$

The energy resulting from linear strain for the kth element is determined by Eq. (3.39)

$$U_l^{(k)} = \frac{1}{2}\int_V \{\epsilon\}_k^T\,\{\sigma\}\,dV \tag{3.39}$$

Further, the constitutive relations (3.3) is used to convert stress terms into strain terms and following expression for strain energy is obtained as follows

$$U_l^{(k)} = \frac{1}{2}\int_V \{\epsilon\}_k^T\,\{\sigma\}\,dV = \frac{1}{2}\int_V \{\epsilon\}_k^T\,\left[\bar{Q}\right]\{\epsilon\}_k\,dV \tag{3.40}$$

Moreover, the expression given in Eq. (3.40) is simplified in terms of field variables by utilising Eq. (3.35) and (3.38) in Eq. (3.40) in the subsequent manner.

$$\begin{aligned} U_l^{(k)} &= \frac{1}{2}\int_V \{\bar{\epsilon}\}_k^T\,[H]_k^T\,\left[\bar{Q}\right][H]_k\,\{\bar{\epsilon}\}_k\,dV \\ &= \frac{1}{2}\int_S \{q_i\}_k^T\,[B]_k^T[D]_k[B]_k\,\{q_i\}_k\,dx_1dx_2 = \frac{1}{2}\,\{q_i\}_k^T\,[K]_k\,\{q_i\}_k \end{aligned} \tag{3.41}$$

Where $[D]_k = \int_{-h/2}^{h/2}[H]_k^T\,\left[\bar{Q}\right][H]_k dx_3$ and $[K]_k = \iint [B]_k^T[D]_k[B]_k dx_1dx_2$

Where $[K]_k$ is elemental stiffness matrix and [D] is the function of the thickness variable. The Gauss quadrature technique is employed to compute the integral involve in elemental

stiffness matrix using the Jacobian as $[K]_k = \int_{-1}^{1}\int_{-1}^{1}[B]_k^T[D]_k[B]_k|J|d\zeta d\eta$ to simplify the transformation between ζ-η and x_1-x_2 coordinates.
Total strain energy, U is calculated by performing assembly over all the elements and is expressed as:

$$U_l = \sum_{k=1}^{nel} \frac{1}{2} \{q_i\}_k^T [K]_k \{q_i\}_k = \frac{1}{2} \{q\}^T [K] \{q\} \tag{3.42}$$

where $\{q\}$ global displacement vector, [K] is global stiffness matrix.

Non-linear strain energy: Geometrical stiffness matrix depends on geometry as well as on the internal in-plane forces and is obtained by using non-linear strain–displacement relationships (Eq. (3.33)). The strain energy for non-linear strains due to external in-plane force for the kth element is derived as:

$$\begin{aligned} U_{nl}^{(k)} &= \frac{1}{2}\int_V \{\epsilon_{nl}\}_k^T \{\sigma\} dV = \frac{1}{2}\int_V \{\epsilon_{nl}\}_k^T \left[\bar{S}\right] \{\epsilon_{nl}\}_k dV = \frac{1}{2}\int_V \{\bar{\epsilon_{nl}}\}_k^T [H_G]_k^T \left[\bar{S}\right] [H_G]_k \{\bar{\epsilon_{nl}}\}_k dV \\ &= \frac{1}{2}\int_S \{q_i\}_k^T [B_G]_k^T [G]_k [B_G]_k \{q_i\}_k dx_1 dx_2 = \frac{1}{2} \{q_i\}_k^T [K_G]_k \{q_i\}_k \end{aligned} \tag{3.43}$$

Where $[G] = \sum_{j=1}^{nl}\int_{-h/2}^{h/2}[H_G]^T \left[\bar{S}\right] [H_G] dx_3$ and $[\bar{S}] = \begin{bmatrix} S_{x_1x_1} & S_{x_1x_2} \\ S_{x_1x_2} & S_{x_2x_2} \end{bmatrix}$

The in-plane stresses, $S_{x_1x_2}$ and$S_{x_2x_2}$ are written in terms of $S_{x_1x_1}$ as $S_{x_2x_2} = \lambda_1 S_{x_1x_1}$ and $S_{x_1x_2} = \lambda_2 S_{x_1x_1}$.
Total strain energy U_{nl} because of non-linear strains is attained by conducting assembly process across all the elements and is given as:

$$U_{nl} = \sum_{k=1}^{nel} U_{nl}^k = \frac{1}{2} \{\bar{q}\}^T [K_G] \{\bar{q}\} \tag{3.44}$$

where $[K_G]$ is global geometric stiffness matrix.

Work done: The work done as a result of an external transverse load can be expressed as follows:

$$W = \sum_{k=1}^{nel} W_k = \sum_{k=1}^{nel} \int_{A_k} p(x_1, x_2) w dA_k = \sum_{k=1}^{nel} \{f\}_k \{q\}_k = \{F\} \{q\} \tag{3.45}$$

where [f]=[0, 0, p_0, 0, 0, 0, 0], p_0 is applied transverse load. For Uniformly distributed load (UDL), p_0=q_0, whereas for sinusoidal load (SSL), $p_0 = q_0\ sin(\pi x_1/a) sin(\pi x_2/b)$

3.5.4 Derivation of Governing System

The energy terms and work done related to the structural analysis of FG plates as discussed in previous section are utilised in the principle of minimal potential energy to formulate the governing equations of system. The Lagrange equations of motion for minimum potential energy is given as follows [160]

$$\frac{\partial U_l}{\partial q} + \frac{\partial U_{nl}}{\partial q} - \frac{\partial W}{\partial q} = 0 \tag{3.46}$$

The terms U_l and U_{nl} and W appearing in Eqs. (3.42), (3.44), and (3.45) are substituted in Eq. (3.46) to obtain the following system of equations.

$$[K]\{q\} + \lambda [K_G]\{q\} = F \tag{3.47}$$

The above system is algebraic system of governing equations in general form which can be solved to yield the desired response of the composite FG plates.

Static Analysis: The static response of the plate under consideration is solely influenced by transverse loads, while any other external forces are neglected. Therefore, for static analysis, the geometric stiffness matrix [K_G] becomes zero and the system of equations for static analysis is reduced as in Eq. (3.48)

$$[K]\{q\} = \{F\} \tag{3.48}$$

Buckling Response: For buckling analysis, the considered plate is subjected to in-plane compressive forces only, due to which instability occurs in the plate. Therefore, in this case, the load vector in Eq. (3.47) will become zero. So the mathematical system of the FG plate are obtained in the form of an eigenvalue problem as given in Eq. (3.49)

$$[K + \lambda K_G]\{q\} = 0 \tag{3.49}$$

The above system is solved mathematically for eigen values, where the eigenvalues are associated with the phenomenon of buckling, and the least eigenvalue specifically represents the critical buckling load.

3.6 Summary

In this chapter, the laminated and FG plate are modeled and analyzed based on non-polynomial shear deformation theories. The formulation of governing differential equations

along with solution methodology are presented in details. The Navier's solution approach is implemented to examine the structural behavior of composite plates. The system of equations are then attained for cross-ply and angle-ply laminated plates. Moreover for FG plate, the material properties are varied accordance to power-law rule of mixture. The algebraic system for FG plate is presented in this chapter to yield the desired mechanical behavior. The finite element methodology also presented in this chapter along with detailed formulation to derive the numerical solution of composite plates subjected to various boundary conditions. The newly developed secant hyperbolic shear deformation theory is proposed in the chapter 4 and 6 to analyze the bending and buckling response of multi-layered structures and FGM plates. The inverse hyperbolic theory is implemented for the first time to predict the structural response of FG porous plate in chapter 5.

Chapter 4

Development of new shear deformation theory

Composite plates are particularly important structural elements that have been extensively studied by researchers in the past. In industry and emerging fields of technology, laminated composite plates are extensively used. These plates are made by stacking layers of different materials in a specific orientation to achieve desired mechanical properties. Over the last few decades, several plate theories have been proposed for modeling of laminated composite plates. In existing literature, there are variety of analytical and numerical methods to analyze laminated composite plates. Kant and Swaminathan [161] presented a review of several methods to investigate the stress analysis of laminated composites. The different higher shear deformation theories (HSDTs) which contain polynomial and non-polynomial types shape function have been developed earlier [27–29, 66–68]. Swaminathan and Ragounadin [162] proposed analytic solutions for the flexural analysis of angle-ply plates employing a higher-order refined theory. Aydogdu [163] evaluated the deflections, buckling and stresses of symmetric cross-ply plates using various HSDTs. Akavci [164] carried out the free vibrations and buckling response of cross-ply laminated composites using hyperbolic shear deformation theories. The analytical solutions are obtained using Navier method. For laminated plates, Karama *et al.* [165] introduced a new shear deformation theory based on exponential strain shape function. Aydogdu [40] modified the model of Karama *et al.* [165] and analyzed the bending, buckling, and free vibrations responses for laminated plates. Further, a novel refined non-polynomial based higher order theory is developed by Mantari *et al.* [166] to study the static and dynamic behavior of laminates. Piskunov *et al.* [167] performed the static analysis of anisotropic cross- and angle-ply plates and shells using rational transverse HSDT. A noval shear deformation theory was introduced by Mahi *et al.* [41] for bending and free vibrations characteristics of FG plates. The theory provides non-linear variation of transverse strains having five degrees of freedom. Dhuria *et al.* [168] evaluated the bending and buckling response for FGM porous plates with simply supported edges using Navier solution technique. Thai and Kim [4] presented analytical solutions for static and free vibration response of FG plates using simple HSDT. Further, different methods

The content of this chapter has been published in Journal Of Applied Mechanics, 90(5):051004, 2023.

have been employed to obtain the mechanical responses of laminated composite plates using different plate theories [145, 169–171]. All of these studies are limited in that they analyze cross-ply laminated plates in most of the research based on higher order theory. Only a few articles have proposed analytical solutions for angle-ply laminated plate employing the recent non-polynomial shear deformation theory.

In this study, a new higher order hyperbolic shear deformation theory is developed in the axiomatic framework which deals with the static and buckling behavior of both cross- and angle-ply laminated composite plates. The assumed plate is subjected to have simply supported conditions along its edges. The Navier-type solution technique is used to solve the governed equations. The independent Navier solutions are obtained for cross- as well as angle-ply plate. The numerical results for deflections and critical buckling load of rectangular and square laminates are presented. To ensure the validity of present theory, the findings are compared with solutions obtained from other theories in existing literature, and they are found to be in good agreement. The new results are taken as benchmark for further study of laminated plates.

4.1 Results and Discussion

In this section, the new shear deformation model (3.1) proposed in chapter 3 and the developed solution methodology is implemented to analyze the structural response of composite laminates. The mathematical formulation performed in chapter 3 is utilised to examine the bending and buckling behavior of cross-ply and angle-ply multi-layered plates. To verify the accuracy of proposed model, various numerical examples are discussed in predicting the mechanical behavior of plates. This is done by comparing our results with those already existed in the literature. The MATLAB generalized program is developed to obtain the analytical solutions for considered laminated plates. The plate under consideration is subjected to a transverse SSL and UDL. Moreover, the effects of shear deformation, side-thickness ratio, lamination sequence, and loading conditions on the mechanical responses are investigated. Different material properties of the laminated plate are as follows

Material properties 1 (MP1) [43]

$$\frac{E_1}{E_2} = 25, \quad \frac{G_{12}}{E_2} = 0.5, \quad \frac{G_{13}}{E_2} = 0.5, \quad \frac{G_{23}}{E_2} = 0.2, \quad \nu_{12} = 0.25 \tag{4.1}$$

Material properties 2 (MP2) [87]

$$\frac{E_1}{E_2} = 40, \quad \frac{G_{12}}{E_2} = 0.6, \quad \frac{G_{13}}{E_2} = 0.6, \quad \frac{G_{23}}{E_2} = 0.5, \quad \nu_{12} = 0.25 \tag{4.2}$$

Material properties 3 (MP3) [162]

$$E_1 = 38.61\ \text{GPa}, \quad E_2 = 8.27\ \text{GPa}, \quad G_{12} = 4.14\,\text{GPa}, \quad G_{13} = 4.14\,\text{GPa}, \quad G_{23} = 3.45\,\text{GPa}, \nu_{12} = 0.26 \tag{4.3}$$

4.1.1 Static Response of Cross-ply Plates

This section focuses on studying the static behaviour of symmetric and anti-symmetric cross ply laminated plates. The bending of plate is assumed in the transverse direction and the load $\bar{q}$ is expressed in the Eq. (3.22). Thus, the system of equations Eq. (4.4) can be solved algebraically to find the deflections and stresses for cross-ply plates.

$$\left[\bar{\mathbb{K}}^{\mathbb{C}}\right]\{\triangle\} = \{\bar{q}\} \tag{4.4}$$

The stress analysis is then carried out by employing the strain-displacement relationship given by (3.2) and the stress-strain relations (3.3). In static response, the stresses and transverse deflection are evaluated at critical points. The results for deflections and stresses are presented in the non-dimensional forms indicated in Eq. (4.5).

$$\overline{W} = w_0\left(\frac{a}{2},\frac{b}{2}\right)\frac{100E_2h^3}{\bar{q}_0a^4}, \quad \bar{\sigma}_{11} = \sigma_{11}\left(\frac{a}{2},\frac{b}{2},\frac{h}{2}\right)\frac{h^2}{\bar{q}_0a^2}, \quad \bar{\sigma}_{22} = \sigma_{22}\left(\frac{a}{2},\frac{b}{2},\frac{h}{4}\right)\frac{h^2}{\bar{q}_0a^2}$$

$$\bar{\tau}_{12} = \tau_{12}\left(0,0,\frac{h}{2}\right)\frac{h^2}{\bar{q}_0a^2}, \quad \bar{\tau}_{13} = \tau_{13}\left(0,\frac{b}{2},0\right)\frac{h}{\bar{q}_0a}, \quad \bar{\tau}_{23} = \tau_{23}\left(\frac{a}{2},0,0\right)\frac{h}{\bar{q}_0a} \tag{4.5}$$

Analysis of square [0/90/90/0] Laminated Plates Subjected to SSL

As a first example, a simply supported four-layered symmetric plate under sinusoidal load is considered for analysis. The non-dimensional maximum deflection ($\overline{W}$) and the stresses are evaluated for various values of thickness parameter a/h using non-dimensional forms Eq. (4.5). The material properties (MP1) are used to examine static response characteristics. The obtained numerical results are presented in Table 4.1 along with the existing results based on different shear deformation theories. The present theory exhibits good agreement of deflection, and normal stresses results when compared with exact solution of Pagano and Hatfield [10]. However, there is a considerable difference of transverse shear stresses with 3D elasticity solution, as in evaluation of transverse stresses, the equilibrium equations are not maintained in the formulation. The average absolute error (%Error) for evaluation of non-dimensional deflection ($\overline{W}$) is 1.43% for the present theory which is lower than previ-

Table 4.1: The dimensionless deflection and stresses for [0/90/90/0] laminated plate

a/h	Theory	$\overline{W}$		$\bar{\sigma}_{11}$		$\bar{\sigma}_{22}$		$\bar{\tau}_{12}$		$\bar{\tau}_{23}$		$\bar{\tau}_{13}$	
			%Error		%Error		%Error		%Error		%Error		%Error
4	Pagano and Hatfield [10]	1.954	-	0.72	-	0.663	-	0.047	-	0.291-		0.219	-
	Present	1.9243	1.52	0.7307	1.48	0.6377	3.81	0.0474	0.85	0.2676	8.04	0.2489	13.65
	Mantari *et al.* [69]	1.921	1.69	0.74	2.78	0.635	4.22	0.048	2.13	0.269	7.56	0.254	15.98
	Grover *et al.* [43]	1.9257	1.45	0.7255	0.76	0.639	3.62	0.0473	0.64	0.27	7.21	0.25	14.15
	Karama *et al.* [165]	1.919	1.79	0.699	2.92	0.636	4.07	0.0459	2.34	0.226	22.34	0.226	3.196
	Reddy [28]	1.893	3.12	0.665	7.64	0.632	4.68	0.044	6.38	0.239	17.87	0.206	5.94
10	Pagano and Hatfield [10]	0.743	-	0.559	-	0.401	-	0.028	-	0.196	-	0.301	-
	Present	0.7289	1.89	0.5589	0.017	0.3949	1.52	0.0275	1.92	0.1749	10.7	0.3275	8.80
	Mantari *et al.* [69]	0.73	1.75	0.561	0.36	0.395	1.50	0.028	0	0.176	10.2	0.335	11.3
	Grover *et al.* [43]	0.7284	1.96	0.5578	0.22	0.3947	1.57	0.0275	1.92	0.1762	10.1	0.3287	9.22
	Karama *et al.* [165]	0.724	2.56	0.553	1.07	0.393	2	0.027	3.57	0.163	16.84	0.294	2.33
	Reddy [28]	0.715	3.77	0.546	2.33	0.389	3	0.027	3.57	0.153	21.94	0.264	12.3
20	Pagano and Hatfield [10]	0.517	-	0.543	-	0.308	-	0.023	-	0.156	-	0.328	-
	Present	0.5103	1.29	0.5428	0.03	0.3065	0.48	0.023	0	0.1401	10.1	0.3531	7.65
	Mantari *et al.* [69]	0.51	1.35	0.542	0.18	0.306	0.65	0.023	0	0.132	15.38	0.323	1.52
	Grover *et al.* [43]	0.5102	1.32	0.5425	0.09	0.3064	0.52	0.023	0	0.1412	9.48	0.3542	7.98
	Karama *et al.* [165]	0.509	1.55	0.541	0.37	0.306	0.65	0.023	0	0.131	16.03	0.316	3.66
	Reddy [28]	0.506	2.13	0.539	0.74	0.304	1.3	0.023	0	0.123	21.15	0.283	13.72
100	Pagano and Hatfield [10]	0.439	-	0.539	-	0.276	-	0.022	-	0.141	-	0.337	-
	Present	0.4345	1.03	0.5388	0.03	0.271	1.81	0.0214	2.73	0.126	10.6	0.3632	7.77
	Mantari *et al.* [69]	0.435	0.91	0.539	0	0.271	1.81	0.021	4.55	0.119	15.6	0.332	1.48
	Grover *et al.* [43]	0.4345	1.03	0.5388	0.03	0.271	1.81	0.0214	2.73	0.1271	9.85	0.3643	8.1
	Karama *et al.* [165]	0.435	0.91	0.538	0.19	0.27	2.18	0.021	4.55	0.118	16.3	0.324	3.86
	Reddy [28]	0.434	1.14	0.538	0.19	0.27	2.18	0.021	4.55	0.112	20.57	0.29	13.95

ously developed theories (1.70% (Karama *et al.* [165]), and 2.54% (Reddy [28])) and well agreement is found with (Grover *et al.* [43] (1.44%), Mantari *et al.* [69](1.425%)). Moreover, for moderate thick to thin plates ($a/h \geq 10$), the proposed theory is more accurate and gives

better results in terms of central deflections, normal stresses and the shear stresses. Also, it is observed that as span-thickness ratio a/h increases, the corresponding deflection of square plate decreases.

The influence of plate aspect ratio on the dimensionless bending of symmetric cross-ply plate is shown in Fig. 4.1 for different side-thickness ratios. It is noted that the transverse deflection increases with the increment in aspect ratio for any value of a/h. So the square plate possess smaller deflection than rectangular plate. Also it is observed that the thick plate (a/h=4) has more non-dimensional deflection than moderately thick or thin plate (a/h=10,100). The variations of in-plane stresses σ_{11} across the thickness and transverse shear stresses σ_{13} for different a/h ratios is obtained for considered laminated plate in Fig. 4.2 and 4.3. The variations in stress σ_{11} decreases with increase in span-thickness ratio.

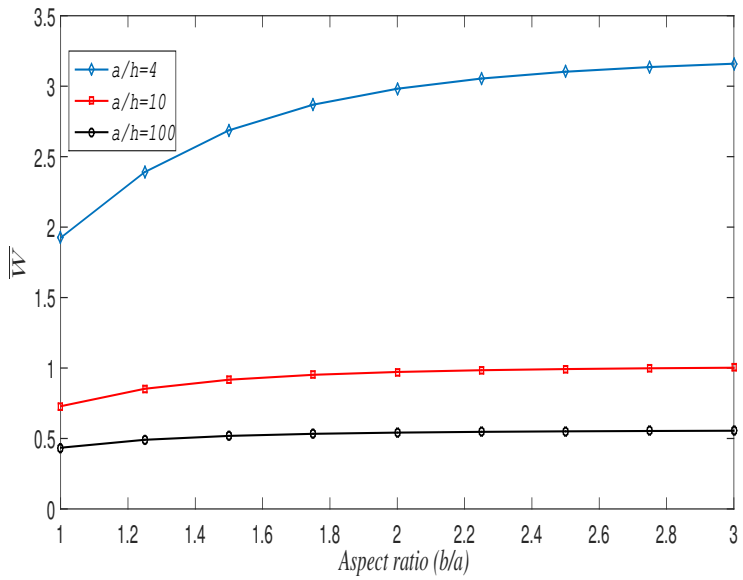

Figure 4.1: The influence of b/a ratio on dimensionless deflections for cross-ply plate.

Anti-symmetric Cross-ply Square Plates Subjected to UDL

As a next example, the multilayered cross-ply $[0/90]_n$ plates subjected to UDL are considered. The results of maximum deflection for two, four, six and eight layered plates are obtained corresponding to various span-thickness ratios and are plotted in Fig. 4.4. It can be noticed that the increasing number of layers decrease the non-dimensional deflection. The decrease in deflection is clearly notable from two to four layered plate. Also, the thick plate (a/h=4) possesses the more deflection as compare to moderately thick and thin plates.

Three-layer [0/90/0] Symmetric Square Plate Under Transverse SSL (MP1)

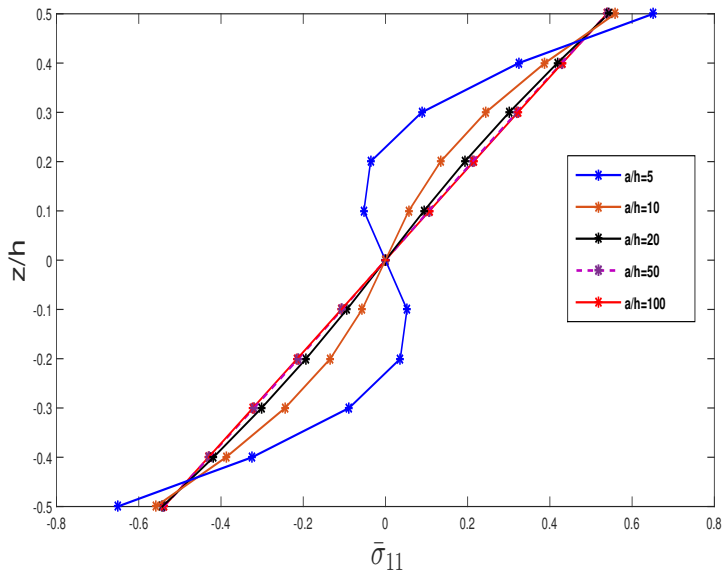

Figure 4.2: Variation of $\bar{\sigma}_{11}$ across thickness for symmetric cross-ply laminates.

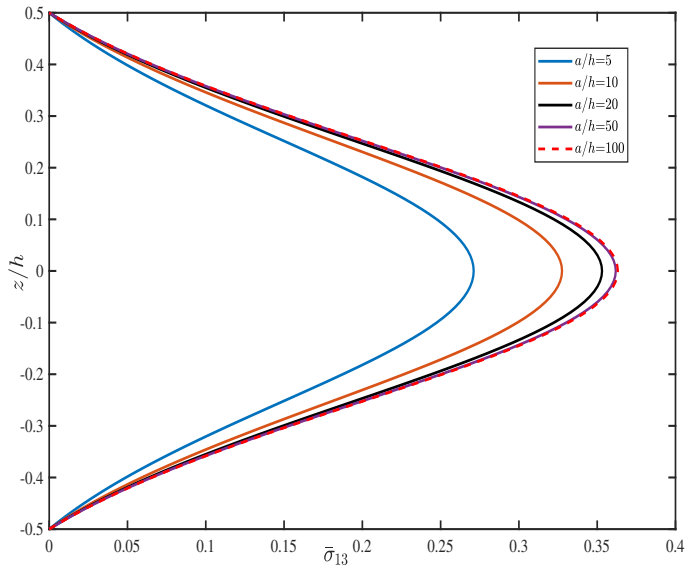

Figure 4.3: Variation of $\bar{\sigma}_{13}$ across thickness for symmetric cross-ply laminated plate.

In the second example, the transverse deflections and stresses for symmetric cross-ply laminated plate under sinusoidal loading are obtained. The results of present theory are compared with 3D-elasticity solution presented by Pagano and Hatfield [10] and the other shear deformation theories ([43], [69], [165], [28]) in Table 4.2 using different values of a/h. The results predicted by the present model agreed well with results due to (Grover *et al.* [43]) for $a/h = \{10, 20, 50, 100\}$ except for transverse shear stresses $\bar{\tau}_{23}$ and $\bar{\tau}_{13}$. The dimensionless deflection, axial stresses ($\bar{\sigma}_{11}$, $\bar{\sigma}_{22}$), in-plane shear stress ($\bar{\tau}_{12}$) and transverse shear stress

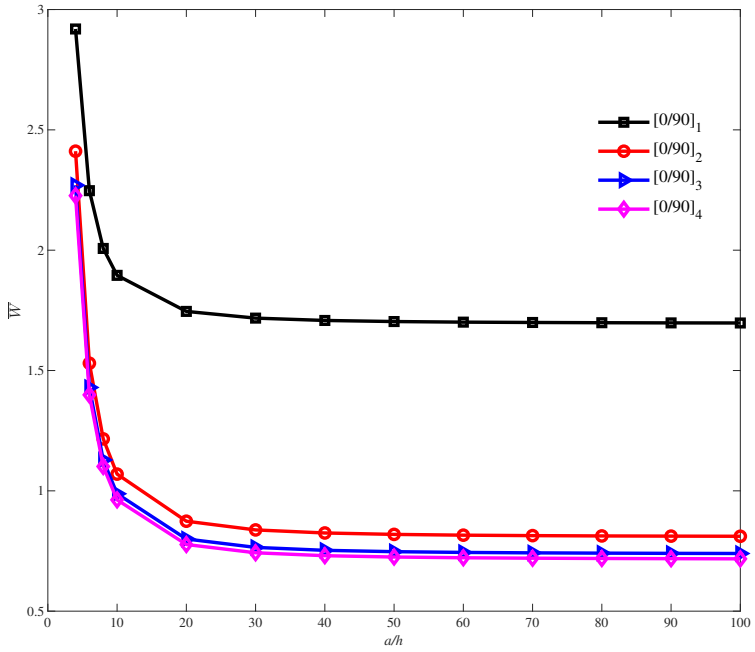

Figure 4.4: Effect of side-thickness ratio on non-dimensional deflection of cross-ply $[0/90]_n$ square laminate.

($\bar{\tau}_{23}$) decrease as a/h ratio increase. However, transverse shear stress ($\bar{\tau}_{13}$) increase with increase in a/h ratio.

4.1.2 Bending Analysis of Angle-ply Laminated Plates

The static bending behavior of laminated angle-ply plates is examined in this study. The SS2 boundary conditions and the material properties MP2 are taken here. The mathematical system of equations for angle-ply plate in the matrix form Eq. (4.6) is solved for components in vector $\{\triangle\}$.

$$\left[\bar{\mathbb{K}}^{\mathbb{A}}\right]\{\triangle\} = \{\bar{q}\} \tag{4.6}$$

Thus, the displacement components and the rotations are then obtained.

In this section, firstly the two and six layered angle-ply plates with different alignment of fiber orientation are considered for analysis. The orientations of fiber are taken as 5, 30 and 45 degree. The flexural behavior of the square anti-symmetric laminated plates is obtained in terms of maximum transverse deflection and non-dimensionality form is given in Eq. (4.5). The results given in Table 4.3 for dimensionless deflection obtained from present theory are compared to those given by using different theories such as IHSDT [157], third order shear

Table 4.2: The deflections and stresses for laminated symmetric [0/90/0] plate subjected to SSL

a/h	Theory	$\overline{W}$	$\bar{\sigma}_{11}$	$\bar{\sigma}_{22}$	$\bar{\tau}_{12}$	$\bar{\tau}_{23}$	$\bar{\tau}_{13}$
4	Pagano and Hatfield [10]	2.006	0.755	0.556	0.0505	0.217	0.282
	Present	1.9490	0.8127	0.5000	0.0532	0.2000	0.2415
	Mantari *et al.* [69]	1.9434	0.823	0.497	0.0536	0.201	0.245
	Grover *et al.* [43]	1.955	0.8079	0.5015	0.0532	0.2019	0.2438
	Karama *et al.* [165]	1.944	0.775	0.502	0.0516	0.191	0.22
	Reddy [28]	1.9218	0.734	-	-	0.183	-
10	Pagano and Hatfield [10]	0.7405	0.59	0.288	0.0289	0.123	0.357
	Present	0.7322	0.5856	0.2755	0.0275	0.1139	0.3068
	Mantari *et al.* [69]	0.7342	0.588	0.276	0.0288	0.115	0.314
	Grover *et al.* [43]	0.7329	0.5845	0.2757	0.0286	0.1148	0.3091
	Karama *et al.* [165]	0.723	0.576	0.272	0.0281	0.108	0.272
	Reddy [28]	0.7125	0.568	-	-	0.103	-
20	Pagano and Hatfield [10]	-	0.552	0.21	0.0234	0.094	0.385
	Present	0.5100	0.5506	0.2065	0.0233	0.0897	0.3228
	Mantari *et al.* [69]	0.5113	0.551	0.206	0.0233	0.09	0.331
	Grover *et al.* [43]	0.5102	0.5503	0.2065	0.0233	0.0903	0.3252
	Karama *et al.* [165]	0.508	0.548	0.205	0.0231	0.086	0.285
50	Pagano and Hatfield [10]	-	0.541	0.185	0.0216	0.084	0.393
	Present	0.4440	0.5406	0.1840	0.0216	0.0819	0.3278
	Mantari *et al.* [69]	0.445	0.541	0.184	0.0217	0.082	0.336
	Grover *et al.* [43]	0.4441	0.5406	0.184	0.0216	0.0825	0.3302
	Karama *et al.* [165]	0.435	0.538	0.27	0.021	0.118	0.324
100	Pagano and Hatfield [10]	-	0.539	0.181	0.0213	0.083	0.395
	Present	0.4344	0.5392	0.1807	0.0214	0.0807	0.3285
	Mantari *et al.* [69]	0.4353	0.539	0.181	0.0214	0.081	0.337
	Grover *et al.* [43]	0.4344	0.5392	0.1807	0.0214	0.0813	0.3309
	Karama *et al.* [165]	0.435	0.538	0.18	0.0213	0.78	0.289
	Reddy [28]	0.4342	0.539	-	-	0.075	-

deformation theory (TSDT) [172] and FSDT [172]. It is evident that this theory is more accurate in predicting the non-dimensional deflections for angle-ply plates ($a/h = 4, 10, 20$)

than other theories presented in Table 4.3. The good agreement of results are found with results due to Joshan *et al.* [157] for thin plates $(a/h = 50, 100)$. Further, it is observed that the deflection corresponding to any particular alignment of fiber-orientation decreases with increase in number of layers from two to six.

Further, a four layered [45/-45/45/-45] square anti-symmetric angle-ply composite plate subjected to transverse sinusoidal loading is considered. The material properties set is used as MP3. The dimensionless maximum deflection $\overline{W}$, in-plane stresses $\bar{\sigma}_{11}$, $\bar{\sigma}_{22}$ and $\bar{\sigma}_{12}$ are evaluated for different value of side-thickness ratios and are presented in Table 4.4 along with other existing results given by Swaminathan and Ragounadin [162]. It is evident that, the deflections and stresses obtained from proposed theory are well agreed with higher order refined theory due to Swaminathan and Ragounadin [162] for $(a/h = 10, 100)$. Moreover, for thick plates $(a/h = 4)$, considerable difference is found with available results.

Fig. 4.5 depicts the dimensionless deflection of two [45/-45] and four layered $[45/\text{-}45]_2$ degree angle-ply square and rectangular $(b/a = 2)$ plates corresponding to various a/h ratios. The material properties MP1 are used for analysis. The results indicate that the plate with two layers has a greater deflection compared to the four-layered plate. Also, it can be seen that for square plate, the dimensionless deflection is significantly lower as compared to the rectangular plate.

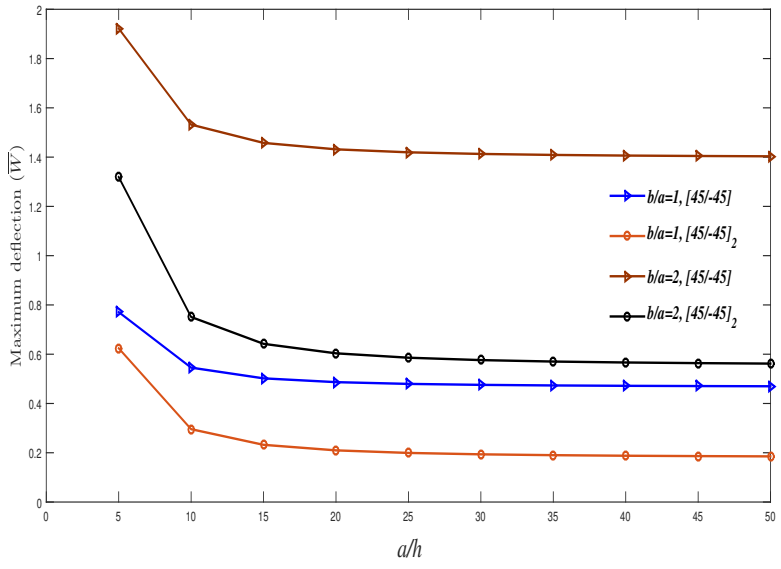

Figure 4.5: The non-dimensional deflection of multi-layered square and rectangular anti-symmetric plate corresponding to span thickness ratios subjected to SSL.

Table 4.3: The deflection for multi-layered angle-ply plates under SSL with respect to different a/h ratios (MP2).

a/h	Theory	$[5/-5]$	$[5/-5]_3$	$[30/-30]$	$[30/-30]_3$	$[45/-45]$	$[45/-45]_3$
4	Present	1.1926	1.1663	0.9945	0.8417	0.9303	0.7935
	Joshan *et al.* [157]	1.1955	1.1689	0.9968	0.843	0.9326	0.7948
	Reddy (TSDT) [172]	1.2625	1.2282	1.0838	0.8851	1.0203	0.8375
	Reddy (FSDT) [172]	1.3675	1.2647	1.2155	0.8994	1.1576	0.8531
10	Present	0.478	0.4431	0.5791	0.2977	0.5455	0.2717
	Joshan *et al.* [157]	0.4783	0.4434	0.5794	0.2978	0.5457	0.2718
	Reddy (TSDT) [172]	0.4848	0.4485	0.5916	0.3007	0.5587	0.2745
	Reddy (FSDT) [172]	0.4883	0.4491	0.6099	0.2989	0.5773	0.2728
20	Present	0.3564	0.3197	0.5149	0.2121	0.4866	0.1899
	Joshan *et al.* [157]	0.3565	0.3198	0.515	0.2121	0.4866	0.1899
	Reddy (TSDT) [172]	0.3579	0.3209	0.518	0.2127	0.4897	0.1905
	Reddy (FSDT) [172]	0.3586	0.3208	0.5221	0.2121	0.4914	0.1899
50	Present	0.3212	0.284	0.4967	0.1877	0.4699	0.1667
	Joshan *et al.* [157]	0.3212	0.284	0.4967	0.1877	0.4699	0.1667
	Reddy (TSDT) [172]	0.3215	0.2842	0.4972	0.1878	0.4704	0.1608
	Reddy (FSDT) [172]	0.3216	0.284	0.4979	0.1877	0.4712	0.1667
100	Present	0.3162	0.2788	0.4941	0.1842	0.4675	0.1633
	Joshan *et al.* [157]	0.3162	0.2788	0.4941	0.1842	0.4675	0.1638
	Reddy (TSDT) [172]	0.3162	0.2789	0.4912	0.1842	0.4676	0.1634
	Reddy (FSDT) [172]	0.3162	0.2789	0.4914	0.1842	0.4678	0.1638

Table 4.4: The non-dimensional deflection and stresses of four layered [45/-45/45/-45] angle-ply plates under the sinusoidal loading (MP3).

a/h	Theory	$\overline{W}(\frac{a}{2}, \frac{b}{2})$	$\bar{\sigma}_{11}(\frac{a}{2}, \frac{b}{2}, \frac{h}{2})$	$\bar{\sigma}_{22}(\frac{a}{2}, \frac{b}{2}, \frac{h}{2})$	$\bar{\sigma}_{12}(0, 0, \frac{h}{2})$
4	Present	1.9838	0.1885	0.1885	-0.1535
	Ref. [162]	2.0392	0.1945	0.1945	-0.1468
10	Present	1.2958	0.1670	0.1670	-0.1359
	Ref. [162]	1.3040	0.1681	0.1681	-0.1348
100	Present	1.1638	0.1628	0.1628	-0.1326
	Ref. [162]	1.1638	0.1628	0.1628	-0.1325

4.1.3 Buckling Analysis of Laminates

In this section, a simply supported symmetric cross-ply multi-layered [0/90/0], [0/90/90/0], [0/90/0/90/0], [0/90/0/90/0/90/0/90/0] square plates are considered and stability analysis is performed under in-plane uni-axial compressive load. The non-dimensional form of buckling load parameter is defined as $\bar{N}_{cr}= \lambda a^2/(E_2 h^3)$. A comparison between the results obtained for non-dimensional buckling load parameter using the various theories given by authors [43] [173], [174], [175] and exact elasticity solutions [176] are shown in Table 4.5. Effect of anisotropy is observed for various types of laminates with constant side-thickness ratio (a/h=10) and the material properties MP2 are used with $\frac{E_1}{E_2}$ as a variable. The obtained results indicate that the proposed HSDT is appropriate in predicting the buckling loads when compared to Putcha and Reddy [173]. Further, it is visible from Table 4.5 that the value of buckling load parameter increases with increase in value of modulus ratio $\frac{E_1}{E_2}$. Moreover, the impact of span thickness ratio on uni and bi-axial buckling load is shown in Fig. 4.6 and Fig. 4.7, respectively for anti-symmetric $(0/90)_n$ square laminated plates. It is observed that the value of critical buckling load parameter is large for higher values of a/h for both axial compressive loads. Also, as the number of layers vary from 2 to 4, the critical buckling experience a significant increment and for a number of layers greater than four, the value of buckling loads comes closer to each other. Moreover, the critical buckling load value corresponding to uni-axial loading is double than that of bi-axial compressive force for any value of a/h.

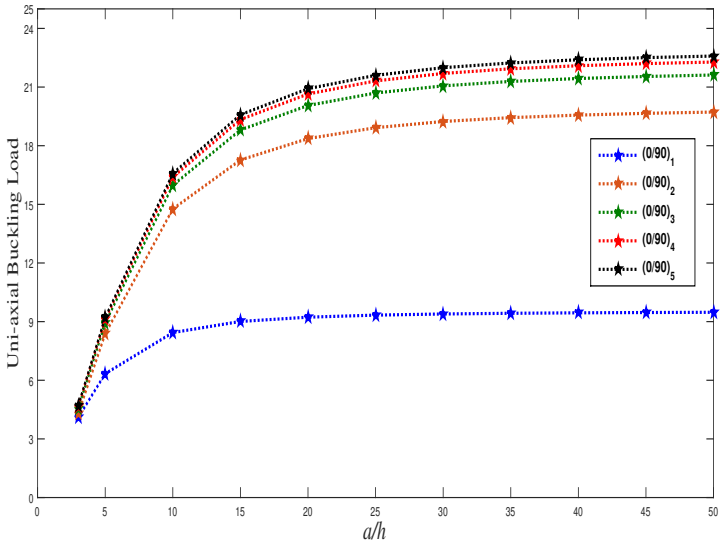

Figure 4.6: Plot of uni-axial buckling load parameter with span thickness ratios for antisymmetric $(0/90)_n$ cross-ply laminated plate.

In Table 4.6, the numerical values of dimensionless buckling load for a two-layer [30/-

Table 4.5: Uniaxial buckling load parameter of symmetric laminated plates ($a/h = 10$).

N	Theory	$\frac{E1}{E2}$				
		3	10	20	30	40
3	Present	5.3955	9.8525	14.9473	18.9854	22.2859
	Grover *et al.* [43]	5.3949	9.8503	14.9415	18.975	22.27
	Putcha and Reddy [173]	5.3933	9.9406	15.298	19.6741	23.34
	Ferreira *et al.* [174]	5.3872	9.8331	14.8975	18.8942	22.1513
	Noor [176]	5.3044	9.7621	15.0191	19.304	22.8807
4	Present	5.4006	9.9757	15.3981	19.8494	23.5916
	Grover *et al.* [43]	5.4002	9.974	15.3936	19.8413	23.579
	Putcha and Reddy [173]	5.114	9.965	15.298	19.6744	23.34
	Liu *et al.* [175]	5.412	10.013	15.309	19.778	23.412
5	Present	5.4167	10.1409	15.9328	20.8337	25.0452
	Grover *et al.* [43]	5.4163	10.139	15.9287	20.8263	25.0344
	Putcha and Reddy [173]	5.4096	10.15	16.008	20.999	25.308
	Ferreira *et al.* [174]	5.4041	10.089	15.7913	20.5914	24.6901
	Noor [176]	5.3255	9.9603	15.6527	20.4663	24.5929
9	Present	5.4207	10.2125	16.1965	21.3510	25.8442
	Grover *et al.* [43]	5.4202	10.21	16.1911	21.3413	25.8298
	Putcha and Reddy [173]	5.4313	10.197	16.172	21.315	25.79
	Ferreira *et al.* [174]	5.4092	10.1767	16.1063	21.1918	25.6088

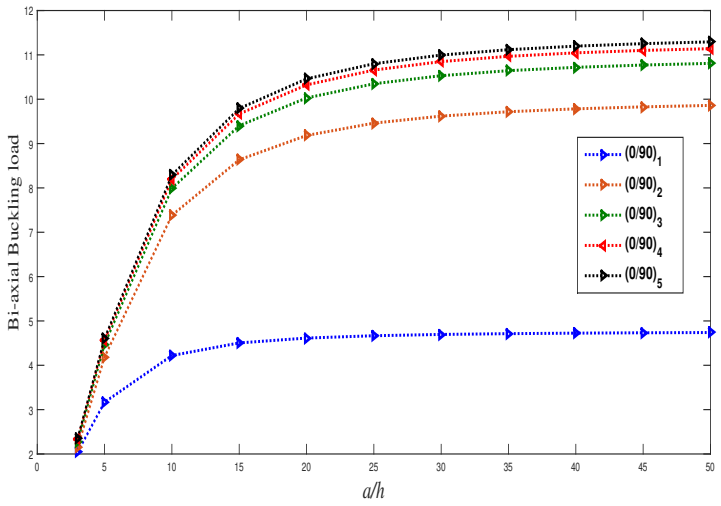

Figure 4.7: Variation of bi-axial buckling loads versus a/h ratio for antisymmetric $(0/90)_n$ cross-ply square laminates.

30] degree and [45/-45] degree angle-ply square laminate subjected to uni-axial loading is presented. The following material properties are used, $E_1 = 40E_2$, $G_{12} = G_{13} = 0.5E_2$, $G_{23} = 0.6E_2$, $\nu_{12} = 0.25$. The present results are compared with the published results reported in Table 4.6. It is seen that, when the angle of fiber is equal to 30° and $a/h = 4$, the percentage error between the buckling load values predicted by present theory and Adim *et al.* [87] is 4.34 %. The percentage error decreases with increase in value of a/h and for thin plate ($a/h = 100$), the current results are agreed upon with those reported by Adim *et al.* [87], Ren [177], and Reddy [172]. Further, the buckling parameter value grows with increment in a/h ratio for any fiber orientation. Fig. 4.8 shows the influence of modulus ratio on the uni-axial buckling stress of a simply supported two-layer [30/-30] and [45/-45] degree square laminate for ($a/h = 4$, 10). The material properties MP2 are used. It can be observed from figure that as modulus ratio increases the corresponding buckling load parameters increase monotonically. Moreover, the value of uni-axial buckling load is higher for fiber orientation θ=45° as compared to θ=30° for any value of a/h. The variation of dimensionless buckling loads with respect to various load index (K_m) are presented in Fig.(4.9) for four layer [0/90/90/0] laminated square plate. The results are graphed for different values of a/h = (4, 10, 20, 50) and material properties MP1 are used. The load index (K_m=0) indicates the uni-axial loading whereas (K_m=1) corresponds to bi-axial compressive force. It is seen that the values of critical buckling load decrease gradually with increase in load index. Also, it is observed from Fig.(4.9) that the thick plate ($a/h = 4$) possess smallest buckling load parameter value relative to thin plate (a/h = 10, 20, 50) plates.

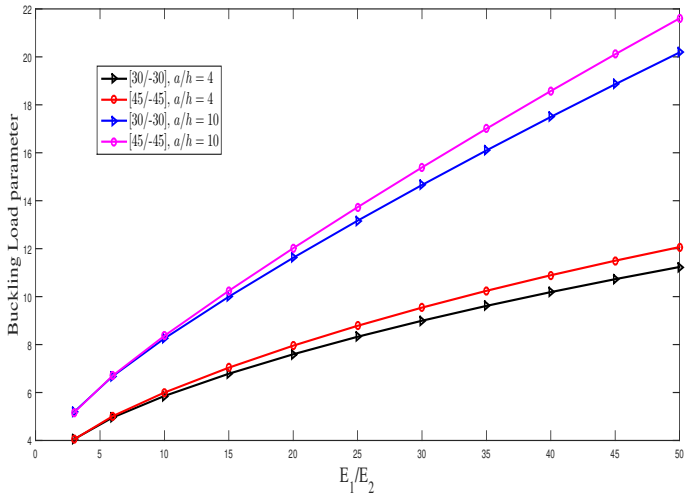

Figure 4.8: Variation of uni-axial buckling load with respect to modulus ratio of antisymmetric two layer angle-ply square plate.

Table 4.6: Buckling load parameter of two-layer (θ/-θ) angle-ply laminates under uni-axial loading.

$\frac{a}{h}$	Theory	Buckling Load	
		θ= 30°	θ= 45°
4	Present	9.9844	10.8912
	Adim *et al.* [87]	9.5688	9.9302
	Ren [177]	9.5368	9.8200
	Reddy [172]	9.3391	8.2377
10	Present	17.3089	18.5749
	Adim *et al.* [87]	17.2795	18.1544
	Ren [177]	15.7517	16.4558
	Reddy [172]	17.1269	18.1544
100	Present	20.4030	21.6719
	Adim *et al.* [87]	20.5020	21.6663
	Ren [177]	20.4793	21.6384
	Reddy [172]	20.5017	21.6663

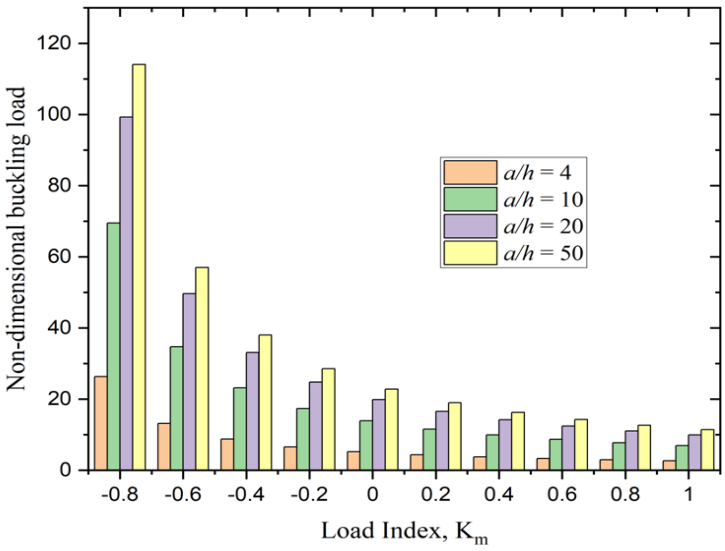

Figure 4.9: The impact of load index values on critical buckling load of cross-ply laminate.

4.2 Conclusions

In this chapter, a new secant hyperbolic shear deformation theory in axiomatic framework is developed for mechanical analysis of laminated composite plates. The closed form solution

are presented to predict structural responses of the cross-ply and angle-ply simply supported plates. The theory accounts for a non-linear variation of transverse strains through thickness and does not require shear correction factors to meet the stress free conditions on the plate surfaces. Distinct solutions for cross- and angle-ply plates are obtained due to differing stiffness characteristics. The deflections and stresses are evaluated for plates subjected to in-plane transverse load (SSL and UDL). The dimensionless buckling load parameters for uni-axial and bi-axial force are found by solving an eigenvalue problem. The accuracy of results due to proposed theory is determined by comparing it with existing solutions of 3D elasticity theory and other higher order plate theories. The effects of different parameters such as aspect ratio, fiber-orientation, span thickness ratio, etc. on the static and buckling response of plate are examined. The following conclusions are drawn on the basis of present theory results.

- The present theory findings for the bending and buckling response of laminated cross-ply and angle-ply plate are well agreed with the published results.
- It is concluded that as aspect ratio (b/a) of cross-ply plate increases, the corresponding deflection also increase. Moreover, the non-dimensional displacement decreases with increment in side-thickness ratio, which conclude that thick plate possesses higher non-dimensional deflection.
- The maximum transverse deflection of anti-symmetric square plate reduces with increase in number of layers.
- For anti-symmetric angle-ply composite plates subjected to SSL, the dimensionless deflection values obtained using present theory are quite accurate as compared to the other existing theories found in the literature.
- Four layered [45/-45/45/-45] angle-ply composite rectangular laminate acquired more deflection than corresponding square plate.
- It is also concluded that multi-layered anti-symmetric plate possess a higher critical buckling load when subjected to uni-axial force as compared to bi-axial force for any side-thickness ratio and fiber-orientation.
- The effect of load index values on critical buckling is also investigated. It is noticed that as load index vary from -0.8 to 1 monotonically, the value of corresponding buckling parameter reduces gradually.
- The newly proposed theory can be taken as benchmark to further study the structural behavior of multi-layered composite structures.

Chapter 5

Mechanical Analysis of Functionally Graded Porous Plates

Functionally graded material (FGM) possess the spatial variation of the properties within one or more specific directions of the material. These materials have seen wide utility in various systems during the last few years due to properties such as specific strength, lightweights, and corrosion resistance etc. This facilitates their utilisation in fundamental structural components as well as in special-purpose applications across various industries such as aerospace industry, electrical devices, optics, and others. [178]. In order to describe the variation of properties in FGMs and structures mathematical laws such as exponential law [179], sigmoid law [180], and power-law [158] are used. The manufacturing process used for the fabrication of FGM causes the porosity within the material [6, 181]. The influence of porosities on the effective material properties of functionally graded materials is significant, since it also affects the macroscopic response of FG structures, including beams, plates, and shells. So it is crucial to incorporate the porosities in order to accurately model the effective material properties and hence predict the response.

In the open literature, some studies about the effect of porosity in the FGM structures have been published. Magnucki and Stasiewicz [182] considered the isotropic porous beams of rectangular cross-section and examined the elastic buckling assuming the degree of porosity varying in the transverse direction, attaining its maximum value at the beam axis. The buckling and bending analysis of FG beam were examined by Chen et al. [183] wherein they considered the Timoshenko beam. Chen et al. [184] carried out the nonlinear free vibration response of a sandwich beam in which they considered a functionally graded porous core. The porous isotropic circular plates were examined by Jabbar et al. [185] and Mojahedin *et al.* [186]. Yu *et al.* [187] calculated the numerical results of thermal buckling for FG plates with internal defects. Mouaici *et al.* [155] carried out the vibration analysis of porous non-homogeneous plates using hyperbolic shear deformation theory. Rezaei *et al.* [159] investigated the natural frequencies of porous FG plates with even and uneven porosity distribution and employed four-variable FSDT for deformation characteristics. Wang *et al.* [188] studied the vibration response of longitudinally traveling FGM plates with evenly and unevenly dis-

The content of this chapter has been published in Journal, Structures, 34: 1458-1474, Elsevier, 2021.

tributed porosities. Kamranfard *et al.* [189] presented the vibration and buckling responses of annular sector porous plates under in-plane compressive force. Demirhan and Taskin [190] performed the bending and free vibration analysis of porous FG plate using the state space approach. They considered even and uneven distributions of porosity and modeled the FGM using the power law. Based on modified FSDT Theory, Trabelsi *et al.* [191] studied the thermal buckling and post-buckling analysis [192] of functionally graded plates and cylindrical shells. The proposed theory assumes the parabolic distribution of the transverse shear deformation across the shell thickness, and the displacement field is approximated by using Four node finite elements. Guellil *et al.* [193] examined the influence of porosity distributions on the static response of FG plates that are supported by a Pasternak foundation based on HSDT. The structural analysis such as static, free vibration, and dynamic analysis have been carried out for the porous plates in the existing literature ([194–202]). The FGM plates are generally modelled in two-dimensional framework under the hypothesis of classical plate theory CPT ([203–206]), FSDT ([207–209]), and HSDT ([4,210–216]). Moreover, various studies have been carried out considering porosities into account ([217–219]). The extensive reviews on the modeling and analysis of FGM plates and beams have been carried out ([220–223])

It is evident from the above literature review and to the best of authors' knowledge, there is no published research examining the impact of porosity distributions on the bending and buckling behaviors of porous FG plates with five different porosity distributions using the IHSDT. In the present work, the IHSDT that contains an inverse hyperbolic shear strain function is employed to model the porous FG plate. The responses for static and buckling analysis are investigated using an analytical approach following Navier's method. Five different types of porosity distributions are considered for analysis. The effects of various parameters such as side-thickness ratio, power index, porosity content, and aspect ratio on the non-dimensional deflections, stresses, uni-axial and bi-axial buckling loads of porous FG plate are evaluated. For static analysis the uniform and sinusoidal distributed transverse loads are considered. To show the applicability and accuracy of this approach, the obtained results are validated with the existing literature and are found to agree well. On the basis of presented results, various conclusions are drawn.

5.1 Modeling of Porous Functionally Graded Plate

In this section, the porous FG plates are modeled mathematically in the framework of inverse hyperbolic shear deformation theory. The plate under consideration is a rectangular FG plate that contains porosities wherein The material properties vary according to a power-law gradient [158] while five different types of porosity distributions are considered. The

considered porosity distributions are even, uneven, symmetrical center enhanced (SCE), bottom enhanced (BE), and top enhanced (TE). The geometry of porous FG plate is depicted in Fig. (5.1). The material property of FG plate for even and uneven porosity distributions are expressed as [159].

Even Distribution:

$$E(x_3) = \left[E_b + (E_t - E_b)\left(\frac{2x_3 + h}{2h}\right)^k\right] - \frac{e}{2}(E_t + E_b) \tag{5.1}$$

Uneven Distribution:

$$E(x_3) = \left[E_b + (E_t - E_b)\left(\frac{2x_3 + h}{2h}\right)^k\right] - \frac{e}{2}(E_t + E_b)\left(1 - \frac{2|x_3|}{h}\right) \tag{5.2}$$

The Young's modulus of porous FG plate for other three distributions is given as follows [196]:

$$E(x_3) = \left[E_b + (E_t - E_b)\left(\frac{2x_3 + h}{2h}\right)^k\right](1 - \Phi(x_3)) \tag{5.3}$$

The E_b and E_t are value of material properties at bottom and top surfaces of plate, respectively. The function $\Phi(x_3)$ represents the distribution of porosity, and it is dependent on both the thickness coordinate and the porosity parameter (e). These functions are listed in Table (5.1).

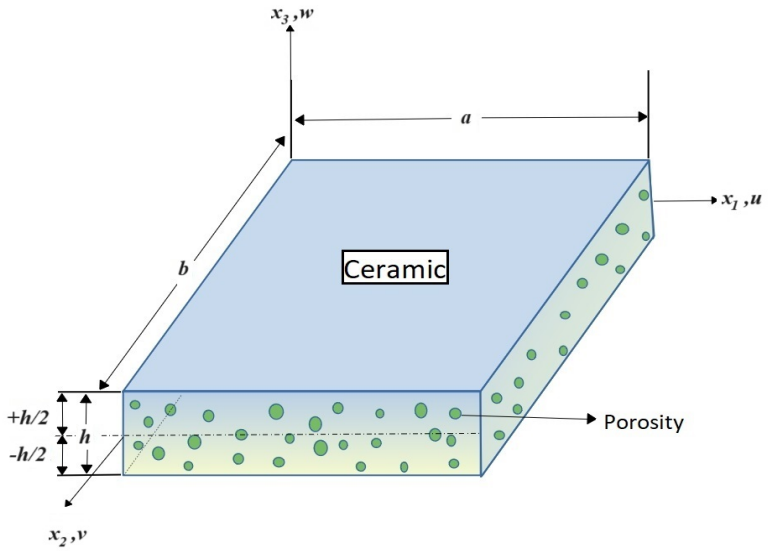

Figure 5.1: FG porous plate

Table 5.1: Porosity distribution functions

Types of Porosity Distribution	$\Phi(x_3)$(Porosity Distribution Function)
Symmetrical Center Enhanced (SCE) Distribution	$e\ \cos(\frac{\pi x_3}{h})$
Bottom Enhanced (BE) Distribution	$e\ \cos\left(\frac{\pi}{2}\left(\frac{x_3}{h}+0.5\right)\right)$
Top Enhanced (TE) Distribution	$e\ \cos\left(\frac{\pi}{2}\left(\frac{x_3}{h}-0.5\right)\right)$

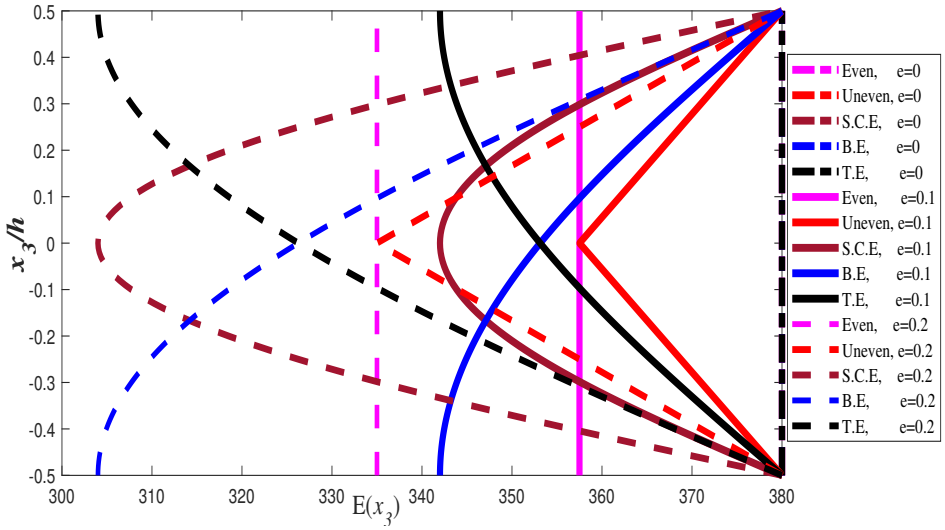

Figure 5.2: Variation of elastic modulus of plate across the thickness

In Fig.(5.2) Young's modulus of porous FG plate with different porosity distributions for power-law index k=0 and for different parameters (e=0, 0.1, 0.2) is plotted against x_3/h (-h/2 to h/2). It can be observed that when both k and e are equal to zero, the Young's modulus exhibits uniformity across all five porosity distributions. At the center of the FG plate, the value of elasticity modulus for e=0.1 and e=0.2 remains same for both even and uneven distributions. It is noted that the elasticity modulus of FG plate for even porosity distribution is constant, whereas for uneven distribution, it shows a linear and symmetric trend. Further, the variation of elasticity modulus (E(x_3)) for SCE porosity distribution is symmetric and parabolic, and with the increment in porosity parameter from e=0.1 to 0.2, the value of E(x_3) tends to decreases for all porosity distributions. This is due to the fact that a higher value of porosity parameter decreases the stiffness of the plate.

Fig.(5.3) shows the distribution of elasticity modulus of plate for the volume fraction index (k=0.1) and porosity indices (e=0, 0.1 ,0.2) with five porosity distribution functions. The figure demonstrates that when the values of k and e are set to 0.1 and 0 respectively,

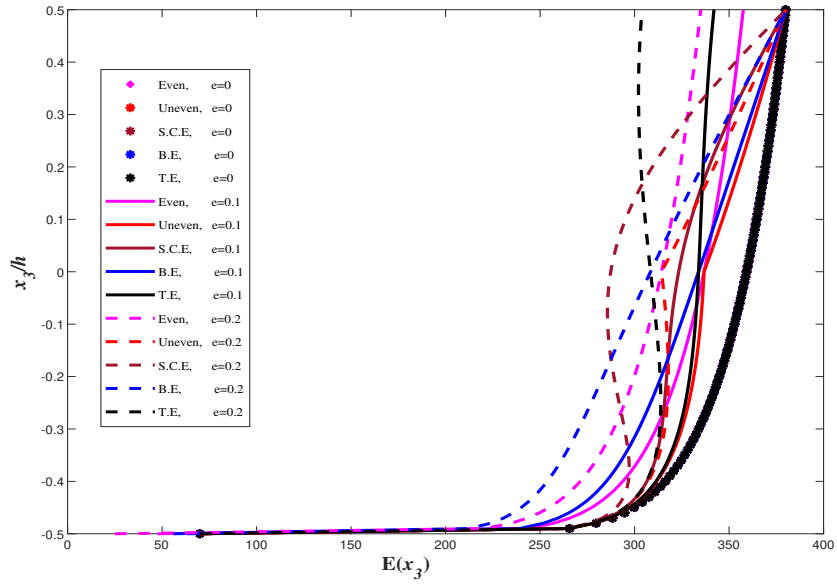

Figure 5.3: Young's modulus of plate for k=0.1 with different porosity distribution

the elasticity modulus remains same throughout all five porosity distributions. The value of elasticity modulus decreases as parameter e increases from 0.1 to 0.2. The analytical solution is obtained to solve these equations under the assumption of simply supported boundary conditions.

5.2 Results and Discussion

In this section, the displacement field model of inverse hyperbolic theory given in (3.1) of Chapter 3 is employed to derive the governing equations. The Navier's methodology is implemented to solve these equations and system of algebraic equations (5.2) is then formed to yield the the structural response of of FG plate.

$$\left[\bar{K} - N_0 G\right] \{\triangle\} = \{\bar{q}\} \tag{5.4}$$

Moreover, this section presents the results for static and buckling response of functionally graded non-porous and porous plates. The FG plates are constituted of metallic phase and ceramic phase, where the metallic phase is Aluminum while the ceramic phase is Alumina. The plate is assumed to be ceramic rich at the top surface and the FG material follows the power law. The material properties of Aluminum-Alumina FG material are listed in Table (5.2). The porosity distributions considered are even, uneven, symmetric center enhanced,

bottom enhanced, and top enhanced. The effect of porosity distribution and the extent of porosity is examined on the bending and stability behavior of FG plates. Also, the impact of span-thickness ratio, aspect ratio, power-law index, and loading conditions is investigated.

Table 5.2: Material properties of top and bottom

	Bottom (Aluminum)	Top (Alumina)
Elastic modulus	$E_b = 70GPa$	$E_t = 380GPa$
Poisson ratio	v_b=0.3	v_t=0.3

5.2.1 Static Analysis

The results for static analysis of FG porous plates are presented in this section. The plate under consideration is subjected to a transverse load. All others loading terms are zero. Therefore, the mathematical system given in Eq. (5.2) reduces to the following form.

$$\left[\bar{K}\right]\{\triangle\} = \{\bar{q}\} \tag{5.5}$$

The above system is solved via matrix inversion method for constant coefficients. These constants are then substituted in the assumed solution (3.20) to find the mid-plane field variables. The strain-displacement and the constitutive relations are employed to obtain the stresses at critical points. The transverse load is considered as sinusoidal load (SSL) and uniformly distributed load (UDL). The static response is evaluated in terms of transverse deflection and stresses. The dimensionless results for deflections and stresses are obtained and the following non-dimensional forms are used.

$\bar{W}= \frac{10h^3E_t}{\bar{q}_0a^4}\ \bar{w}(\frac{a}{2},\frac{b}{2},\frac{h}{2}), \quad \bar{\sigma}_{11}= \frac{h}{\bar{q}_0a}\sigma_{11}(\frac{a}{2},\frac{b}{2},\frac{h}{2}), \quad \bar{\tau}_{13}= \frac{h}{\bar{q}_0a}\tau_{13}(0,\frac{b}{2},0)$

The numerical results of the non-dimensional deflections of nonporous and porous FG plates subjected to UDL are tabulated in Table (5.3) for a variety of span-thickness ratio ($a/h = 5, 10, 20$), power law index ($k = 0, 0.1, 0.5, 1$), porosity parameter ($e = 0, 0.2, 0.4$), and porosity distributions. It is noted that the materials properties are negative for the even type porosity distribution for the value of e greater than 0.32. Therefore, the results correspondence to e=0.4 for even type distribution are not reported in the present work. The non-dimensional deflections obtained through the use of IHSDT are being compared to the previously reported results in existing literature based on four variable refined plate

theory given by Demirhan and Taskin [190]. The comparison is being conducted for both even and uneven distributions of porosity. The results of IHSDT are also compared with newly developed theory in chapter 4 for all porosity distributions in tables (5.3) and (5.4). This is observed that, present results show good agreement with the results obtained due to Demirhan and Taskin [190] and also with theory proposed in [168]. for all the values of a/h ratio and power law index. The deflections corresponding to $e = 0$ indicate the responses of non-porous FG plate. From the tabulated results, it is noted that the non-dimensional deflection increases as the value of porosity parameter increase for any value of a/h and k. This is accounted towards the fact that the increase in porosity parameter value reduces stiffness of the plate, therefore increasing the deflection. Additionally, when the span-thickness ratio increases, the deflection of plate reduces consistently for all porosity distributions. The effect of variation in the porosity distribution on the non-dimensional deflection reveals that the response of porous plate depends not only on the type of distribution but also on the span-thickness ratio. For isotropic plate (k=0), the plate with uneven porosity distribution possesses the lowest bending deflection. In contrast, the plate with bottom or top enhanced distribution possesses the highest non-dimensional deflection. However, for FG plates ($k \neq 0$), it is seen that the plate exhibiting an uneven distribution of porosity has the least non-dimensional deflection, whereas the plate with a even porosity distribution experiences the maximum deflection.

Further, the normal ($\bar{\sigma}_{11}$) and transverse shear stresses ($\bar{\tau}_{13}$) are evaluated for the porous FG plates subjected to UDL. The distribution of these stresses across the thickness of the plate is obtained and is depicted in Figures 5.4 to 5.8. Fig. (5.4) and Fig. (5.5) shows the dimensionless normal and shear stress for different values of the power-law index and porosity parameter. In Fig. (5.4), the even porosity and Fig. (5.5), the uneven porosity type is considered. For $k = 0$, the distribution of non-dimensional normal stress is linear in nature and symmetric as shown in Fig. (5.4) and Fig. (5.5). As the value of k increases, the stress distribution becomes non-linear and non-symmetric. This is due to the reason that there is a change in material properties of plate with an increase in power-law index values ($k > 0$). Moreover, it can be observed from the data that the largest value of the normal stress occurs at the top of the plate. It is observed that for a particular value of k, with an increase in porosity parameter (e), the maximum normal stresses of porous FG plate increases for both types of porosity distributions. Moreover, for the isotropic plate ($k = 0$), the shear stress is maximum at the center of the plate, and for higher values of k, the maximum shear stress shifts to the upper surface.

In Figures 5.6 to 5.8, the non-dimensional stresses are presented for FG porous plate subjected to UDL for various power-law index values and porosity parameters with SCE, BE,

Table 5.3: The non-dimensional deflection of FG plate subjected to uniform distributed load

a/h	k	e	Even Present(IHSDT)	Even Present(New)	Even Demirhan *et al.* [190]	Uneven Present(IHSDT)	Uneven Present(New)	Uneven Demirhan *et al.* [190]
5	0	0	0.533	0.5329	0.5352	0.533	0.5329	0.5352
		0.2	0.6046	0.6045	0.60706	0.5545	0.5544	0.58052
		0.4	–	–	0.70111	0.5785	0.5785	0.63466
	0.1	0	0.5881	0.5879	0.58992	0.5881	0.5879	0.58992
		0.2	0.6769	0.6768	1.57969	0.6141	0.6139	0.64981
		0.4	–	–	0.80066	0.6433	0.6431	0.71393
	0.5	0	0.8053	0.8052	0.8083	0.8053	0.8052	0.8083
		0.2	0.9968	0.9966	0.98705	0.8578	0.8576	0.92411
		0.4	–	–	1.3267	0.9201	0.9198	1.08409
	1	0	1.0410	1.0408	1.04469	1.041	1.0408	1.04469
		0.2	1.4328	1.4325	1.43735	1.1424	1.1421	1.27236
		0.4	–	–	2.47062	1.2748	1.2744	1.66012
10	0	0	0.4660	0.4660	0.46655	0.4660	0.4660	0.46655
		0.2	0.5286	0.5286	0.52922	0.4816	0.4815	0.5045
		0.4	–	–	0.61134	0.4984	0.4983	0.54923
	0.1	0	0.5162	0.5162	0.51714	0.5162	0.5162	0.51714
		0.2	0.5946	0.5946	0.59566	0.5354	0.5354	0.56398
		0.4	–	–	0.89806	0.5563	0.5563	0.64537
	0.5	0	0.7147	0.7146	0.71361	0.7147	0.7146	0.71361
		0.2	0.8887	0.8887	0.8895	0.7561	0.7561	0.81751
		0.4	–	–	1.18947	0.8042	0.8042	0.95489
	1	0	0.9279	0.9278	0.92873	0.9279	0.9278	0.92873
		0.2	1.2913	1.2913	1.29241	1.0115	1.0114	1.13392
		0.4	–	–	2.29216	1.119	1.1189	0.8372
20	0	0	0.4492	0.4492	0.44939	0.4492	0.4492	0.44939
		0.2	0.5096	0.5096	0.50971	0.4633	0.4632	0.48543
		0.4	–	–	0.5888	0.4782	0.4782	0.52782
	0.1	0	0.4982	0.4982	0.49834	0.4982	0.4982	0.49834
		0.2	0.574	0.574	0.57412	0.5157	0.5157	0.54338
,		0.4	–	–	0.67728	0.5345	0.5345	1.38928
	0.5	0	0.6919	0.6919	0.69209	0.6919	0.6919	0.69209
		0.2	0.8616	0.8616	0.86177	0.7306	0.7306	0.79069
		0.4	–	–	1.551	0.7751	0.7751	0.92626
	1	0	0.8995	0.8995	0.89968	0.8995	0.8995	0.89968
		0.2	1.2558	1.2558	1.25611	0.9786	0.9786	1.09915
		0.4	–	–	2.24366	1.0799	1.0799	1.44418

and TE porosity distribution. It is noted that non-dimensional normal stress reaches its maximum value when the plate is composed of ceramic material and with higher power law index values, the maximum normal stress is higher. Also, Fig. 5.8 shows that in the case of top enhanced porosity distribution, the maximum normal stress decreases with an increase

Table 5.4: The non-dimensional deflection of FG plate subjected to uniform distributed load

a/h	k	e	SCE Present(IHSDT)	SCE Present (New)	BE Present(IHSDT)	BE Present (New)	TE Present(IHSDT)	TE Present (New)
5	0	0	0.533	0.5329	0.533	0.5329	0.533	0.5329
		0.2	0.5850	0.5848	0.6075	0.6074	0.6075	0.6074
		0.4	0.6519	0.6517	0.7151	0.7149	0.7151	0.7149
	0.1	0	0.5881	0.5879	0.5881	0.5879	0.5881	0.5879
		0.2	0.6462	0.646	0.6703	0.6701	0.6706	0.6704
		0.4	0.7210	0.7208	0.7889	0.7887	0.7894	0.7892
	0.5	0	0.8053	0.8052	0.8053	0.8052	0.8053	0.8052
		0.2	0.8887	0.8885	0.9179	0.9177	0.9195	0.9193
		0.4	0.9969	0.9967	1.080	1.0797	1.083	1.0828
	1	0	1.041	1.0408	1.041	1.0408	1.041	1.0408
		0.2	1.1512	1.151	1.1877	1.1874	1.188	1.1877
		0.4	1.2953	1.2949	1.3986	1.3982	1.3971	1.3968
10	0	0	0.4660	0.4660	0.4660	0.4660	0.466	0.4660
		0.2	0.5050	0.5050	0.5302	0.5302	0.5302	0.5302
		0.4	0.5521	0.5521	0.6236	0.6235	0.6236	0.6235
	0.1	0	0.5162	0.5162	0.5162	0.5162	0.5162	0.5162
		0.2	0.5604	0.5603	0.5875	0.5875	0.5874	0.5874
		0.4	0.6139	0.6139	0.6913	0.6913	0.6907	0.6907
	0.5	0	0.7147	0.7146	0.7147	0.7146	0.7147	0.7146
		0.2	0.7804	0.7804	0.8143	0.8143	0.8138	0.8137
		0.4	0.8617	0.8616	0.9591	0.9591	0.9561	0.9561
	1	0	0.9279	0.9278	0.9279	0.9278	0.9279	0.9278
		0.2	1.0161	1.0161	1.0591	1.0591	1.0552	1.0551
		0.4	1.1267	1.1266	1.2499	1.2498	1.2365	1.2365
20	0	0	0.4492	0.4492	0.4492	0.4492	0.4492	0.4492
		0.2	0.4849	0.4849	0.5108	0.5108	0.5108	0.5108
		0.4	0.527	0.527	0.6006	0.6006	0.6006	0.6006
	0.1	0	0.4982	0.4982	0.4982	0.4982	0.4982	0.4982
		0.2	0.5388	0.5388	0.5668	0.5668	0.5666	0.5665
		0.4	0.5870	0.5870	0.6669	0.6669	0.6659	0.6659
	0.5	0	0.6919	0.6919	0.6919	0.6919	0.6919	0.6919
		0.2	0.7532	0.7532	0.7883	0.7883	0.7872	0.7872
		0.4	0.8277	0.8277	0.9288	0.9288	0.9243	0.9243
	1	0	0.8995	0.8995	0.8995	0.8995	0.8995	0.8995
		0.2	0.9822	0.9822	1.0269	1.0269	1.0219	1.0219
		0.4	1.0844	1.0844	1.2126	1.2126	1.1963	1.1962

in porosity coefficient from e=0.2 to e=0.4.

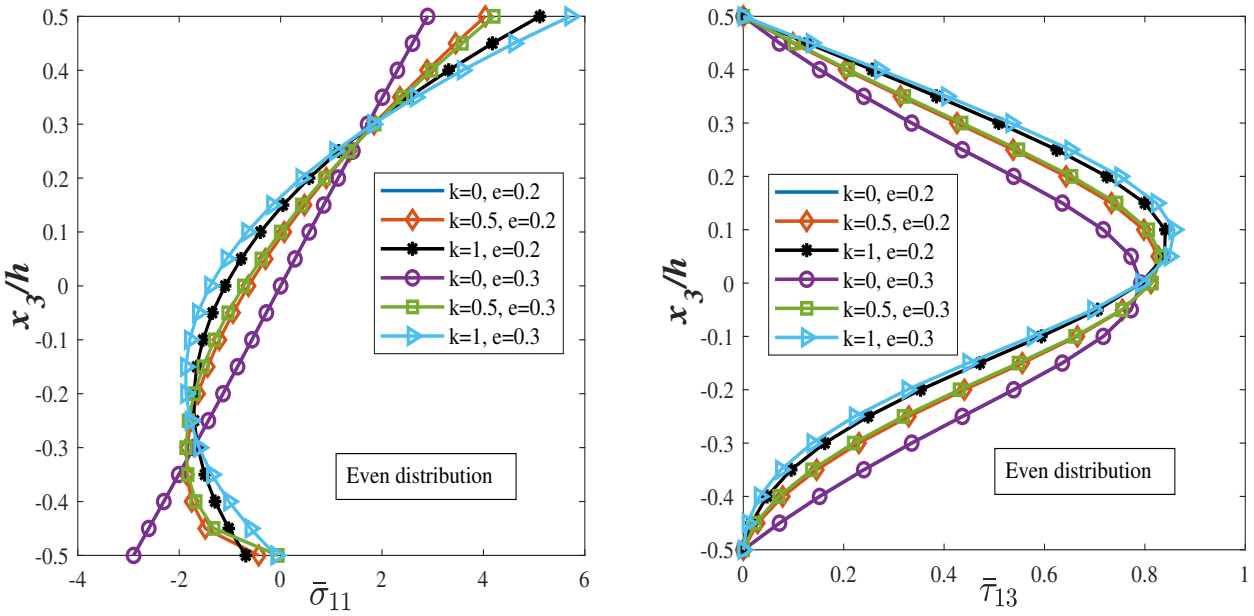

Figure 5.4: The dimensionless normal and shear stress of uniform loaded FG plate

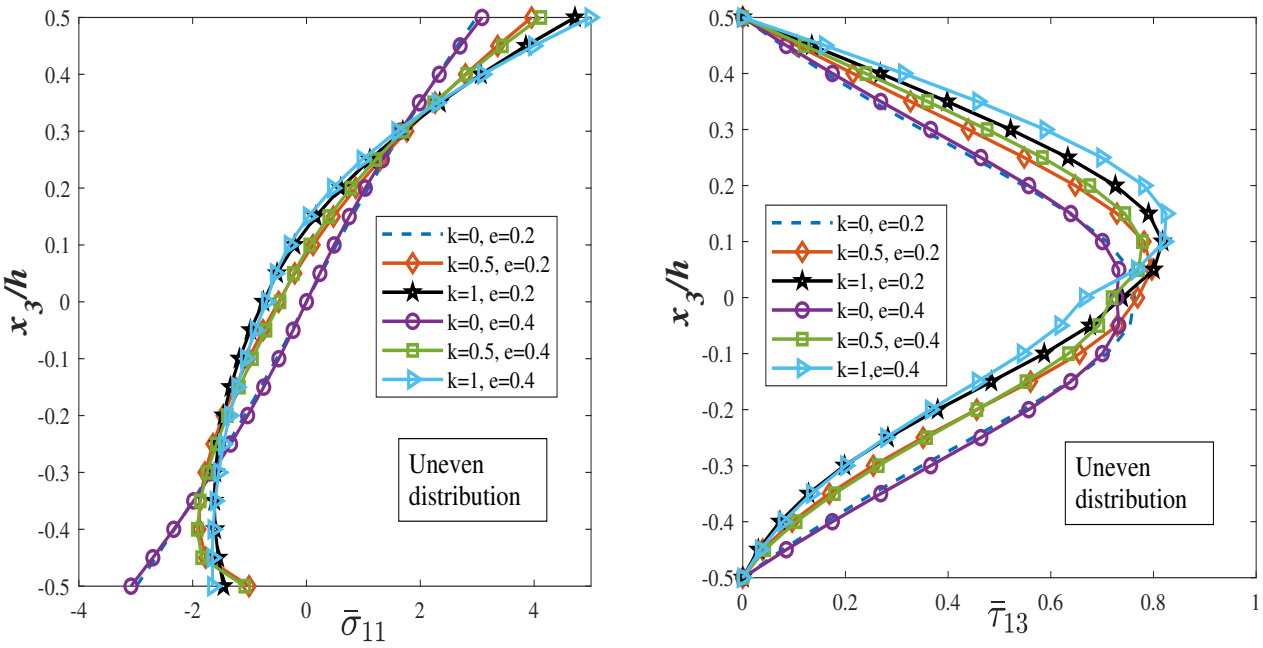

Figure 5.5: The distribution of normal and shear stress across the thickness for uneven porosity distribution.

As a next example, the porous FG plates are assumed to be subjected to transverse SSL. The dimensionless deflection and stresses (normal and transverse shear) are evaluated for the considered types of porosity distributions. The effects of porosity, span-thickness ratio, and volume fraction index on the static response of plates are examined.

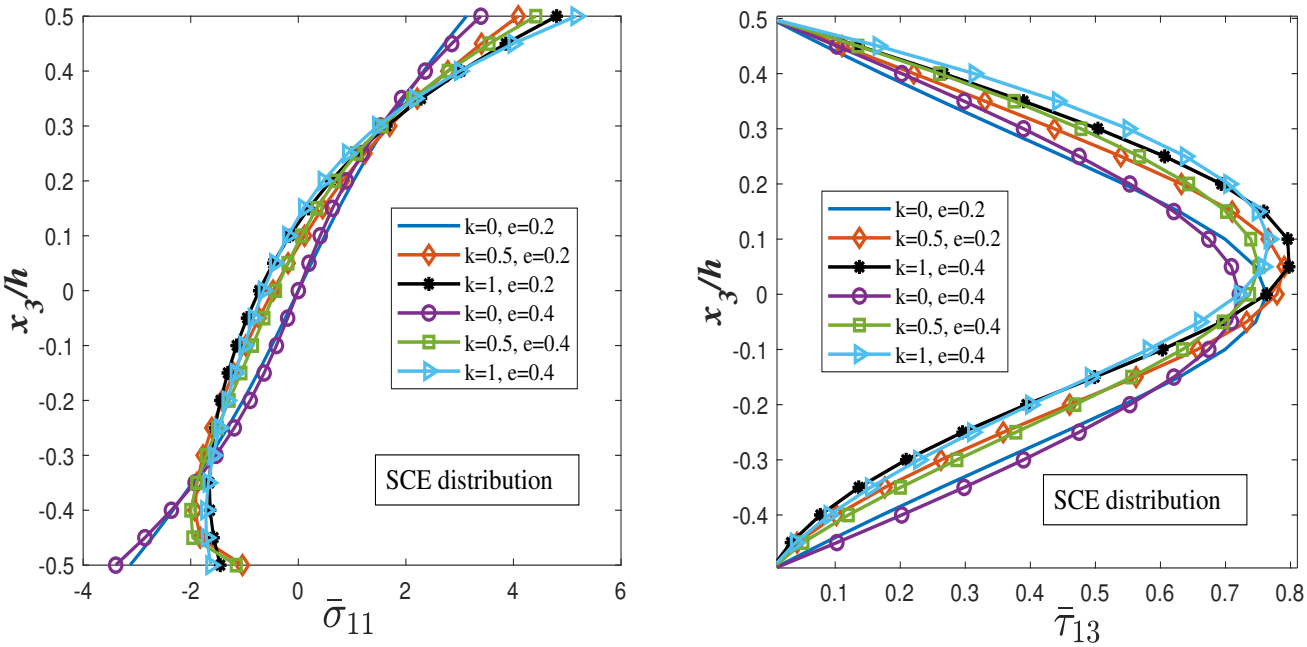

Figure 5.6: The normal and shear stress of uniformly loaded FG plate with symmetric center enhanced (SCE) porosity distribution.

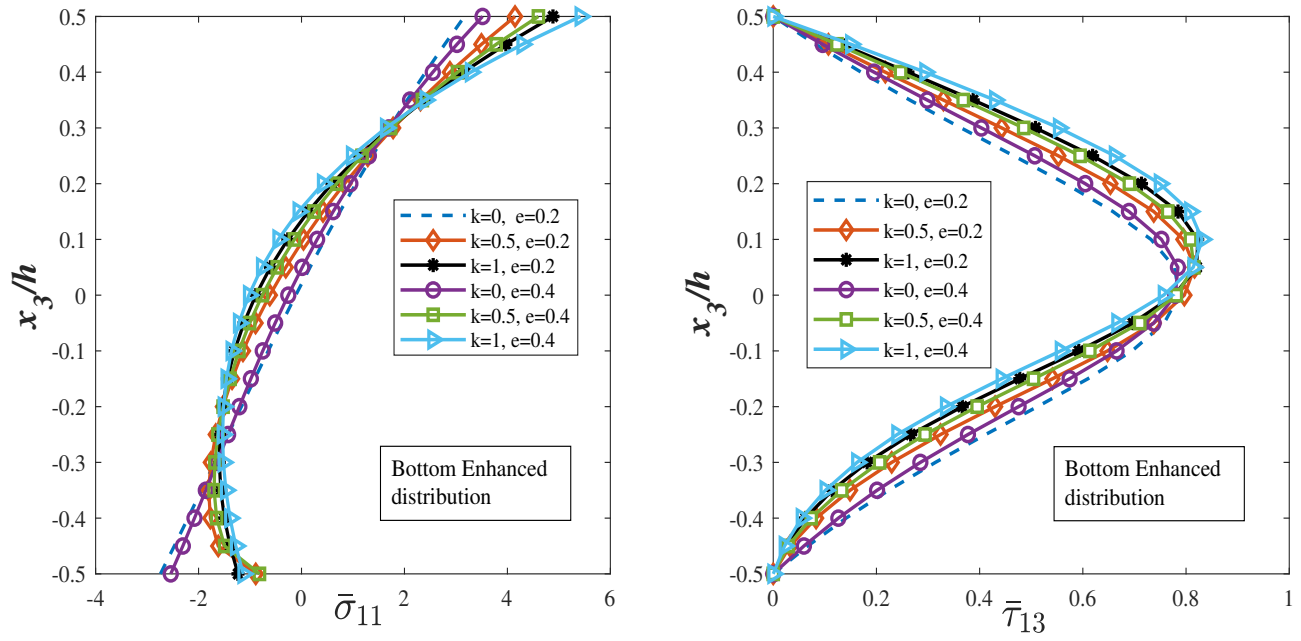

Figure 5.7: The distribution of dimensionless normal and shear stress across the thickness of plate with BE porosity distribution.

In Table (5.5), the results of dimensionless deflections of sinusoidal loaded porous and non-porous FG plates are presented for various power law exponent (k=0, 0.1, 0.5, 1), porosity parameter (e=0, 0.2, 0.4) and a/h ratios (5, 10, 20). It is seen that for all types of porosity

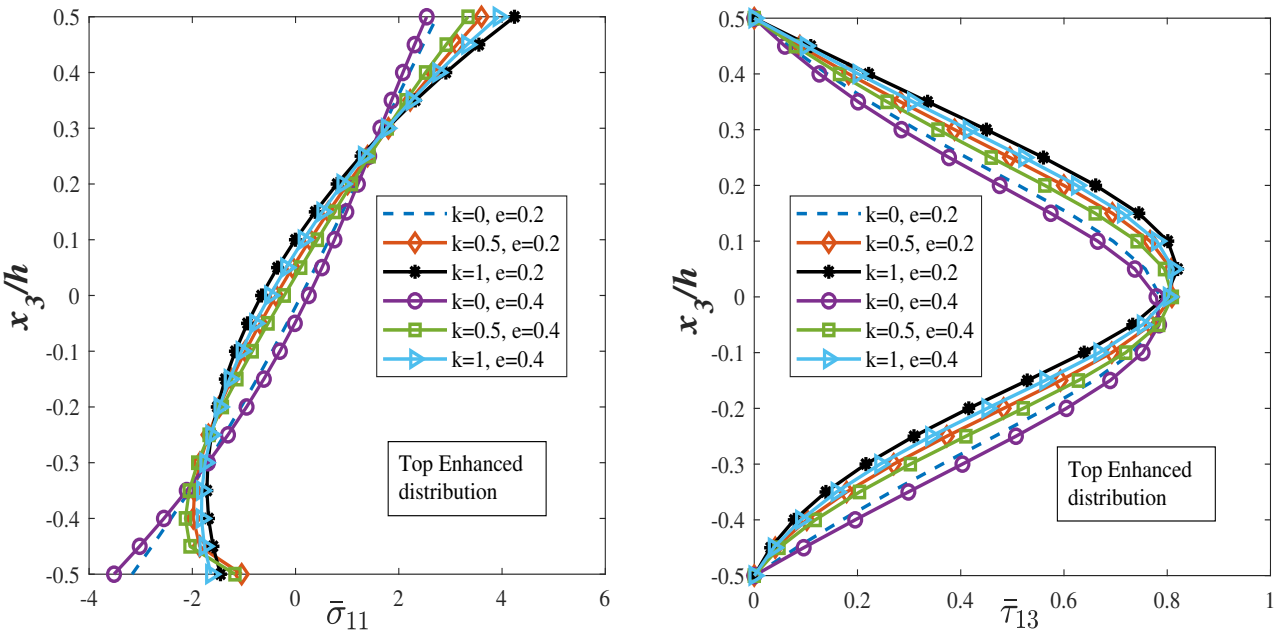

Figure 5.8: The normal and shear stress of FG uniformly loaded porous plate with TE distribution.

distributions, increasing a/h ratio leads to decreasing non-dimensional deflection of the plate for a particular value of e and k. Further, when e=0, the deflections correspond to all types of porosity distributions are the same, as it corresponds to the non-porous plate. Moreover, it can observe that for non-porous plates, the value of non-dimensional deflections for even porosity model is higher than the uneven distribution. As depicted from Table (5.5), the deflection increases with an increase in power law exponent from 0 to 1. This is due to the fact that overall stiffness of the plate reduces as the power law exponent increases.

The normal and shear stresses for different values of k and e are presented with even and uneven porosity distribution in Fig. (5.9) and Fig. (5.10). In both distribution, we see that at the bottom surface of the plate, the value of normal stress is minimum, and with moving towards the upper surface, its value is increasing. The maximum normal stress occurs at the surface, where the plate is ceramic rich. The maximum normal stress increases as the power law and porosity index increase. This is due to the reason that there is a change in material properties of plate with an increase in power-law index values (k >0). Also, it is observed that for isotropic plates, the dimensionless shear stress shows the symmetric distribution and its value is maximum at center. As evident from Fig. (5.8) and Fig. (5.10), the non-dimensional normal and shear stresses possess higher values for even porosity distribution relative to uneven distribution for any value of exponent k and porosity parameter.

Table 5.5: The non-dimensional deflection of nonporous and porous FG plate for sinusoidal load

a/h	k	e	Even	Uneven	SCE	BE	TE
5	0	0	0.3416	0.3416	0.3416	0.3416	0.3416
		0.2	0.3875	0.3556	0.3754	0.3894	0.3894
		0.4	—	0.3713	0.4191	0.4584	0.4584
	0.1	0	0.3768	0.3768	0.3768	0.3768	0.3768
		0.2	0.4336	0.3937	0.4145	0.4295	0.4297
		0.4	—	0.4127	0.4632	0.5055	0.5059
	0.5	0	0.5154	0.5154	0.5154	0.5154	0.5154
		0.2	0.6376	0.5493	0.5693	0.5874	0.5886
		0.4	—	0.5897	0.6396	0.6911	0.6934
	1	0	0.6659	0.6659	0.6659	0.6659	0.6659
		0.2	0.9155	0.7313	0.7371	0.7597	0.7602
		0.4	—	0.8166	0.8305	0.8943	0.8943
10	0	0	0.2957	0.2957	0.2957	0.2957	0.2957
		0.2	0.3354	0.3056	0.3205	0.3364	0.3364
		0.4	—	0.3163	0.3506	0.3957	0.3957
	0.1	0	0.3275	0.3275	0.3275	0.3275	0.3275
		0.2	0.3772	0.3397	0.3556	0.3727	0.3727
		0.4	—	0.3531	0.3898	0.4386	0.4382
	0.5	0	0.4532	0.4532	0.4532	0.4532	0.4532
		0.2	0.5635	0.4796	0.4951	0.5164	0.5161
		0.4	—	0.5102	0.5469	0.6082	0.6064
	1	0	0.5883	0.5883	0.5883	0.5883	0.5883
		0.2	0.8184	0.6415	0.6445	0.6715	0.6691
		0.4	—	0.7098	0.7149	0.7924	0.7842
20	0	0	0.2841	0.2841	0.2841	0.2841	0.2841
		0.2	0.3223	0.2930	0.3067	0.3231	0.3231
		0.4	—	0.3025	0.3334	0.3799	0.3799
	0.1	0	0.3151	0.3151	0.3151	0.3151	0.3151
		0.2	0.3630	0.3261	0.3408	0.3585	0.3583
		0.4	—	0.3381	0.3714	0.4218	0.4212
	0.5	0	0.4376	0.4376	0.4376	0.4376	0.4376
		0.2	0.5448	0.4621	0.4764	0.4985	0.4978
		0.4	—	0.4902	0.5235	0.5873	0.5845
	1	0	0.5688	0.5688	0.5688	0.5688	0.5688
		0.2	0.7941	0.6189	0.6212	0.6494	0.6462
		0.4	—	0.6830	0.6859	0.7668	0.7565

In Figures (5.11), (5.12) and (5.13) the non-dimensional normal and shear stress is presented for SCE, BE, and TE porosity distribution. The stresses are evaluated for a variety of power-

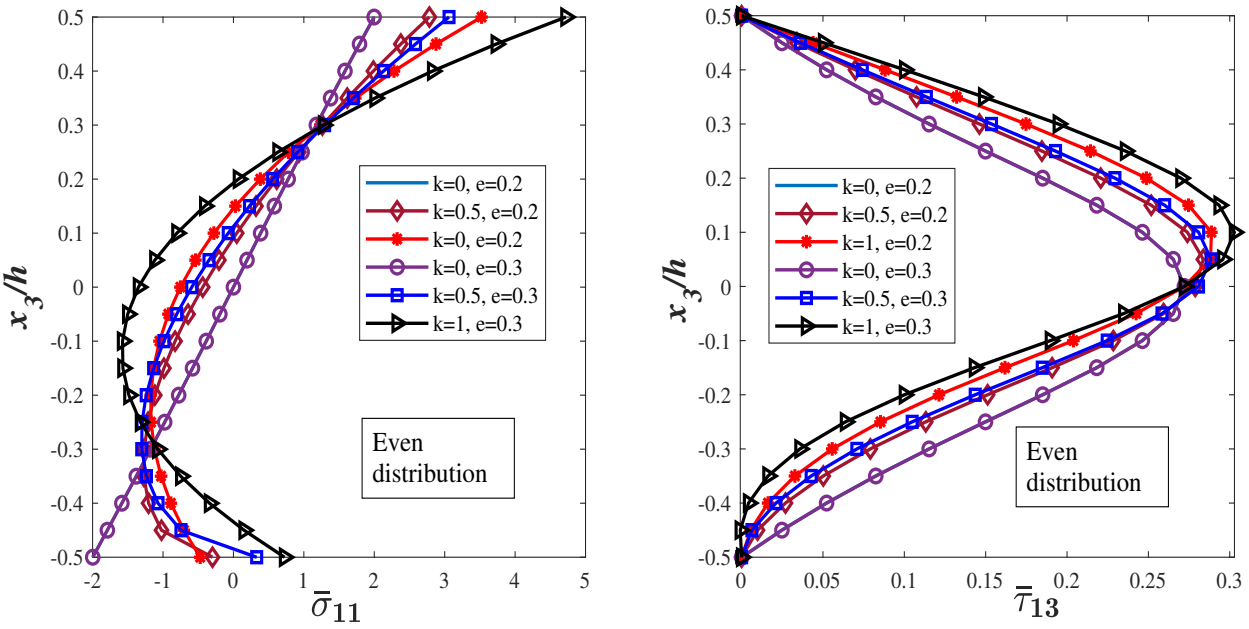

Figure 5.9: The normal and transverse shear stress of porous plate subjected to SSL

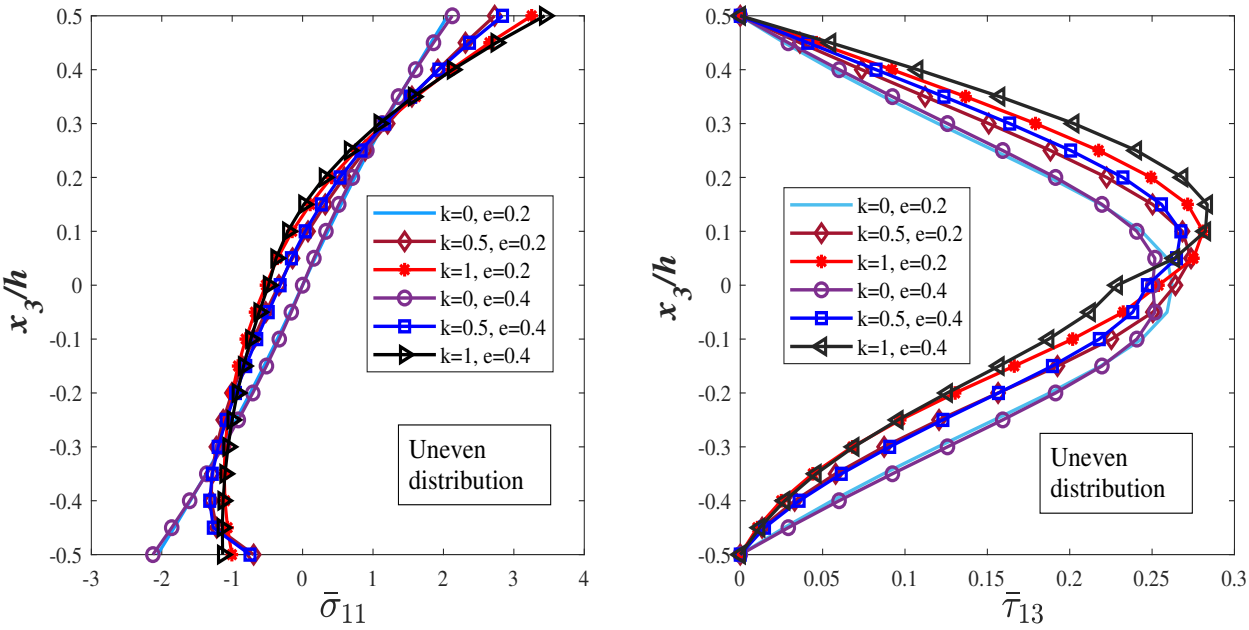

Figure 5.10: The normal and transverse shear stress of porous FG plate with uneven porosity distribution

law index and porosity parameters. From Fig. (5.11) and Fig.(5.12), it is observed that the maximum normal stress at the top surface increases with an increase in the value of e for a particular value of k. On the other hand, for the top enhanced (TE) porosity distribution in Fig. (5.13), the maximum normal stress decreases as the porosity parameter increases.

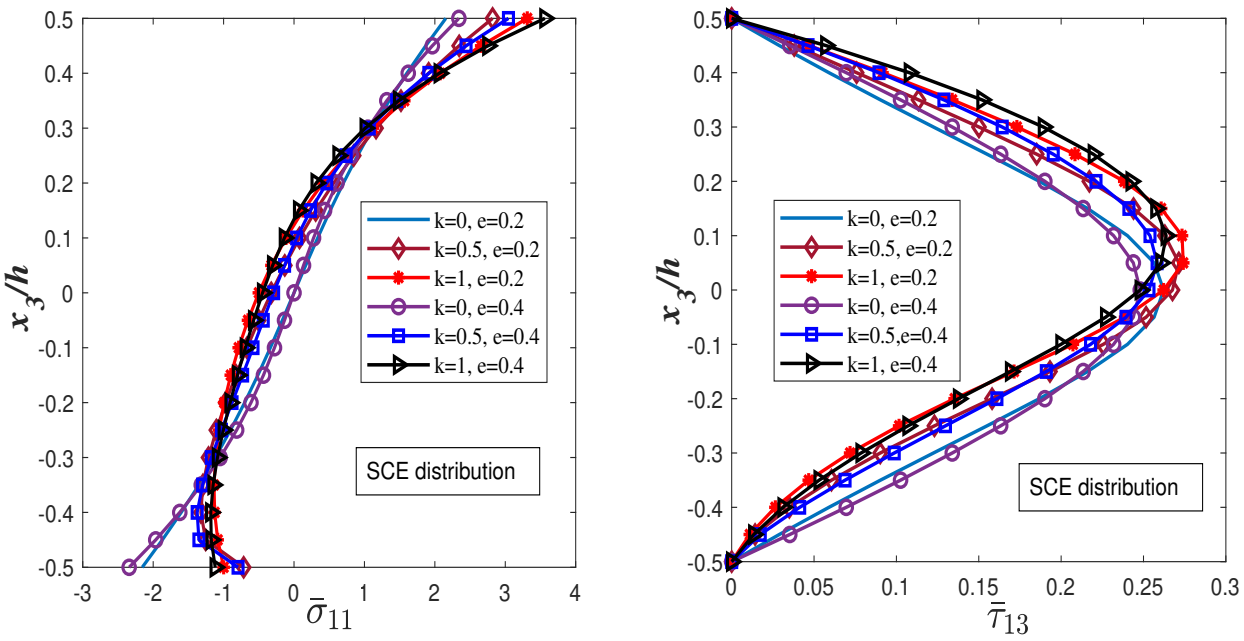

Figure 5.11: The dimensionless normal and transverse shear stress of porous FG plate subjected to SSL

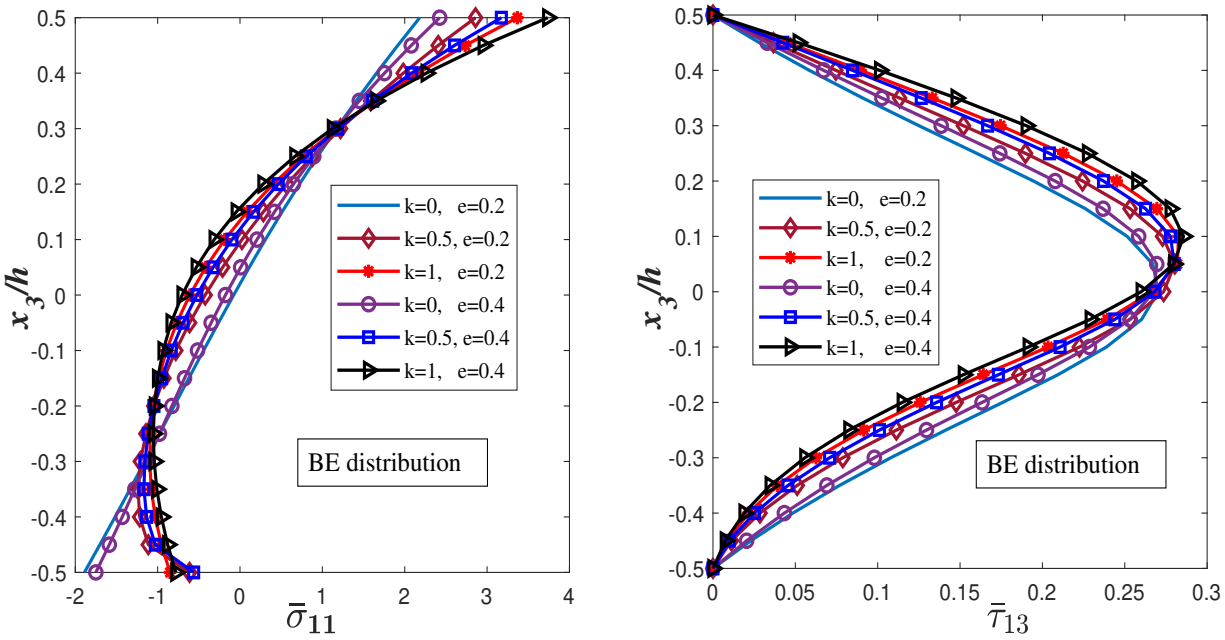

Figure 5.12: The effect of porosity parameter and power law index on dimensionless normal and shear stress for porous FG plate

Further, it is evident that for SCE distribution, the non-dimensional shear stress for isotropic plate (k=0) is maximum at the center of a plate and its value at the center decreases as the value of e increases. Furthermore, it is evident from Fig. (5.13) that an increase in the

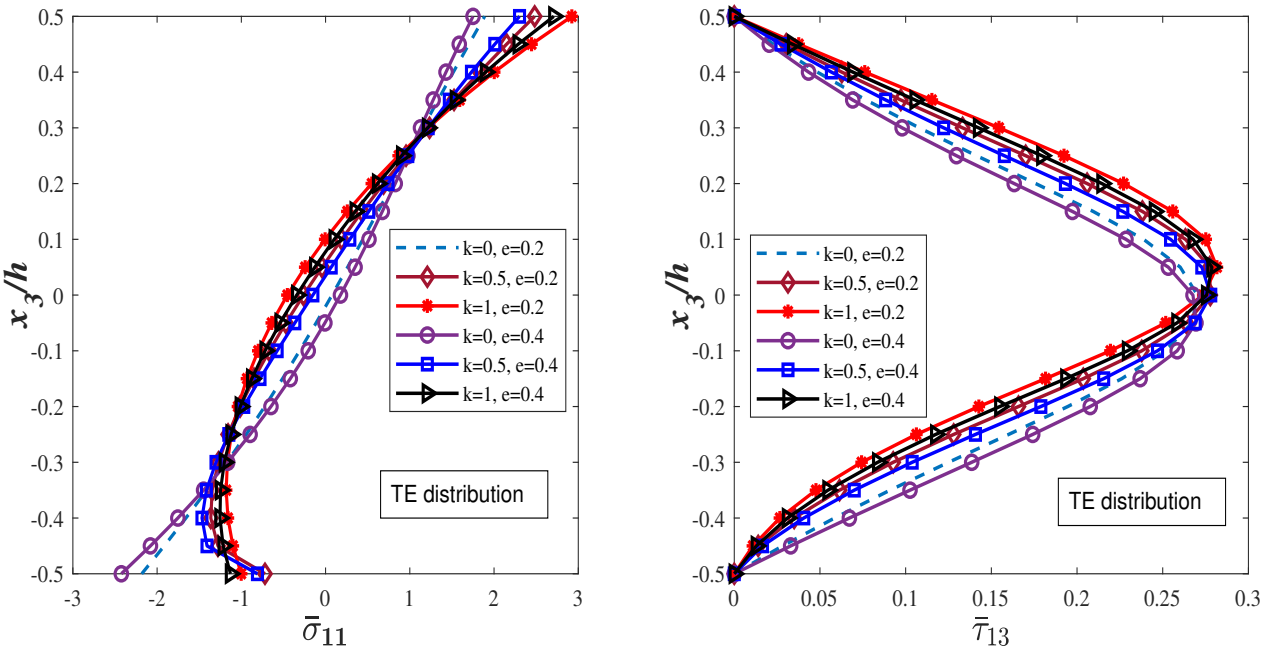

Figure 5.13: The non-dimensional normal and shear stress of porous FG plate with top enhanced porosity distribution.

porosity index leads to an increase in the values of dimensionless shear stress for values of x_3/h below the centre, while it results in a decrease for values of x_3/h above the centre. Additionally, the dimensionless shear stress remains zero at the top and bottom surfaces of the plate for all values of the power-law index and porosity parameter.

5.2.2 Buckling Analysis

In order to assess the buckling behavior, the plate is subjected to in-plane uni-axial and bi-axial compressive forces only. Hence, the mathematical system presented in Eq. (5.2) can be simplified to the subsequent expression:

$$\left[\bar{K} - N_0 G\right] \{\triangle\} = 0 \tag{5.6}$$

[G] is the geometric matrix due to uni-axial and bi-axial load. The parameter N_0 corresponds to the buckling load. The above system of equations is an eigenvalue problem. The eigenvalues correspond to the buckling, and the minimum eigenvalue corresponds to the critical buckling load.

The analysis is carried out for square as well as rectangular plates. The critical buckling load parameter of FG plates subjected to uni-axial loads is examined for a variety of power-law exponent (0, 0.1, 0.5, 1), porosity parameter (0.2, 0.4), side-to-thickness ratio (5, 10), and

aspect ratio (b/a=2, 1). The obtained results are listed in Table (5.6). It is observed that the plate with uneven porosity distribution possesses the highest buckling load. Moreover, the increment in porosity parameter reduces the buckling load. This is accounted towards the fact that the density of internal pores becomes higher and hence the stiffness of plate decreases thereby causing reduction in the buckling load parameter. The plate with higher span-thickness ratio possess the higher buckling load parameter. Further, it is observed that as the value of k increases, the dimensionless buckling load values decrease. Due to increment in k, the FG plate becomes metallic rich. Since the metal has less Young's modulus relative to ceramic, therefore the buckling load decreases. Table (5.7) shows the results of bi-axial buckling loads considering various parameters. The tables (5.6) and (5.7) indicate that the uni-axial and bi-axial buckling loads for uneven type porosity distribution surpass those of all other porosity distributions for specified values of parameters k, e, a/h, and b/a. From the Table (5.6), it is deduced that the effect of aspect ratio is significant between b/a=2 and b/a=1, since uni-axial buckling load values experience a sudden increase with a small change in aspect ratio b/a=2 to b/a=1 for all porosity distributions. As seen from Table (5.6) and Table (5.7), the value of critical buckling load for a porous FG square plate (b/a=1) subjected to bi-axial compressive force is lower compared to that under uni-axial compression.

In order to study the response of FG plates subjected to bi-axial force, the non-porous and porous (e=0.1) plate with five different porosity distributions are considered. The effect of load index on the dimensionless buckling load is investigated. The load index term K_m defines the magnitude of axial load in the y-direction in terms of axial load in the x-direction. The value of K_m=0 corresponds to uni-axial compressive force. The bi-axial loads are applied by assuming non-zero values of K_m. The impact of the load index parameter on the buckling load is assessed, and the corresponding outcomes are presented in Fig. (5.14). The load values for both uni-axial load (K_m=0) and bi-axial load (K_m=-0.8, -0.6, -0.4, -0.2, 0.2, 0.4, 0.6, 0.8, and 1) are shown in Fig. (5.14). The values of non-dimensional critical buckling loads reduce with an increase in load index values. This is because higher loads increase the tendency for the structure to buckle under compressive force. Also, it is seen that the FG non-porous plate possesses the higher non-dimensional buckling load relative to the porous plate. This is due to that young's modulus of non-porous plate is higher than porous plate. Further, for porous FG plates, the plate with uneven porosity distribution possesses the highest non-dimensional buckling load value, while the plate with even porosity possesses the lowest critical buckling load.

The effect of span-thickness (a/h) ratio on dimensionless buckling load is studied for porous FG square plate subjected to a uni-axial and bi-axial compressive forces. The results in

Table 5.6: The critical buckling loads of porous FG plate under in-plane uni-axial loading

a/h	b/a	k	e	Even	Uneven	SCE	BE	TE
5	2	0	0.2	5.9434	6.4978	6.1739	5.9192	5.9192
			0.4	—	6.2480	5.5815	5.0307	5.0307
		0.1	0.2	5.2989	5.8585	5.5792	5.3558	5.3549
			0.4	—	5.6103	5.0362	4.5511	4.5510
		0.5	0.2	3.5772	4.1758	4.0365	3.8925	3.8893
			0.4	—	3.9062	3.6211	3.3069	3.3055
		1	0.2	2.4780	3.1299	3.1098	3.0021	3.0061
			0.4	—	2.8146	2.7800	2.5472	2.5598
	1	0	0.2	14.1937	15.4666	14.6528	14.1232	14.1232
			0.4	—	14.8138	13.1249	11.9991	11.9991
		0.1	0.2	12.6838	13.9721	13.2711	12.8068	12.8005
			0.4	—	13.3263	11.8734	10.8815	10.8729
		0.5	0.2	8.6261	10.0131	9.6607	9.3631	9.3442
			0.4	—	9.3275	8.5994	7.9591	7.9320
		1	0.2	6.0082	7.5217	7.4619	7.2405	7.2354
			0.4	—	6.7353	6.6228	6.1501	6.1503
10	2	0	0.2	6.5338	7.1785	6.8507	6.5161	6.5161
			0.4	—	6.9436	6.2816	5.5407	5.5407
		0.1	0.2	5.8054	6.4535	6.1700	5.8768	5.8785
			0.4	—	6.2175	5.6452	4.9946	5.0002
		0.5	0.2	3.8773	4.5634	4.4234	4.2341	4.2381
			0.4	—	4.2951	4.0144	3.5943	3.6081
		1	0.2	2.6649	3.4094	3.3952	3.2532	3.2669
			0.4	—	3.0852	3.0676	2.7560	2.7891
	1	0	0.2	16.4000	17.9991	17.1606	16.3508	16.3508
			0.4	—	17.3877	15.6863	13.9018	13.9018
		0.1	0.2	14.5825	16.1914	15.4669	14.7570	14.7598
			0.4	—	15.5787	14.1096	12.5413	12.5523
		0.5	0.2	9.7617	11.4689	11.1104	10.6519	10.6581
			0.4	—	10.7802	10.0578	9.0440	9.0704
		1	0.2	6.7205	8.5746	8.5347	8.1909	8.2204
			0.4	—	7.7486	7.6934	6.9413	7.0141

terms of non-dimensional buckling load are obtained for non-porous and porous FG plate with five different porosity distributions. The obtained results are depicted in Fig. (5.15). Also, it is seen that the increase in the side-to-thickness ratio increases the buckling loads,

Table 5.7: The non-dimensional buckling loads of porous FG plate for bi-axial in-plane force

a/h	b/a	k	e	Even	Uneven	SCE	BE	TE
5	2	0	0.2	4.7547	5.1982	4.9391	4.7354	4.7354
			0.4	—	4.9984	4.4652	4.0245	4.0245
		0.1	0.2	4.2391	4.6868	4.4634	4.2847	4.2839
			0.4	—	4.4882	4.0289	3.6409	3.6408
		0.5	0.2	2.8618	3.3407	3.2292	3.1140	3.1115
			0.4	—	3.1249	2.8968	2.6456	2.6444
		1	0.2	1.9824	2.5039	2.4879	2.4017	2.4048
			0.4	—	2.2516	2.2240	2.0378	2.0478
	1	0	0.2	7.0968	7.7333	7.3264	7.0616	7.0616
			0.4	—	7.4069	6.5625	5.9995	5.9995
		0.1	0.2	6.3419	6.9861	6.6355	6.4034	6.4002
			0.4	—	6.6632	5.9367	5.4408	5.4364
		0.5	0.2	4.3130	5.0065	4.8303	4.6815	4.6721
			0.4	—	4.6637	4.2997	3.9796	3.9660
		1	0.2	3.0041	3.7609	3.7310	3.6202	3.6177
			0.4	—	3.3676	3.3114	3.0750	3.0752
10	2	0	0.2	5.2271	5.7428	5.4805	5.2129	5.2129
			0.4	—	5.5549	5.0252	4.4326	4.4326
		0.1	0.2	4.6443	5.1628	4.9360	4.7015	4.7028
			0.4	—	4.9740	4.5162	3.9957	4.0002
		0.5	0.2	3.1018	3.6507	3.5387	3.3872	3.3905
			0.4	—	3.4361	3.2115	2.8755	2.8865
		1	0.2	2.1319	2.7275	2.7161	2.6026	2.6136
			0.4	—	2.4681	2.4541	2.2048	2.2312
	1	0	0.2	8.2000	8.9995	8.5803	8.1754	8.1754
			0.4	—	8.6938	7.8431	6.9509	6.9509
		0.1	0.2	7.2912	8.0957	7.7335	7.3785	7.3799
			0.4	—	7.7894	7.0548	6.2707	6.2761
		0.5	0.2	4.8809	5.7344	5.5552	5.3259	5.3290
			0.4	—	5.3901	5.0289	4.5220	4.5352
		1	0.2	3.3602	4.2873	4.2673	4.0954	4.1102
			0.4	—	3.8743	3.8467	3.4707	3.5070

which concludes that the thin FG plates possess larger buckling loads. However, the rate of increment decreases with increase in a/h ratio. The type of porosity distribution also influence the buckling load of porous FG plate. Among the considered porosity distributions, the plate with uneven porosity distribution possess the highest buckling load parameter while the plate with even porosity distribution possess the lowest buckling load for a specific porosity parameter and a/h ratio. This is due to the fact that the elasticity modulus of the uneven FG plate is greater than the even one nearby lower and upper surface. The non-dimensional buckling for porous and non-porous FG square plate subjected to uni-axial load is twice of the same plate subjected to bi-axial load.

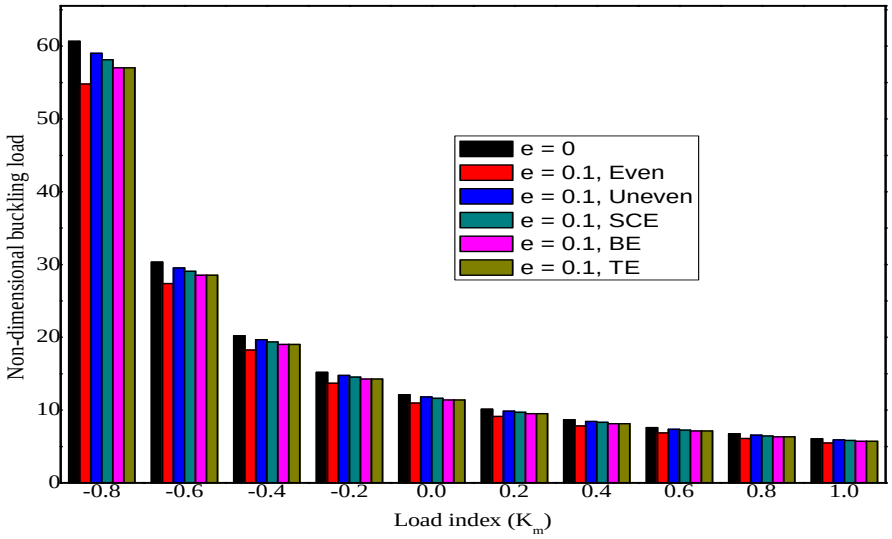

Figure 5.14: The effect of load index on the non-dimensional buckling load

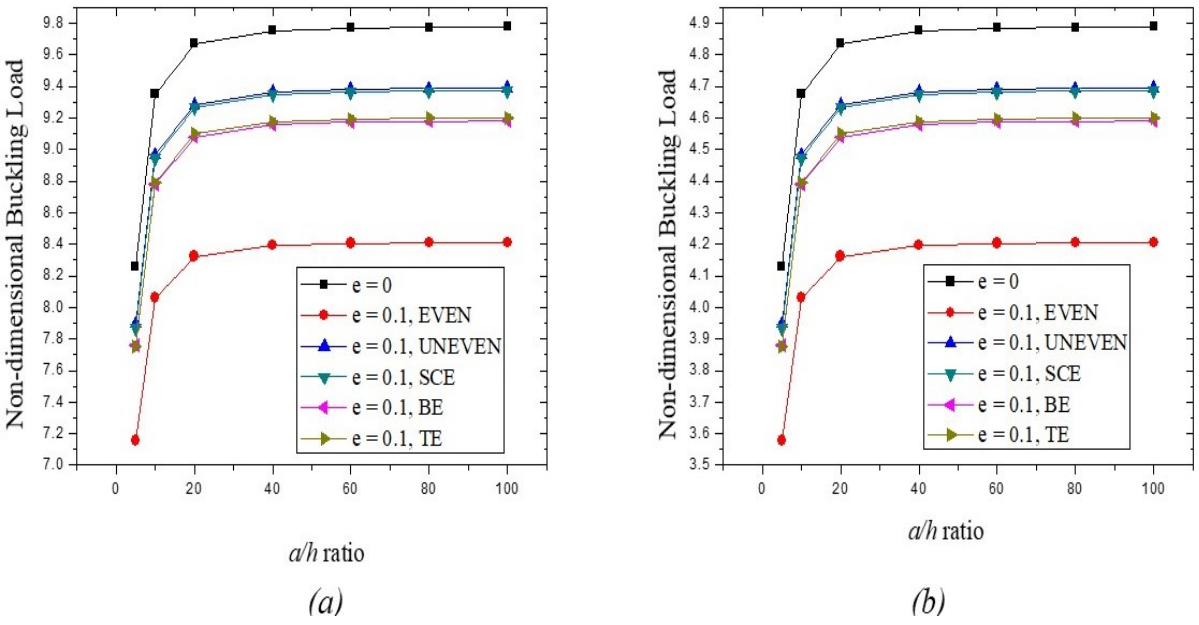

Figure 5.15: The dimensionless critical buckling load of FG plate under (a) uni-axial load (b) bi-axial load.

5.3 Conclusions

In the present work, the porosity in the FG plates is mathematically modeled based on five different distributions. These distributions are chosen as even, uneven, symmetric center enhanced, symmetric bottom enhanced, and top enhanced to account for the porosities present in the material. The FG plate is modeled in a displacement-based axiomatic framework wherein inverse hyperbolic shear deformation theory is chosen. The IHSDT employs a non-polynomial function of thickness co-ordinate to express the shear deformations. The use of such functions in the theory enables to introduce the traction free boundary conditions on top and bottom surfaces of the plate without using the shear correction factor. The mathematical system of equations is obtained by using the principle of virtual work by employing linear strain- displacement relations and generalized Hook's law. These equations are then solved via an analytical approach following the Navier method for simply supported boundary conditions. The static and buckling response of FG porous plates is examined. The effects of various parameters such as types of porosity distribution, porosity parameter,span-thickness ratio, aspect ratio, power-law index, and loading conditions on dimensionless deflection and critical buckling loads are evaluated. On the basis of the presented results, the following conclusion are observed:

- The present results for the static response of porous FG plates agree well with the

existing results, whichever available.

- The non-dimensional deflection of the FG porous plate is affected by the kind of porosity distribution. In case, when (e $\neq$ 0), the FG porous plate with uneven porosity distribution possesses the lowest non-dimensional deflection while the plate with even porosity distribution possesses the highest non-dimensional deflection.
- The non-dimensional deflection increases with increase in porosity parameter due to the fact that the increment in porosity parameter reduces the stiffness of FG plate. However, the increment rate depends on the type of porosity distribution, power index, and span-thickness ratio.
- The FG porous plates subjected to UDL possesses higher dimensionless deflections relative to the corresponding plates subjected to SSL.
- The non-dimensional buckling loads of porous FG plates subjected to bi-axial load possess a lower value than uni-axial buckling load for any value of side-thickness ratio, power-law index, and porosity parameter.
- The value of critical buckling load for square plate (b/a=1) subjected to uniaxial compressive force is double than in case of biaxial loading.

The response of FG plate with different porosity distributions have been examined via Navier's method in this chapter. As Navier's solutions are well accurate as well as easy to implement in comparison with exact solutions, but they can applicable to simply supported boundary conditions only. Therefore, several numerical techniques are available in literature to model and analyze the FGM structures with various boundary conditions. Therefore, next chapter deals with implementation of numerical technique to examine the mechanical behavior of FG plate under different boundary conditions.

Chapter 6

Finite element analysis of newly developed secant hyperbolic shear deformation theory

In this Chapter, we investigated the static and buckling behavior of composite laminated and FG porous plates for various combination of boundary conditions in the framework of finite element (FE) formulation. In order to accurately predict the response of structures, power law (P-FGM), and exponential law (E-FGM) functions are commonly used for modeling of the FGM plate [129, 224]. In both P-FGM and E-FGM distributions, the stress concentrations occur in the interfaces of material where it is varies continuously. Thus, the sigmoid law (S-FGM) which is amalgamation of two piecewise exponent functions is introduced by Chung and Chi [225] to define a new volume distribution. The advantage of S-FGM is that it can reduce the stress intensity factor more effectively. Stress concentrations do not occur to any appreciable extent at the interface of the materials when the FGM plate is modeled by sigmoid law distributions. Many researchers have adopted the power-law, exponential-law and sigmoid-law distributions to study the mechanical behavior of FGM structures using different plate theories. Lee *et al.* [226] carried out bending analysis of P-FGM, and S-FGM plates on elastic foundation using a four-variable higher order plate theory. Chi and Chung [227] studied the dynamical behavior of FGM plates subjected to transverse force and further they investigated the impacts of loadings, and aspect ratio on static deflection. Grover *et al.* [85] adopted an 8 noded bi-quadratic FE to predict the free vibration behavior of laminated composite and sandwich plates. They used inverse hyperbolic strain shape function in displacement field to investigate the response of general laminates with arbitrary boundary conditions. Duc and Cong [228] computed the non-linear dynamic response of thin sigmoid FG plates by employing CPT. Fazzolari [229] determined the modal characteristics of FG plates subjected to temperature environment whose material properties follow power- and sigmoid-law distributions by employing improved higher order plate theory. Further, bending, stress analysis, and vibration response of FG plates in the framework of P-FGM and E-FGM distributions have been conducted by researchers using various techniques [41, 70, 230–234]. Duc and Cong [235] obtained the nonlinear postbuckling response of thick FG plates on elastic foundations using third order deformation theory. Singh and Harsha [236] presented the free vibration and buckling anal-

ysis of sandwich plate whose material properties varied according to sigmoid distribution law. The inverse hyperbolic HSDT is adopted to formulate the plate governing equations. Jung *et al.* [237] proposed the four variable refined higher order plate theory to yield the non-dimensional frequencies of sigmoid FG plates on elastic foundation Thang *et al.* [238] developed the analytical approach to study the post-buckling behavior of imperfect S-FGM plates by employing classical plate theory. Mehar *et al.* [239] used finite element approach to investigate the deflection, and stress values of CNT reinforced sandwich plate under the effect of the mechanical loading. Jung and Han [240] examined the influence of power-law index, and loading conditions on static deflection of S-FGM nanoscale plates. Using Hamilton's principle, the governing equations of plate are formed and analytical solutions are obtained in framework of a nonlocal elasticity theory. Ali *et al.* [241] computed the vibration characteristics of FGM Levy plates assuming sigmoid distribution law. The dynamic stiffness method is proposed to asses the effect of different parameters on natural frequencies and mode shapes. The finite element modeling have been carried out in analysis of smart shells and beams in following articles [242–244]. Apart from the existing literature on the research of FGM plates, there exist various articles that investigate the mechanical analysis of FGM beams and shells as well [183, 245–253]

Based on aforementioned research, it can be concluded that the most of the study for FGM structures analysis is based upon P-FGM and E-FGM distribution. But so far the research leading to the bending analysis of sigmoid FGM plates considering porosity effect is somehow limited. Further, the majority of researchers have almost focused on free vibration response of the S-FGM plate. In view of the research gap, this study deals with static, buckling and stress analysis of both P-FGM and S-FGM plates with porosity effect by using a new hyperbolic shear deformation theory. The finite element procedures illustrated for composite, and porous FG plates with power-law as well as sigmoid law gradient. The FE approach with C^0 isoparametric eight noded quadrilateral element is proposed to examine the bending and buckling behavior. Furthermore, the effects of porosity index, power-law exponent, loading conditions, and the aspect ratio are investigated on computing deflections and critical buckling loads.

6.1 Mathematical Modeling

In this section, the functionally graded plate in which the material properties vary along the thickness direction is considered. The volume fraction of constituent materials is defined by adopting power-law and sigmoid-law distributions. Three different choices of distributions are also taken to evaluate the effect of porosity in modeling the FG plate. The geometric representation of FGM plate is illustrated using Cartesian coordinates $(x_1 - x_2 - x_3)$ in

Figure (6.1).

The Young's modulus of assumed porous FG plate along the thickness is represented by

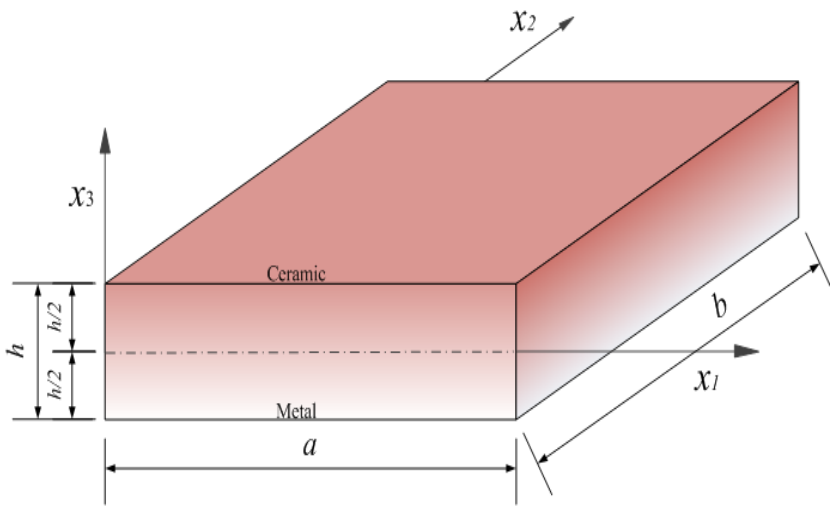

Figure 6.1: Geometry of FG plate

P-FGM and S-FGM distributions as follows.

Power-law function (P-FGM):

According to rule of mixture, the material property of P-FGM can be defined by [226]

$$E(x_3) = \left[E_b + (E_t - E_b)\left(\frac{x_3 + \frac{h}{2}}{h}\right)^k\right] \quad \text{where, } 0 \leq x_3 \leq h \tag{6.1}$$

Sigmoid-law function (S-FGM):

The volume fractions of material in accordance with sigmoid-law distribution are given as [226, 240]

$$E_1(x_3) = \left[E_b + (E_t - E_b)\left(1 - \frac{1}{2}\left(\frac{\frac{h}{2} - x_3}{\frac{h}{2}}\right)^k\right)\right] \quad \text{where, } 0 \leq x_3 \leq \frac{h}{2} \tag{6.2}$$

$$E_2(x_3) = \left[E_b + (E_t - E_b)\frac{1}{2}\left(\frac{\frac{h}{2} + x_3}{\frac{h}{2}}\right)^k\right] \quad \text{where, } -\frac{h}{2} \leq x_3 \leq 0 \tag{6.3}$$

Where E_t and E_b are properties of material at top and bottom of plate and k denotes the power-law exponent that indicates the volume fraction of the material. Fig. (6.2) and (6.3) represent the variation of Young's modulus for P-FGM and S-FGM plates with respect to the transverse direction for various values of parameter k.

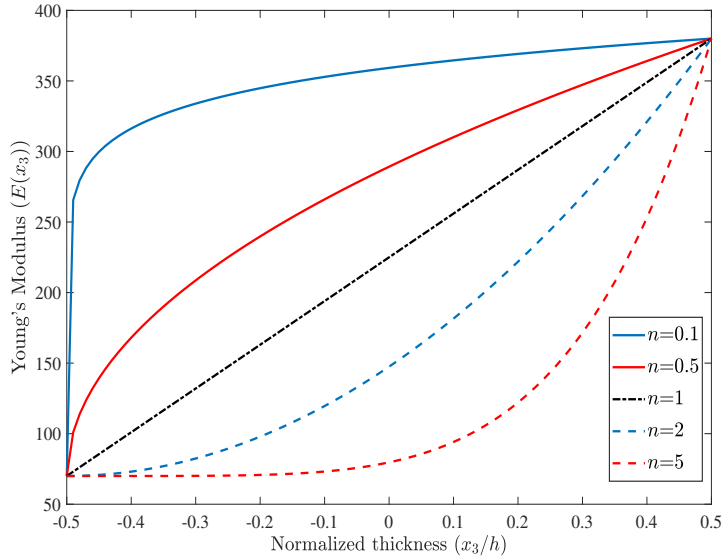

Figure 6.2: Variation of Elasticity modulus of P-FGM plate with respect to x_3/h ratios.

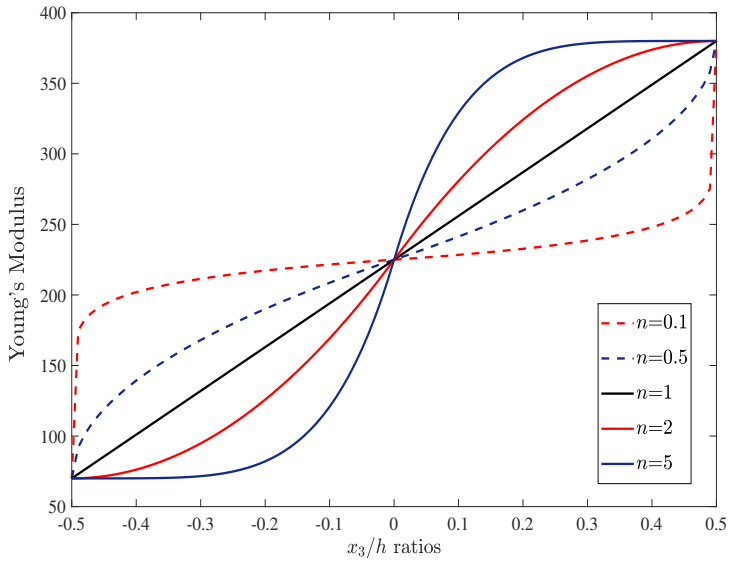

Figure 6.3: Young's Modulus of S-FGM plate with respect to normalized thickness ratios for different material indexes k.

6.1.1 Porous Functionally Graded Material

In this paper, three types of porosity distributions are proposed using different mathematical functions. The symmetric center enhanced (SCE), bottom (BE) and top (TE) enhanced distributions are employed to determine the material properties of porous plates. Taking into consideration the impact of porosity distribution, the Young's modulus of FG plate

obeying P-FGM law are written as follows:

$$E(x_3) = \left[E_b + (E_t - E_b)\left(\frac{x_3 + \frac{h}{2}}{h}\right)^k\right](1 - \Phi(x_3)) \quad \text{where, } 0 \leq x_3 \leq h \tag{6.4}$$

Further, according to the sigmoid-law rule, the material property of porous plate are written as below:

$$E_1(x_3) = \left[E_b + (E_t - E_b)\left(1 - \frac{1}{2}\left(\frac{\frac{h}{2} - x_3}{\frac{h}{2}}\right)^k\right)\right](1 - \Phi(x_3)) \quad \text{where, } 0 \leq x_3 \leq \frac{h}{2} \tag{6.5}$$

$$E_2(x_3) = \left[E_b + (E_t - E_b)\frac{1}{2}\left(\frac{\frac{h}{2} + x_3}{\frac{h}{2}}\right)^k\right](1 - \Phi(x_3)) \quad \text{where, } -\frac{h}{2} \leq x_3 \leq 0 \tag{6.6}$$

Where $\Phi(x_3)$ is porosity distribution function depending on parameter e and thickness co-ordinate. The different types of distributions functions are given in Table 7.1. Where e is porosity index and the FGM plate becomes perfect for e=0. The distribution of porosity with different types through thickness is shown in Fig. 6.4.

Table 6.1: Porosity distribution functions

Types of Distributions	$\Phi(x_3)$ (Different Porosity Functions)
SCE (Symmetric Center Enhanced Distribution)	$e\ \cos(\frac{\pi x_3}{h})$
BE (Bottom Enhanced Distribution)	$e\ \cos\left(\frac{\pi}{2}\left(\frac{x_3}{h} + 0.5\right)\right)$
TE (Top Enhanced Distribution)	$e\ \cos\left(\frac{\pi}{2}\left(\frac{x_3}{h} - 0.5\right)\right)$

6.2 Results and Discussion

In this study, the results of numerical analyses of the bending and buckling of perfect and porous FGM plates are calculated. The considered FGM plate is made of ceramic phase on its top surface while bottom of FG material is metallic rich. The finite element modeling is proposed to ensure the accuracy and applicability of present formulation to analyze FG plates subjected to various boundary conditions. For validation of the proposed theory, a comparison study is conducted between the present results and some existing FG plate

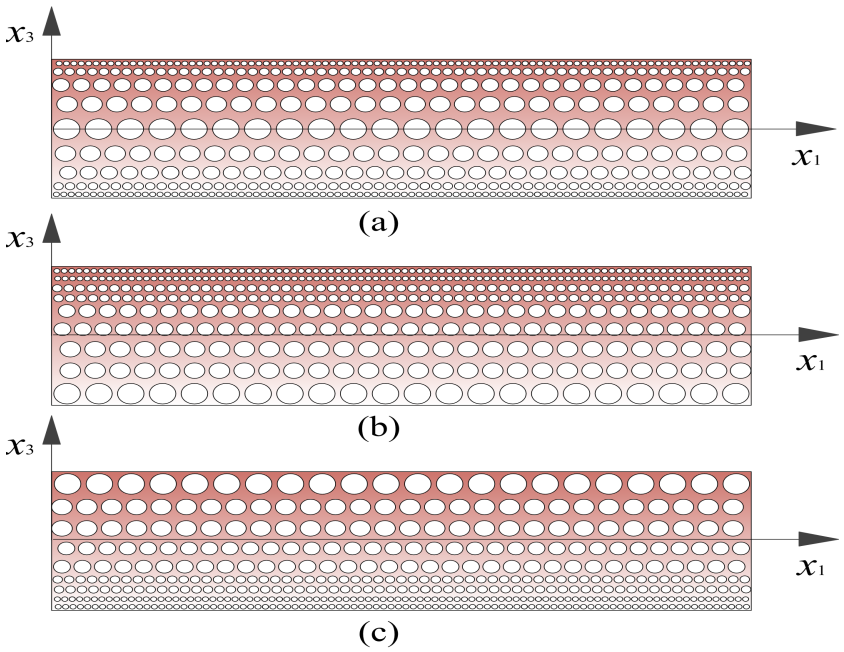

Figure 6.4: Porosity distribution:(a) SCE (b) BE (c) TE

theories results. Also the significances of boundary conditions, material characteristics, porosity parameter, and side to thickness ratio on the static deflections and buckling loads of FG plates are discussed. In order to evaluate the flexural response of FGM plates, a MATLAB program was developed using the present finite element formulation. After evaluating the elemental stiffness and geometrical matrix, the assembly of plate over whole domain is carried out. The Gaussian Quadrature scheme is used to compute the integral over domain. It should be noted that problem of shear locking arises particularly for the thin plates. In order to eliminate the same, selective integration is adopted wherein bending terms are integrated with 3x3 order while the shear terms are integrated with 2x2 order. The following boundary conditions are implemented for solving problems related to bending and buckling responses.

- Simply supported Conditions (S):

  $u_0 = w_0 = \Theta_{x_1} = \phi_{x_1} = 0$ (Edge parallel to x_1-axis)

  $v_0 = w_0 = \Theta_{x_2} = \phi_{x_2} = 0$ (Edge parallel to x_2-axis)

- Clamped Condition (C): $u_0 = v_0 = w_0 = \Theta_{x_1} = \Theta_{x_2} = \phi_{x_1} = \phi_{x_2} = 0$

The material properties of ceramic-metal FG plate are given in Table 6.2. Where v is constant poison ratio of assumed material.

Table 6.2: Material properties

	Material Properties (MM1)		Material Properties (MM2)	
	Metal	Ceramic	Metal(Aluminum)	Ceramic(Alumina)
Elastic modulus	$E_b = 1.44GPa$	$E_t = 14.4GPa$	$E_b = 70GPa$	$E_t = 380GPa$
Poisson ratio	v_b=0.38	v_t=0.38	v_b=0.3	v_b=0.3

6.2.1 Static Analysis

The aforementioned system (3.48) is solved to obtain the nodal displacements after implementing the boundary conditions. Firstly, the non-dimensional deflections and stresses are evaluated for four layered simply supported symmetric plates under transverse SSL for different a/h ratio in Table (6.3). The non-dimensional forms given is Eq. (4.5) are taken for analysis. Convergence analysis for laminated plate is performed for various mesh sizes. The results are being compared with exact solutions and other available results in literature. It is observed that well convergence is achieved for deflection for mesh size upto 8 and for stresses, converges to exact results is obtained for size of mesh upto 14. The variation in convergence between deflection and stresses is due to fact that displacements are primary variable, whereas stresses are derived quantities in the assumed displacement field.

Further, the numerical results for deflection of P-FGM and S-FGM plates subjected to SSL and UDL are presented. As a second example, the non-dimensional deflections obtained from proposed theory for perfect S-FGM simple supported plate are presented in Table (6.4) for various values of a/h. The results are validated with published results of Jung and Han [254] for homogeneous (k=0) plate and for power-law exponent (k=1,5) under uniform load. Further, the non-dimensional displacements are evaluated for P-FGM plate (k=0,1,5) and results are validated with those obtained by Thai and Cho [255] for power-law index 0, and 1 in Table 6.5. It is apparent that the results of present study are in excellent agreement with those found in previous literature. The non-dimensional forms and material properties (MM1) are used as follows [254]:

$$W = \frac{h^3 E_b \times 10^2}{q_0 a^4} w(\frac{a}{2}, \frac{b}{2}, \frac{h}{2}), \quad E_t = 14.4GPa, \quad E_b = 1.44GPa, \quad v = 0.38, \quad q = 1N/m^2 \tag{6.7}$$

It is also observed from Table (6.4) and (6.5) that the maximum deflection for P- and S-FGM plates does not differ for values of k=0 and k=1. This occurs due to the fact that material characteristics of P- and S-FGM are same for k= 0 and 1.

Table 6.3: The dimensionless deflection and stresses for [0/90/90/0] laminate subjected to transverse SSL

a/h	Theory	$\overline{W}$	$\bar{\sigma}_{11}$	$\bar{\sigma}_{22}$	$\bar{\tau}_{12}$	$\bar{\tau}_{23}$	$\bar{\tau}_{13}$
4	Present(4×4)	1.9172	0.5786	0.5286	0.0551	0.2512	0.2377
	Present(6×6)	1.9263	0.6401	0.5849	0.0509	0.2597	0.2329
	Present(8×8)	1.9277	0.6648	0.6075	0.0492	0.2625	0.2307
	Present(10×10)	1.9281	0.6769	0.6185	0.0484	0.2638	0.2296
	Present(14×14)	1.9283	0.6877	0.6284	0.0476	0.2649	0.2286
	Present (Analytical)	1.9243	0.7307	0.6377	0.0474	0.2676	0.2489
	Grover *et al.* [43]	1.9257	0.7255	0.639	0.0473	0.27	0.25
	Reddy [28]	1.893	0.665	0.632	0.044	0.239	0.206
	Exact [9]	1.954	0.72	0.663	0.047	0.291	0.219
10	Present(4×4)	0.7275	0.4636	0.3267	0.0323	0.1695	0.3490
	Present(6×6)	0.7285	0.5129	0.3613	0.0299	0.1767	0.3426
	Present(8×8)	0.7286	0.5327	0.3753	0.0289	0.1788	0.3394
	Present(10×10)	0.7286	0.5424	0.3821	0.0284	0.1797	0.3377
	Present(14×14)	0.7287	0.5511	0.3882	0.0280	0.1804	0.3362
	Present (Analytical)	0.7289	0.5589	0.3949	0.0275	0.1749	0.3275
	Grover *et al.* [43]	0.7284	0.5578	0.3947	0.0275	0.1762	0.3287
	Reddy [28]	0.715	0.546	0.389	0.027	0.163	0.294
	Exact [9]	0.743	0.559	0.401	0.028	0.196	0.301
100	Present(4×4)	0.4339	0.4445	0.2235	0.0253	0.1165	0.3825
	Present(6×6)	0.4344	0.4930	0.2478	0.0232	0.1234	0.3843
	Present(8×8)	0.4344	0.5121	0.2575	0.0224	0.1256	0.3837
	Present(10×10)	0.4343	0.5214	0.2621	0.0221	0.1265	0.3828
	Present(14×14)	0.4343	0.5298	0.2664	0.0217	0.1273	0.3815
	Present (Analytical)	0.4345	0.5388	0.271	0.0214	0.126	0.3632
	Grover *et al.* [43]	0.4345	0.5388	0.271	0.0214	0.1271	0.3643
	Reddy [28]	0.434	0.538	0.27	0.021	0.112	0.29
	Exact [9]	0.439	0.539	0.276	0.022	0.141	0.337

As an next example, the maximum non-dimensional deflections are shown in Table (6.6) for different mesh density for square ($b/a = 1$) and rectangular ($b/a = 2$) homogeneous P-FGM plate. The material properties (MM2) given in Table (6.2) and dimensionality form $W = \frac{10E_t h^3}{q_0 a^4} w(\frac{a}{2}, \frac{b}{2}, \frac{h}{2})$, is used for analysis. The results for simply supported (SSSS) and clamped (CCCC) conditions on all the edges are presented along with different porosity distributions. The convergence study of FEM for central deflection with various mesh sizes is performed for porous FG plate. it is evident from the analysis that convergence is monotonic and size of mesh 8×8 is adequate for the precise prediction of maximum displacement.

Table 6.4: Comparison of dimensionless deflection of S-FGM square plates under uniform loads (MM1).

a/h	Homogeneous plate(k=0)		k=1		k=5	
	Present (S-FGM)	Jung and Han [254]	Present (S-FGM)	Jung and Han [254]	Present (S-FGM)	Jung and Han [254]
5	0.5136	0.5145	1.1517	1.1533	1.5578	1.5599
10	0.4413	0.4415	1.0201	1.0205	1.4338	1.4344
20	0.4231	0.4232	0.9871	0.9873	1.4027	1.4029
100	0.4173	0.4173	0.9765	0.9766	1.3927	1.3929

Hence, mesh of size eight is taken into account for subsequent study. It is also observed that deflection corresponding to SSSS boundary conditions is larger than the plate with all edges clamped for any value of b/a ratio. Several numerical studies are further discussed to examine the effects of parameters such as boundary conditions, porosity coefficient, volume fraction index and some others on transverse deflection of porous FG plate.

For an S-FGM simply supported plate, the non-dimensional displacements evaluated by present theory are given in Table (6.7) for different porosity distributions, power-law exponent ($k = 0, 0.1, 0.5, 1$) and side-thickness ratio. The impact of porosity coefficient ($e = 0, 0.2, 0.4, 0.8$) is also investigated on deflections of square plate subjected to UDL. The material properties given in equation (6.7) are employed for analysis. It is observed from Table (6.7) that with the increase of span-thickness ratio a/h the magnitude of deflection decreases and with the increment in power-law exponent (k) corresponding deflection of S-FGM plate increases significantly. For k=0, the properties of material are identical at top and bottom of plate, hence deflection values remain same for BE and TE porosity distributions for any value of a/h.

Table 6.5: Comparison of non-dimension deflection of simply-supported P-FGM plates under uniform loads (b=a).

a/h	Homogeneous plate		k=1		k=5
	Present (P-FGM)	Thai *et al.* [255]	Present (P-FGM)	Thai *et al.* [255]	Present (P-FGM)
5	0.5136	0.5147	1.1517	1.1536	2.4301
10	0.4413	0.4415	1.0201	1.0205	2.0340
20	0.4232	0.4231	0.9871	0.9873	1.9343

As an another example, the influence of different combination of boundary conditions on non-dimensional deflection of S-FGM plate under SSL and UDL load is assessed in Table (6.8). Also, the results are presented for perfect and porous FG along with three porosity

Table 6.6: Mesh convergence: Maximum non-dimensional center deflection under UDL (a/h=10, e=0.5)

b/a	Boundary Conditions	Mesh density	e=0	SCE	BE	TE
1	SSSS	4×4	0.4660	0.5795	0.6895	0.6895
		6×6	0.4663	0.5799	0.6901	0.6901
		8×8	0.4664	0.5799	0.6901	0.6901
		12×12	0.4664	0.5800	0.6902	0.6902
1	CCCC	4×4	0.1632	0.2109	0.2418	0.2418
		6×6	0.1639	0.2112	0.2428	0.2428
		8×8	0.1638	0.2110	0.2427	0.2427
		12×12	0.1638	0.2110	0.2426	0.2426
2	SSSS	4×4	1.1409	1.4092	1.6879	1.6879
		6×6	1.1410	1.4093	1.6880	1.6880
		8×8	1.1412	1.4095	1.6883	1.6883
		12×12	1.1413	1.4097	1.6884	1.6884
2	CCCC	4×4	0.3132	0.4009	0.4639	0.4639
		6×6	0.3152	0.4023	0.4669	0.4669
		8×8	0.3151	0.4019	0.4667	0.4667
		12×12	0.3151	0.4019	0.4667	0.4667

distributions and power-law indices (k=1, 2, 5). It is noticed from tabulated results that the central maximum deflection for considered boundary conditions are in sequence of decreasing order as SSSS>SCSC>SCCC>CCCC, i.e plate with simply supported (SSSS) conditions possess largest deflection while clamped (CCCC) plate possesses smallest. The average decrease in normalized deflection from SSSS to CCCC is approximate 35% for uniform load and decrement is almost 40% for plate subjected to SSL. It is also observed that the dimensionless bending corresponding to SCE (symmetric center enhanced) porosity distribution is lowest whereas TE (Top enhanced) distribution attained highest deflection. This is due to that plate is more stiffer at mid-plane than top and bottom surfaces. Furthermore, higher deflections are observed for S-FGM plate subjected to UDL than transverse SSL for any value of power-law exponent.

Next, a perfect P-FGM square plate composed of alumina (ceramic) and aluminum (metal) is taken. The proposed theory results of non-dimensional displacements for plate under SSL are shown in Table 6.9 along with available results in literature reported by by Carrera *et al.* [256], Neves *et al.* [257] and Nguyen *et al.* [258]. The non-dimensional form

Table 6.7: The non-dimensional deflection of porous S-FGM Simply supported plate for UDL

a/h	Porosity Model	e	k			
			0	0.1	0.5	1
5	SCE	0	0.5136	0.9409	1.0277	1.1517
		0.2	0.5643	1.0344	1.1363	1.2803
		0.4	0.63	1.1556	1.2787	1.4505
		0.8	0.8832	1.6233	1.83	2.1153
	BE	0	0.5136	0.9409	1.0277	1.1517
		0.2	0.5855	1.072	1.1707	1.3115
		0.4	0.6891	1.2611	1.3763	1.5398
		0.8	1.2062	2.1971	2.3583	2.5888
	TE	0	0.5136	0.9409	1.0277	1.1517
		0.2	0.5855	1.0733	1.1746	1.3187
		0.4	0.6891	1.2639	1.3847	1.5563
		0.8	1.2062	2.2203	2.4338	2.7235
10	SCE	0	0.4413	0.8092	0.8956	1.0201
		0.2	0.4784	0.878	0.9793	1.1239
		0.4	0.5233	0.9615	1.0838	1.2567
		0.8	0.6615	1.2197	1.4238	1.7122
	BE	0	0.4413	0.8092	0.8956	1.0201
		0.2	0.502	0.9207	1.0204	1.163
		0.4	0.5905	1.0832	1.2019	1.3692
		0.8	1.0521	1.9242	2.1037	2.3489
	TE	0	0.4413	0.8092	0.8956	1.0201
		0.2	0.502	0.9209	1.0201	1.1637
		0.4	0.5905	1.0829	1.1988	1.3677
		0.8	1.0521	1.9322	2.1212	2.3921
50	SCE	0	0.418	0.767	0.8532	0.9779
		0.2	0.4507	0.8277	0.9289	1.0737
		0.4	0.4891	0.8992	1.0212	1.1943
		0.8	0.5899	1.0893	1.2926	1.582
	BE	0	0.418	0.767	0.8532	0.9779
		0.2	0.4752	0.8722	0.9721	1.1153
		0.4	0.5588	1.0261	1.1459	1.3144
		0.8	1.0026	1.8365	2.0219	2.2718
	TE	0	0.418	0.767	0.8532	0.9779
		0.2	0.4752	0.872	0.9705	1.1139
		0.4	0.5588	1.0249	1.1391	1.3071
		0.8	1.0026	1.8397	2.0209	2.2859

Table 6.8: The effects of boundary conditions on central deflection of S-FGM plates subjected to UDL and SSL (a/h=10)

Power-law	Boundary conditions	e=0	e=0.2			e=0.4		
			SCE	BE	TE	SCE	BE	TE
UDL								
1	SSSS	1.0201	1.1239	1.163	1.1637	1.2567	1.3692	1.3677
	SCSC	0.5212	0.5774	0.5937	0.5961	0.6509	0.6977	0.7024
	SCCC	0.4398	0.4875	0.501	0.5031	0.5499	0.5885	0.593
	CCCC	0.3538	0.3926	0.4029	0.4049	0.4437	0.4731	0.4776
2	SSSS	1.2073	1.3372	1.3757	1.3791	1.5062	1.616	1.6208
	SCSC	0.6091	0.6775	0.6933	0.6976	0.7678	0.8125	0.8224
	SCCC	0.5134	0.5712	0.5842	0.5881	0.6477	0.6846	0.6935
	CCCC	0.4117	0.4586	0.4684	0.4719	0.5207	0.5486	0.5569
5	SSSS	1.4338	1.5847	1.632	1.6363	1.7808	1.9111	1.9179
	SCSC	0.7148	0.7928	0.8125	0.818	0.8954	0.9493	0.9621
	SCCC	0.6018	0.6677	0.6839	0.6888	0.7544	0.7989	0.8104
	CCCC	0.4813	0.5344	0.5468	0.5512	0.6045	0.6384	0.6491
SSL								
1	SSSS	0.6467	0.7128	0.7373	0.7379	0.7973	0.868	0.8673
	SCSC	0.3532	0.3912	0.4024	0.4039	0.4409	0.4728	0.4759
	SCCC	0.303	0.3358	0.3452	0.3465	0.3787	0.4056	0.4084
	CCCC	0.2536	0.2814	0.2889	0.2902	0.3178	0.3393	0.3422
2	SSSS	0.765	0.8474	0.8716	0.8739	0.9548	1.0237	1.0272
	SCSC	0.4129	0.4592	0.47	0.4729	0.5204	0.5509	0.5574
	SCCC	0.3539	0.3937	0.4027	0.4053	0.4463	0.472	0.4779
	CCCC	0.2955	0.329	0.3362	0.3386	0.3734	0.3938	0.3995
5	SSSS	0.9079	1.0037	1.0334	1.0363	1.1281	1.2099	1.2148
	SCSC	0.4848	0.5376	0.5511	0.5547	0.6071	0.6439	0.6523
	SCCC	0.415	0.4604	0.4717	0.475	0.5201	0.5511	0.5588
	CCCC	0.3457	0.3837	0.3928	0.3958	0.434	0.4586	0.466

$W = \frac{10E_T h^3}{q_0 a^4} w(\frac{a}{2}, \frac{b}{2}, \frac{h}{2})$ for deflection and $\bar{\sigma}_{11} = \frac{h}{q_0 a}\sigma_{11}(\frac{a}{2}, \frac{b}{2}, \frac{h}{3})$ for in-plane stress is assumed for study. The influence of material index k=(1, 4, 10) and side-to-thickness ratio a/h=(4, 10, 100) is also investigated. Higher the material index, stiffness of the plate will decreases, hence more will be corresponding deflection. An increment in the a/h ratio leads to an decrease in the maximum deflections, which concludes that thick plates provides more deflection than moderately thick and thin plats. The variations of dimensionless deflection

Table 6.9: The non-dimensional deflection of perfect P-FGM plate for sinusoidal distributed load MM2

a/h	Method	k=1		k=4		k=10	
		Deflection	$\bar{\sigma}_{11}$	Deflection	$\bar{\sigma}_{11}$	Deflection	$\bar{\sigma}_{11}$
4	Present	0.7266	0.5649	1.1613	0.4267	1.3861	0.3126
	Carrera *et al.* [256]	0.7289	0.7856	1.1673	0.5986	1.3925	0.4345
	Neves *et al.* [257]	0.7308	0.5806	1.1553	0.4338	1.376	0.3112
	Nguyen *et al.* [258]	0.7279	0.5811	1.1588	0.4391	1.3882	0.3218
10	Present	0.5885	1.4425	0.8817	1.1393	1.0079	0.8487
	Carrera *et al.*	0.5890	2.0068	0.8828	1.5874	1.0090	1.1807
	Neves *et al.* [257]	0.5913	1.4874	0.877	1.1592	0.9952	0.8468
	Nguyen *et al.* [258]	0.5882	1.4896	0.8791	1.1757	1.0051	0.87581
100	Present	0.5623	14.4833	0.8284	11.5350	0.9359	8.6177
	Carrera *et al.*	0.5625	20.149	0.8286	16.047	0.9361	11.989
	Neves *et al.* [257]	0.5648	14.944	0.8241	11.737	0.9228	8.6011
	Nguyen *et al.* [258]	0.5622	14.989	0.8280	11.939	0.9354	8.9198

with parameter (e) for three types of porosity distributions functions are depicted in Fig. (6.5). The deflections are evaluated for P-FGM plate under uniform distributed force for different material index ($k = 0.1, 0.5, 1$) and thickness of plate is assumed to be $h = a/10$. The figure shows that, higher porosity index (e) results in more central deflections, as the elasticity modulus of plate reduces with increasing values of e. The curves corresponding to SCE distribution always locate below the BE and TE distributions curves for any value of material index. This reveals that porosity distribution type has unique impact on non-dimensional deflection.

The influence of span-thickness ratio on the static deflection of porous ($e = 0.2$) plate for different porosity distributions is assessed in Fig. (6.6). The results are displayed for P-FGM and S-FGM simply supported plates with power-law exponent (k=2) subjected to SSL and material properties MM2 are considered. It is seen that the central deflection for higher span-thickness (a/h) value is less than corresponding to smaller a/h ratio. Moreover, the deflection decreases significantly as a/h ratio increase from 2 to 4, i.e maximum reduction

in deflection is approximately 39%. Also the influence of P-FGM and S-FGM distribution is observed on predicting the maximum deflection at center. The S-FGM plate possesses smaller deflections at the middle of plate than P-FGM distribution. The non-dimensional deflections for various aspect ratio and different kind of boundary conditions are shown in Fig. (6.7). It is seen that the increase in aspect ratio have increasing effect on normalized deflection for any type of porosity distribution. As it is clear that SSSS plate obtained more deflection value than plate with SCSC boundary conditions. The percentage decrease in deflection between SSSS and SCSC FG porous plate is approximately 45% for b/a=1, whereas the difference is increases significantly as b/a ratio approaches towards 3.

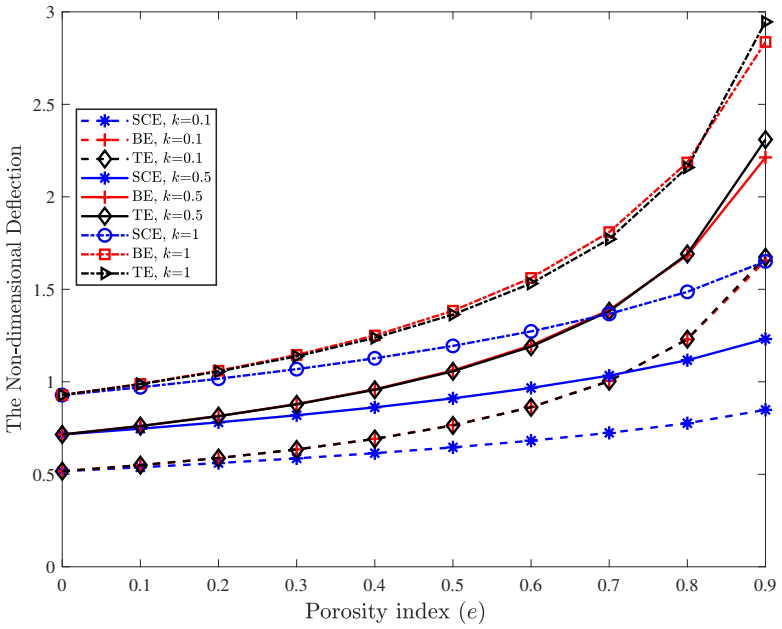

Figure 6.5: Effect of porosity parameter on dimensionless deflection of P-FGM plate subjected to UDL (a/h=10).

6.2.2 Buckling Response

The mathematical system given in Eq. (3.49) is solved to yield the buckling response of the FG plate. The several numerical results for buckling analysis are presented in this section for perfect and porous plates. The assumed FG plate is subjected to compressive uni-axial and bi-axial loads. The non-dimensional form for the buckling load parameter is defined as $\bar{N_\sigma} = \frac{N_\sigma a^2}{E_B h^3}$. Initially, the stability behavior of simply supported S-FGM plate is investigated and the non-dimensional buckling loads for uni-axial loading are evaluated for perfect FG plate by using present theory. The obtained results for critical buckling are tabulated in Table (6.10) along with previous published results given by Jung and Han [254] for different

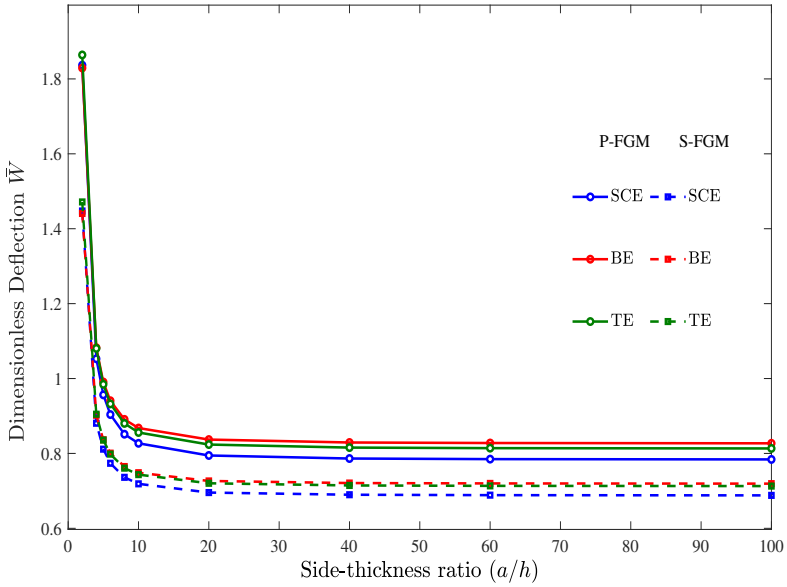

Figure 6.6: Effect of side to thickness ratio on central deflection of P-FGM and S-FGM plate subjected to SSL (MM2).

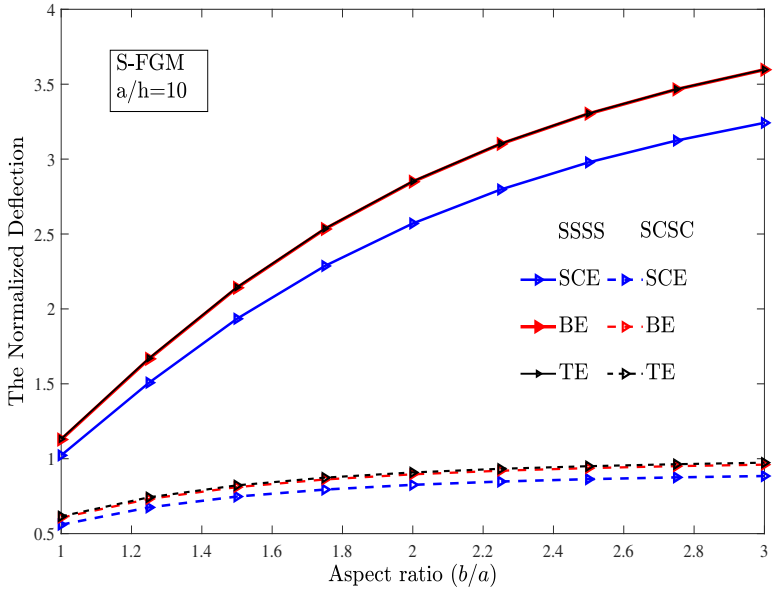

Figure 6.7: The effect of aspect ratio on normalized deflection of S-FGM plate under different boundaries conditions ($k = 2, e = 0.5$)

values of thickness ratio and material index (k). It is found that present approach results are well agreed with those obtained form Jung and Han [254] for S-FGM plate. In second example, an P-FGM plate made of Aluminum/Alumina (MM2) is taken and effect of porosity distributions, power-law indices and a/h ratios on the non-dimensional buckling load

Table 6.10: The critical buckling load of simply supported perfect S-FGM square plates (MM1).

a/h	(k=1)		k=5		k=10	
	Present (S-FGM)	Jung and Han [254]	Present (S-FGM)	Jung and Han [254]	Present (S-FGM)	Jung and Han [254]
5	13.7420	13.7221	10.1995	10.1852	9.6914	9.6792
10	15.6616	15.6552	11.1566	11.1520	10.5346	10.5306
20	16.2304	16.2284	11.4252	11.4238	10.7693	10.7681
100	16.4216	16.4209	11.5142	11.5137	10.8468	10.8464

parameter is assessed. In Table (6.11), the numerical results due to newly developed secant hyperbolic theory for uni-axial buckling loads for porous FG simply supported plate are also compared with analytical (IHSDT) results for various porosity parameters e and porosity distributions. It is concluded from Table (6.11) that the porosity has significant influence on buckling behavior of FGM plate, that is perfect plate possess higher critical buckling load as compare to porous plate. Also, it is noted that the fundamental buckling loads are reduced with increment in material index (k), which concludes that the homogeneous plate (k=0) attained the higher critical buckling load. This is due to that the FG plate become softer when power-law index changes from 0 to 1, hence value of buckling load parameter decreases.

As an next example, additional results of uniaxial and biaxial buckling load parameters for S-FGM plate (MM1) are presented in Table (6.12) for various material exponent, span-thickness ratio (a/h) and porosity distributions. It is noticed that, a/h ratio has the considerable effect on non-dimensional buckling load, i.e with rise in a/h ratio the corresponding buckling load value increases for any porosity distribution type. Moreover, the effect of in-plane loading conditions on the buckling behavior is clearly shown in Table (6.12), the values of critical loads in case of uni-axial buckling are double relative to the bi-axial compressive force.

The critical loads for uni-axial case are depicted in Fig. (6.8) for P-FGM plate and effects of different boundary conditions are studied. The properties of material are taken as MM2 in this case. The porosity effect on non-dimensional buckling load is also shown for three types of porosity models, where dimensionless buckling load decreases as the magnitude of porosity increases. Moreover, the plate with SSSS boundary conditions possesses less critical buckling value as compare to SCSC and CCCC boundary conditions. The SCE distribution attained the highest buckling load parameter among others porosity distributions.

Table 6.11: The stability behavior of porous P-FGM plate subjected to uni-axial load

a/h	Porosity Model	e	$k=0$		$k=0.5$		$k=1$	
			Present (New)	Analytical (IHSDT)	Present (New)	Analytical (IHSDT)	Present (New)	Analytical (IHSDT)
5	Perfect Plate	0	16.0466	16.1003	10.6396	10.6722	8.2359	8.2597
	SCE	0.2	14.6133	14.6528	9.6367	9.6607	7.4447	7.4619
		0.4	13.1027	13.1249	8.5857	8.5994	6.6133	6.6228
	BE	0.2	14.0777	14.1232	9.3367	9.3631	7.2218	7.2405
		0.4	11.9626	11.9991	7.9391	7.9591	6.1365	6.1501
	TE	0.2	14.0777	14.1232	9.3152	9.3442	7.2135	7.2354
		0.4	11.9626	11.9991	7.907	7.9320	6.1305	6.1503
10	Perfect plate	0	18.5869	18.6030	12.1276	12.1370	9.3427	9.3496
	SCE	0.2	17.1488	17.1606	11.1034	11.1104	8.5298	8.5347
		0.4	15.6798	15.6863	10.0539	10.0578	7.6908	7.6934
	BE	0.2	16.3371	16.3508	10.6519	10.6442	8.1856	8.1909
		0.4	13.8909	13.9018	9.0383	9.0440	6.9376	6.9413
	TE	0.2	16.3371	16.3508	10.6496	10.6581	8.2141	8.2204
		0.4	13.8909	13.9018	9.063	9.0704	7.0083	7.0141

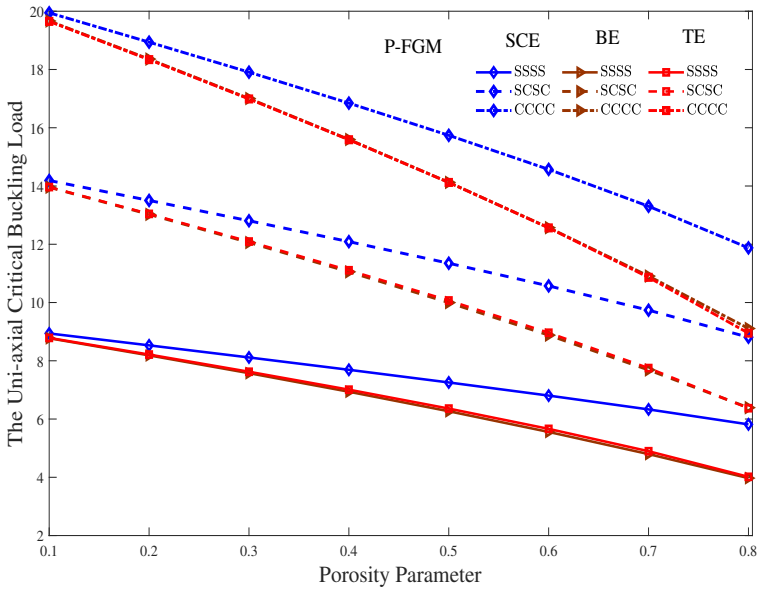

Figure 6.8: The plotting of uni-axial buckling loads w.r.t various porosity indices for different boundary conditions. (a/h=10, k=1).

Table 6.12: The critical buckling load for S-FGM plates subjected to uni-axial and bi-axial force

a/h	Material index (k)	e=0	e=0.2			e=0.4		
			SCE	BE	TE	SCE	BE	TE
Uni-axial Buckling								
5	0	30.719	27.923	26.942	26.942	24.968	22.892	22.892
	0.5	15.3752	13.8899	13.4967	13.4468	12.3244	11.4828	11.4028
	1	13.742	12.3511	12.0684	11.9964	10.8876	10.2824	10.161
	5	10.1995	9.1721	8.9816	8.8975	8.09	7.6986	7.5463
10	0	36.170	33.349	31.788	31.788	30.462	27.028	27.028
	0.5	17.8299	16.299	15.6487	15.6507	14.719	13.286	13.3167
	1	15.6616	14.2106	13.7381	13.7275	12.704	11.6699	11.6784
	5	11.1566	10.0921	9.8021	9.7748	8.9787	8.3716	8.338
50	0	38.355	35.571	33.737	33.737	32.783	28.693	28.693
	0.5	18.7937	17.2614	16.4937	16.5204	15.7007	13.9924	14.0755
	1	16.3973	14.9332	14.3772	14.3946	13.4247	12.1991	12.2667
	5	11.5029	10.4278	10.0981	10.0941	9.3071	8.6132	8.6283
Bi-axial Buckling								
5	0	15.359	13.961	13.471	13.471	12.484	11.446	11.446
	0.5	7.6876	6.94495	6.74835	6.7234	6.1622	5.7414	5.7014
	1	6.871	6.17555	6.0342	5.9982	5.4438	5.1412	5.0802
	5	5.0998	4.5861	4.4908	4.4488	4.045	3.8493	3.7732
10	0	18.085	16.674	15.894	15.894	15.231	13.514	13.514
	0.5	8.9149	8.1495	7.8244	7.8254	7.3595	6.643	6.6584
	1	7.8308	7.1053	6.8691	6.8638	6.352	5.835	5.8392
	5	5.5783	5.0461	4.9011	4.8874	4.4894	4.1858	4.169
50	0	19.178	17.785	16.869	16.869	16.392	14.347	14.347
	0.5	9.3969	8.6307	8.2469	8.2602	7.8504	6.9962	7.0378
	1	8.1987	7.4666	7.1886	7.1973	6.7124	6.0996	6.1334
	5	5.7515	5.2139	5.0491	5.0471	4.6536	4.3066	4.3142

6.3 Conclusions

The FE analysis for newly developed theory has been done in this chapter. The results are provided for laminated and porous FG plate. In the present study, stress analysis, bending

and buckling response of S-FGM and P-FGM plates are evaluated. Three types of porosity distribution in terms of cosine functions are taken for modeling of FG porous plates. The higher shear deformation theory involving secant hyperbolic based shear strain function is proposed to assess the static and stability behavior of considered plates. The finite element formulation in framework of minimum energy principle is employed to derive the equations of motion. The numerical solutions of non-dimensional deflections and critical buckling loads are determined for FG plate under various boundary conditions. Two types of distributed loads UDL and SSL are considered under plate deformation. Through the comparison study of results, it is observed that the proposed theory is well accurate for analysis of laminated and FGM plates and revealed good agreement with available results in literature. The influences of parameters such as span-thickness ratio, power-law index, porosity factor, aspect ratio, boundary constraints etc. on mechanical behavior of FG plates have also assessed. After confirming the accuracy, the present results will be used as the foundation for further research. The concluded summary of the proposed work is as follows:

- The non-dimensional deflections for P-FGM and S-FGM plates remains same for homogeneous plate (k=0, 1).
- As the value of aspect ratio increases from b/a= 1 to 2, the magnitude of deformation also increase significantly.
- The non-dimensional displacement increases with increasing the porosity parameter for all boundary constraints.
- It is noticed that the critical buckling loads decrease significantly when material index (k) increases for any porosity distribution. Due to increment in k, the FG plate becomes metallic rich. Since the metal has less Young's modulus relative to ceramic, therefore the buckling load decreases.

Chapter 7

Summary and Future Scope

The final chapter of this thesis is to briefly summarise the main findings and provide an perspective on potential future research. The primary outcomes of the thesis focus on developing the the modeling and analysis techniques for investigating laminated and functionally graded composite structures. The efficiency of proposed model on analysing such structures has been achieved by comparing the results with existing models. Furthermore, we also describe a number of intriguing potential extensions of the proposed models for future research ideas.

7.1 Summary

This thesis explores the use of mathematical modelling as an effective tool for understanding and predicting the mechanical behavior of composite structures. The study focuses on the development and implementation of mathematical models to examine the mechanical behaviour of these composite structures under different loading conditions. The thesis begins by providing a comprehensive review of existing mathematical models and solution methodologies, discussing their strengths and limitations. Subsequently, it introduces novel mathematical formulations that aim to enhance the accuracy and efficiency of predicting the mechanical responses of composite structures. Thus, the literature review concerning about the static, buckling and free vibration response of composite structures employing various analytical and numerical methods has presented in detailed. In industry and emerging fields of technology, laminated and functionally graded composite plates are extensively utilised. Different plate theories are available for accurately model these plates and to consider the shear deformation effect. In addition to the advancement in plate theories, significant progress has been achieved in solution methodologies. The method used to derive the governing mathematical framework for practical applications is an important feature for accurate analysis. Thus the literature revealed that the Navier's solution approach is most accurate and simplest to obtain analytical solutions for simply supported structures. Thus the literature survey on solution and modeling approaches have motivated us to complete our first objective.

For the first objective, the multi-layered composite rectangular plate is considered and a new higher order shear deformation theory is developed to model the plate. The Navier technique is employed to solve the governing equations and yield the desired mechanical responses. The static and buckling responses are evaluated for cross-ply and angle-ply laminated plates. The accuracy of the results obtained from the proposed theory is assessed by comparing them with existing solutions of 3D elasticity theory and other higher order plate theories. The proposed theory for evaluating non-dimensional deflections and stresses agree well with previously developed theories for thick plate (a/h=4) and gives better results for moderate thick to thin plates ($a/h \geq 10$). An investigation is also conducted to analyse the impact of several factors, including aspect ratio, lamination sequence, and span thickness ratio, on the static and buckling behaviour of laminated plates.

- It may be inferred that when the aspect ratio (b/a) of a laminated plate rises, the deflection correspondingly increases. Moreover, the non-dimensional displacement decreases with increment in side-thickness ratio, which conclude that thick plate possesses higher non-dimensional deflection.

- The maximum transverse deflection of anti-symmetric square plate reduces with increase in number of layers.

- Furthermore, it has been determined that the multi-layered rectangular laminate exhibited greater deflection than corresponding square plate.

- The dimensionless uni-axial buckling load value for symmetric cross-ply composite plate increases with increment in modulus ratio and decreases as number of layers increase.

- The newly proposed theory can be taken as benchmark to further study the structural behavior of multi-layered composite structures.

As an other application, the FGM plate with porosity was considered and analyzed by implementation of Navier's method. Thus to complete the third objective, the IHSDT is proposed for the first time to investigate the bending and buckling response of FG porous plate incorporating different porosity distributions. Moreover, the stresses are plotted against different z/h ratios for different distributions of porosity. The current findings on the static response of porous FG plates under UDL are in good agreement with the available prior results. Also new results are generated for bending and buckling loads for further applications in structural responses. The influence of various parameters including the distribution of porosity types, porosity parameter, power-law index, and loading conditions on dimensionless deflection and critical buckling loads are evaluated.

- It is revealed that the increase in porosity parameter decreases the stiffness of the FG plate, hence corresponding deflection increases.
- The FG plate under a UDL exhibit greater dimensionless deflections compared to the plates under a SSL.
- The mechanical response of the FG plate is influenced by the type of porosity distribution. The non-dimensional uniaxial and biaxial buckling loads of the plate with an uneven distribution are greater than those of the plate with an even porosity distribution.
- The increasing of span-thickness ratio a/h reduces the bending deflection of porous FG square plate subjected to uniformly as well as sinusoidal distributed load. In contrast, the uni-axial and bi-axial buckling loads of porous FG plate increase with increases in span-thickness ratio from 5 to 10.

The proposed solution methodology in objective first and third is efficient to derive the analytical solutions for structural response of composite simply supported plates. The Navier's method is well known to analyze the plate behavior under simply supported boundary conditions only. Therefore, to analyze structures with curved geometries and various boundary conditions, different numerical techniques have been developed in literature. Thus, the finite element method is proposed to find the numerical solutions and overcome the limitations of existing method. In order to fulfill the second objective, the secant hyperbolic shear deformation theory is applied to mathematically model the sigmoid FGM porous plate. Further, to enhance the applicability of FEM, the structural response of FGM porous plate is predicted subjected to general boundary conditions. The governing equations are derived by employing the C^0 isoparametric eight noded quadrilateral finite element in the mathematical formulations. The new numerical results are evaluated for flexural and stability responses for P-FGM and S-FGM plates and comparison study have also carried out with some analytical results. It is seen that the non-dimensionalized deflection of FGM plate decreases as the span-thickness ratio (a/h) increases.

- It is observed that the dimensionless deflection diminishes when the boundary conditions change from simply-supported to clamped edge condition.
- The average reduction in normalised deflection from simply supported to clamped end conditions is approximately 35% for a uniform load, while the decrease is nearly 40% for a plate subjected to SSL.
- The non-dimensional deflections for P-FGM and S-FGM plates remains same for homogeneous plate (k=0, 1).

The research not only enhances our understanding of analysis of composite structures but also provides practical tools for engineers and researchers to optimize the mechanical performance of composite structures in real-world applications. The modeling and solution techniques presented in this thesis have demonstrated their improvement over previous research. Our work is expected to make a valuable contribution to the advancement in analysis of laminated and FGM structures. The present results will be used as the foundation for further research.

7.2 Future Scope

This section explores potential research areas for future extensions of the proposed work. Some possible research directions are outlined below.

- The present work deals with static loading conditions to examine the behavior of composite FGM plates. Therefore, to understand the dynamic response and failure mechanisms of FGM plates, modeling techniques can also be extended to dynamic loading conditions, including impact and vibration analysis.
- The present work studied the static and buckling response of rectangular laminated plate. The proposed theory can be extended to analyze the structural behavior of laminated skew plates.
- The research can be extended to nonlinear analysis of composite structures to predict the dynamic behavior of these structures under various loading conditions and large deformations.
- The research can also be extended to artificial neural network methodologies for estimating structural damage in modeling the composites.

Appendix

Appendix A

$\bar{\mathbb{K}}^C_{11} = A_{11}\beta^2 + A_{66}\gamma^2$, $\bar{\mathbb{K}}^C_{12} = A_{12}\beta\gamma + A_{66}\beta\gamma$, $\bar{\mathbb{K}}^C_{13} = -(B_{11}\beta^2 + (B_{12} + 2B_{66})\gamma^2)\beta$

$\bar{\mathbb{K}}^C_{14} = \left[(\Omega B_{11} + E_{11})\beta^2 + (\Omega B_{66} + E_{66})\gamma^2\right]$, $\bar{\mathbb{K}}^C_{15} = (\Omega B_{12} + E_{12} + \Omega B_{66} + E_{66})\beta\gamma$,

$\bar{\mathbb{K}}^C_{21} = \bar{\mathbb{K}}^C_{12}$, $\bar{\mathbb{K}}^C_{22} = A_{66}\beta^2 + A_{22}\gamma^2$, $\bar{\mathbb{K}}^C_{23} = -(B_{22}\gamma^2 + (B_{12} + 2B_{66})\beta^2)\gamma$

$\bar{\mathbb{K}}^C_{24} = (\Omega B_{66} + E_{66} + \Omega B_{12} + E_{12})\beta\gamma$, $\bar{\mathbb{K}}^C_{25} = \left[(\Omega B_{66} + E_{66})\beta^2 + (\Omega B_{22} + E_{22})\gamma^2\right]$

$\bar{\mathbb{K}}^C_{31} = \bar{\mathbb{K}}^C_{13}$, $\bar{\mathbb{K}}^C_{32} = \bar{\mathbb{K}}^C_{23}$, $\bar{\mathbb{K}}^C_{33} = \left[D_{11}\beta^4 + (2D_{12} + 4D_{66})\beta^2\gamma^2 + D_{22}\gamma^4\right]$,

$\bar{\mathbb{K}}^C_{34} = -\left[(\Omega D_{11} + F_{11})\beta^2 + (\Omega D_{12} + F_{12})\gamma^2 + (2\Omega D_{66} + 2F_{66})\gamma^2\right]\beta$

$\bar{\mathbb{K}}^C_{35} = -\left[(\Omega D_{12} + F_{12})\beta^2 + (2\Omega D_{66} + 2F_{66})\beta^2 + (\Omega D_{22} + F_{22})\gamma^2\right]\gamma$

$\bar{\mathbb{K}}^C_{41} = \bar{\mathbb{K}}^C_{14}$, $\bar{\mathbb{K}}^C_{42} = \bar{\mathbb{K}}^C_{24}$, $\bar{\mathbb{K}}^C_{43} = \bar{\mathbb{K}}^C_{34}$

$$\bar{\mathbb{K}}^C_{44} = [\Omega(\Omega D_{11} + F_{11})\beta^2 + (\Omega F_{11} + H_{11})\beta^2 + \Omega(\Omega D_{66} + F_{66})\gamma^2 + (\Omega F_{66} + H_{66})\gamma^2 + \Omega^2 A_{55} + 2\Omega K_{55} + L_{55}]$$

$\bar{\mathbb{K}}^C_{45} = [\Omega(\Omega D_{12} + F_{12}) + (\Omega F_{12} + H_{12}) + \Omega(\Omega D_{66} + F_{66}) + (\Omega F_{66} + H_{66})]\beta\gamma$

$\bar{\mathbb{K}}^C_{51} = \bar{\mathbb{K}}^C_{15}, \bar{\mathbb{K}}^C_{52} = \bar{\mathbb{K}}^C_{25}, \bar{\mathbb{K}}^C_{53} = \bar{\mathbb{K}}^C_{35}, \bar{\mathbb{K}}^C_{54} = \bar{\mathbb{K}}^C_{45}$

$$\bar{\mathbb{K}}^C_{55} = [\Omega(\Omega D_{22} + F_{22})\gamma^2 + (\Omega F_{22} + H_{22})\gamma^2 + \Omega(\Omega D_{66} + F_{66})\beta^2 + (\Omega F_{66} + H_{66})\beta^2 + \Omega^2 A_{44} + 2\Omega K_{44} + L_{44}]$$

Appendix B

$\bar{\mathbb{K}}^A_{11} = A_{11}\beta^2 + A_{66}\gamma^2$, $\bar{\mathbb{K}}^A_{12} = A_{12}\beta\gamma + A_{66}\beta\gamma$, $\bar{\mathbb{K}}^A_{13} = -(3B_{16}\beta^2\gamma + (B_{26}\gamma^3))$

$\bar{\mathbb{K}}^A_{14} = [(2\Omega B_{16}\beta\gamma + 2E_{16}\beta\gamma]$, $\bar{\mathbb{K}}^A_{15} = (\Omega\beta^2 B_{16} + \beta^2 E_{16} + \Omega B_{26}\gamma^2 + E_{26}\gamma^2)$,

$\bar{\mathbb{K}}^A_{21} = \bar{\mathbb{K}}^A_{12}$, $\bar{\mathbb{K}}^A_{22} = A_{22}\gamma^2 + A_{66}\beta^2$, $\bar{\mathbb{K}}^A_{23} = -(B_{16}\beta^3 + 3B_{26}\beta\gamma^2)$

$\bar{\mathbb{K}}^A_{24} = (\Omega B_{16}\beta^2 + E_{16}\beta^2 + \Omega B_{26}\gamma^2 + E_{26}\gamma^2)$, $\bar{\mathbb{K}}^A_{25} = (2\Omega B_{26}\beta\gamma + 2E_{26}\beta\gamma)$

$\bar{\mathbb{K}}^A_{31} = \bar{\mathbb{K}}^A_{13}$, $\bar{\mathbb{K}}^A_{32} = \bar{\mathbb{K}}^A_{23}$, $\bar{\mathbb{K}}^A_{33} = \left[D_{11}\beta^4 + (2D_{12} + 4D_{66})\beta^2\gamma^2 + D_{22}\gamma^4\right]$,

$$\bar{\mathbb{K}}^A_{34} = -\left[(\Omega D_{11} + F_{11})\beta^2 + (\Omega D_{12} + F_{12})\gamma^2 + (2\Omega D_{66} + 2F_{66})\gamma^2\right]\beta$$

$$\bar{\mathbb{K}}^A_{35} = -\left[(\Omega D_{12} + F_{12})\beta^2 + (2\Omega D_{66} + 2F_{66})\beta^2 + (\Omega D_{22} + F_{22})\gamma^2\right]\gamma$$

$$\bar{\mathbb{K}}^A_{41} = \bar{\mathbb{K}}^A_{14},\ \bar{\mathbb{K}}^A_{42} = \bar{\mathbb{K}}^A_{24},\ \bar{K}^A_{43} = \bar{K}^A_{34}$$

$$\bar{\mathbb{K}}^A_{44} = [\Omega(\Omega D_{11} + F_{11})\beta^2 + (\Omega F_{11} + H_{11})\beta^2 + \Omega(\Omega D_{66} + F_{66})\gamma^2 + (\Omega F_{66} + H_{66})\gamma^2 + \Omega^2 A_{55} + 2\Omega K_{55} + L_{55}]$$

$$\bar{\mathbb{K}}^A_{45} = [\Omega(\Omega D_{12} + F_{12}) + (\Omega F_{12} + H_{12}) + \Omega(\Omega D_{66} + F_{66}) + (\Omega F_{66} + H_{66})]\,\beta\gamma$$

$$\bar{\mathbb{K}}^A_{51} = \bar{\mathbb{K}}^A_{15}, \bar{\mathbb{K}}^A_{52} = \bar{\mathbb{K}}^A_{25}, \bar{\mathbb{K}}^A_{53} = \bar{\mathbb{K}}^A_{35}, \bar{\mathbb{K}}^A_{54} = \bar{\mathbb{K}}^A_{45}$$

$$\bar{\mathbb{K}}^A_{55} = [\Omega(\Omega D_{22} + F_{22})\gamma^2 + (\Omega F_{22} + H_{22})\gamma^2 + \Omega(\Omega D_{66} + F_{66})\beta^2 + (\Omega F_{66} + H_{66})\beta^2 + \Omega^2 A_{44} + 2\Omega K_{44} + L_{44}]$$

Appendix C

$$\bar{K}_{11} = A_{11}\beta^2 + A_{66}\gamma^2,\ \bar{K}_{12} = A_{12}\beta\gamma + A_{66}\beta\gamma,\ \bar{K}_{13} = -(B_{11}\beta^2 + (B_{12} + 2B_{66})\gamma^2)\beta$$

$$\bar{K}_{14} = \left[(\Omega B_{11} + E_{11})\beta^2 + (\Omega B_{66} + E_{66})\gamma^2\right],\ \bar{K}_{15} = (\Omega B_{12} + E_{12} + \Omega B_{66} + E_{66})\beta\gamma,$$

$$\bar{K}_{21} = A_{66}\beta\gamma + A_{12}\beta\gamma,\ \bar{K}_{22} = A_{66}\beta^2 + A_{22}\gamma^2,\ \bar{K}_{23} = -(B_{22}\gamma^2 + (B_{12} + 2B_{66})\beta^2)\gamma$$

$$\bar{K}_{24} = (\Omega B_{66} + E_{66} + \Omega B_{12} + E_{12})\beta\gamma,\ \bar{K}_{25} = \left[(\Omega B_{66} + E_{66})\beta^2 + (\Omega B_{22} + E_{22})\gamma^2\right]$$

$$\bar{K}_{31} = -(B_{11}\beta^2 + (B_{12} + 2B_{66})\gamma^2)\beta,\ \bar{K}_{32} = -(B_{22}\gamma^2 + (B_{12} + 2B_{66})\beta^2)\gamma$$

$$\bar{K}_{33} = \left[D_{11}\beta^4 + (2D_{12} + 4D_{66})\beta^2\gamma^2 + D_{22}\gamma^4\right],$$

$$\bar{K}_{34} = -\left[(\Omega D_{11} + F_{11})\beta^2 + (\Omega D^{(0)}_{12} + F_{12})\gamma^2 + (2\Omega D_{66} + 2F_{66})\gamma^2\right]\beta$$

$$\bar{K}_{35} = -\left[(\Omega D_{12} + F_{12})\beta^2 + (2\Omega D_{66} + 2F_{66})\beta^2 + (\Omega D_{22} + F_{22})\gamma^2\right]\gamma$$

$\bar{K}_{41} = \bar{K}_{14}$, $\bar{K}_{42} = \bar{K}_{24}$, $\bar{K}_{43} = \bar{K}_{34}$

$$\bar{K}_{44} = [\Omega(\Omega D_{11} + F_{11})\beta^2 + (\Omega F_{11} + H_{11})\beta^2 + \Omega(\Omega D_{66} + F_{66})\gamma^2 + (\Omega F_{66} + H_{66})\gamma^2 + \Omega^2 A_{55} + 2\Omega K_{55} + L_{55}]$$

$$\bar{k}_{45} = [\Omega(\Omega D_{12} + F_{12}) + (\Omega F_{12} + H_{12}) + \Omega(\Omega D_{66} + F_{66}) + (\Omega F_{66} + H_{66})]\,\beta\gamma$$

$\bar{K}_{51} = \bar{K}_{15}, \bar{K}_{52} = \bar{K}_{25}, \bar{K}_{53} = \bar{K}_{35}, \bar{K}_{54} = \bar{K}_{45}$

$$\bar{K}_{55} = [\Omega(\Omega D_{22} + F_{22})\gamma^2 + (\Omega F_{22} + H_{22})\gamma^2 + \Omega(\Omega D_{66} + F_{66})\beta^2 + (\Omega F_{66} + H_{66})\beta^2 + \Omega^2 A_{44} + 2\Omega K_{44} + L_{44}]$$

Appendix D

Gauss Quadrature method: This method is employed to compute the integral involve in elemental stiffness matrix using the Jacobian as $[K]_k = \int_{-1}^{1}\int_{-1}^{1}[B]_k^T[D]_k[B]_k|J|d\zeta d\eta$ to simplify the transformation between ζ-η and x_1-x_2 coordinates.To evaluate the surface integration, following gaussian quadrature formula is used in general

$$\int_{-1}^{1}\int_{-1}^{1} f(x,y)dxdy = \sum_{i=1}^{n}\sum_{j=1}^{m}\omega_i\omega_j f(x_i,y_j)$$

where n and m are the number of quadrature points in the x and y directions. (x_i, y_j) are the quadrature points and ω_i, ω_j are the corresponding quadrature weights.

Table 7.1: Guassian locations and weights

Number of Points (n)	weight functions ω_i	Sampling Points
2	ω_1=1	λ_1=-0.577350269
	ω_2=1	λ_2=0.577350269
3	ω_1=0.55555556	λ_1=-0.77459667
	ω_2=0.88888889	λ_2=0
	ω_3=0.55555556	λ_3=0.77459667
4	ω_1=0.34785485	λ_1=–0.86113631
	ω_2=0.65214515	λ_2=-0.33998104
	ω_3=0.65214515	λ_3=0.33998104
	ω_4=0.34785485	λ_4=0.86113631

Bibliography

[1] M. Koizumi, FGM activities in Japan, Composites Part B: Engineering 28 (1-2) (1997) 1–4.

[2] M. Naebe, K. Shirvanimoghaddam, Functionally graded materials: A review of fabrication and properties, Applied Materials Today 5 (2016) 223–245.

[3] C. L. Thanh, L. V. Tran, T. Q. Bui, H. X. Nguyen, M. Abdel Wahab, Isogeometric analysis for size-dependent nonlinear thermal stability of porous FG microplates, Composite Structures 221 (2019) 110838.

[4] H. T. Thai, S. E. Kim, A simple higher-order shear deformation theory for bending and free vibration analysis of functionally graded plates, Composite Structures 96 (2013) 165–173.

[5] P. Tan, N. Nguyen-Thanh, T. Rabczuk, K. Zhou, Static, dynamic and buckling analyses of 3D FGM plates and shells via an isogeometric-meshfree coupling approach, Composite Structures 198 (2018) 35–50.

[6] J. Zhu, Z. Lai, Z. Yin, J. Jeon, S. Lee, Fabrication of Zro2–Nicr functionally graded material by powder metallurgy, Materials Chemistry and Physics 68 (1-3) (2001) 130–135.

[7] N. Wattanasakulpong, V. Ungbhakorn, Linear and nonlinear vibration analysis of elastically restrained ends FGM beams with porosities, Aerospace Science and Technology 32 (1) (2014) 111–120.

[8] G. Kaur, M. Singh, J. Kumar, T. De Beer, I. Nopens, Mathematical modelling and simulation of a spray fluidized bed granulator, Processes 6 (10) (2018) 195.

[9] N. J. Pagano, Exact solutions for rectangular bidirectional composites and sandwich plates:, Journal of Composite Materials 4 (1970) 20–34.

[10] N. J. Pagano, S. J. Hatfield, Elastic behavior of multilayered bidirectional composites, AIAA Journal 10 (7) (1972) 931–933.

[11] A. K. Noor, Stability of multilayered composite plates, Fibre Science and Technology 8 (2) (1975) 81–89.

[12] A. K. Noor, W. S. Burton, Three-dimensional solutions for antisymmetrically laminated anisotropic plates, Journal of Applied Mechanics, Transactions of ASME 57 (1990) 182–188.

[13] S. Srinivas, A. K. Rao, Bending, vibration and buckling of simply supported thick orthotropic rectangular plates and laminates, International Journal of Solids and Structures 6 (11) (1970) 1463–1481.

[14] L. Demasi, Three-dimensional closed form solutions and exact thin plate theories for isotropic plates, Composite Structures 80 (2) (2007) 183–195.

[15] E. Carrera, Theories and finite elements for multilayered, anisotropic, composite plates and shells, Archives of Computational Methods in Engineering 9 (2) (2002) 87–140.

[16] R. Singh, J. Kumar, G. Nelakanti, Numerical solution of singular boundary value problems using green's function and improved decomposition method, Journal of Applied Mathematics and Computing 43 (2013) 409–425.

[17] A. E. H. Love, A treatise on the mathematical theory of elasticity. cambridge university press 4th edition (1927).

[18] W. Koiter, A consistent first approximation in the general theory of thin elastic shells, The Theory of Thin Elastic Shells (1960) 12–33.

[19] E. Reissner, On the theory of bending of elastic plates, Journal of Mathematics and Physics 23 (1-4) (1944) 184–191.

[20] E. Reissner, The effect of transverse shear deformation on the bending of elastic plates, Journal of Applied Mechanics 12 (2) (1945) 69–77.

[21] R. D. Mindlin, Influence of rotatory inertia and shear on flexural motions of isotropic, elastic plates, Journal of Applied Mechanics 18 (1951) 31–38.

[22] P. C. Yang, C. H. Norris, Y. Stavsky, Elastic wave propagation in heterogeneous plates, International Journal of Solids and Structures 2 (1966) 665–684.

[23] F. P. Pai, A new look at shear correction factors and warping functions of anisotropic laminates, International Journal of Solids and Structures 32 (16) (1995) 2295–2313.

[24] E. Reissner, Reflections on the theory of elastic plates, Applied Mechanics Reviews 38 (1985).

[25] J. N. Reddy, A review of refined theories of laminated composite plates, The Shock and Vibration Digest 22 (7) (1990) 3–17.

[26] F. B. Hildebrand, E. Reissner, G. B. Thomas, Notes on the foundations of the theory of small displacements of orthotropic shells, Vol. 1833, National Advisory Committee for Aeronautics Washington, DC, 1949.

[27] M. Levinson, An accurate simple theory of the statics and dynamics of elastic plates, Mechanics Research Communication 7 (1980) 343–50.

[28] J. N. Reddy, A simple higher-order theory for laminated composite plates, Journal of Applied Mechanics 51 (4) (1984) 745–752.

[29] T. Kant, B. N. Pandya, A simple finite element formulation of a higher-order theory for unsymmetrically laminated composite plates, Composite Structures 9 (3) (1988) 215–246.

[30] D. K. Maiti, P. K. Sinha, Bending, free vibration and impact response of thick laminated composite plates, Computers & Structures 59 (1) (1996) 115–129.

[31] A. A. Khdeir, J. N. Reddy, Free vibrations of laminated composite plates using second-order shear deformation theory, Computers & Structures 71 (6) (1999) 617–626.

[32] T. Kant, K. Swaminathan, Analytical solutions for free vibration of laminated composite and sandwich plates based on a higher-order refined theory, Composite Structures 53 (1) (2001) 73–85.

[33] T. Kant, K. Swaminathan, Analytical solutions for the static analysis of laminated composite and sandwich plates based on a higher order refined theory, Composite Structures 56 (4) (2002) 329–344.

[34] K. Swaminathan, S. S. Patil, Higher order refined computational model with 12 degrees of freedom for the stress analysis of antisymmetric angle-ply plates–analytical solutions, Composite Structures 80 (4) (2007) 595–608.

[35] A. J. M. Ferreira, C. M. C. Roque, P. A. L. S. Martins, Analysis of composite plates using higher-order shear deformation theory and a finite point formulation based on the multiquadric radial basis function method, Composites Part B: Engineering 34 (7) (2003) 627–636.

[36] M. Touratier, An efficient standard plate theory, International Journal of Engineering Science 29 (8) (1991) 901–916.

[37] K. P. Soldatos, A transverse shear deformation theory for homogeneous monoclinic plates, Acta Mechanica 94 (3-4) (1992) 195–220.

[38] N. Grover, B. N. Singh, D. K. Maiti, New nonpolynomial shear-deformation theories for structural behavior of laminated-composite and sandwich plates, AIAA Journal 51 (8) (2013) 1861–1871.

[39] D. B. Singh, B. N. Singh, New higher order shear deformation theories for free vibration and buckling analysis of laminated and braided composite plates, International Journal of Mechanical Sciences 131 (2017) 265–277.

[40] M. Aydogdu, A new shear deformation theory for laminated composite plates, Composite Structures 89 (1) (2009) 94–101.

[41] A. Mahi, A. Tounsi, E. A. A. Bedia, A new hyperbolic shear deformation theory for bending and free vibration analysis of isotropic, functionally graded, sandwich and laminated composite plates, Applied Mathematical Modelling 39 (2015) 2489–2508.

[42] K. Kulkarni, B. Singh, D. Maiti, Analytical solution for bending and buckling analysis of functionally graded plates using inverse trigonometric shear deformation theory, Composite Structures 134 (2015) 147–157.

[43] N. Grover, D. K. Maiti, B. N. Singh, A new inverse hyperbolic shear deformation theory for static and buckling analysis of laminated composite and sandwich plates, Composite Structures 95 (2013) 667–675.

[44] T. Kant, et al., A critical review and some results of recently developed refined theories of fiber-reinforced laminated composites and sandwiches, Composite Structures 23 (4) (1993) 293–312.

[45] J. N. Reddy, D. H. Robbins Jr, Theories and computational models for composite laminates, Applied Mechanics Reviews 47 (6) (1994) 147–169.

[46] Y. M. Ghugal, R. P. Shimpi, A review of refined shear deformation theories for isotropic and anisotropic laminated beams, Journal of Reinforced Plastics and Composites 20 (3) (2001) 255–272.

[47] E. Carrera, S. Brischetto, A survey with numerical assessment of classical and refined theories for the analysis of sandwich plates, Applied Mechanics Reviews 62 (1) (2009) 1–17.

[48] D. K. Jha, T. Kant, R. K. Singh, A critical review of recent research on functionally graded plates, Composite Structures 96 (2013) 833–849.

[49] E. Carrera, Historical review of zig-zag theories for multilayered plates and shells, Applied Mechanics Reviews 56 (3) (2003) 287–308.

[50] S. A. Ambartsumyan, Theory of anisotropic plates, J. E. Ashton Edition, Technomic Publication Co., Stanford, CT (1970).

[51] S. Srinivas, A refined analysis of composite laminates, Journal of Sound and Vibration 306 (1973) 495–507.

[52] J. N. Reddy, A generalization of two-dimensional theories of laminated composite plates, Communications in Applied Numerical Methods 3 (3) (1987) 173–180.

[53] A. Toledano, H. Murakami, A composite plate theory for arbitrary laminate configurations, Journal of Applied Mechanics 54 (1987) 181–189.

[54] K. N. Cho, C. W. Bert, A. G. Striz, Free vibrations of laminated rectangular plates analyzed by higher order individual-layer theory, Journal of Sound and Vibration 145 (3) (1991) 429–442.

[55] A. J. M. Ferreira, C. M. C. Roque, R. M. N. Jorge, Analysis of composite plates by trigonometric shear deformation theory and multiquadrics, Computers & structures 83 (27) (2005) 2225–2237.

[56] M. Ćetković, D. Vuksanović, Bending, free vibrations and buckling of laminated composite and sandwich plates using a layerwise displacement model, Composite Structures 88 (2) (2009) 219–227.

[57] C. H. Thai, A. J. M. Ferreira, E. Carrera, H. Nguyen-Xuan, Isogeometric analysis of laminated composite and sandwich plates using a layerwise deformation theory, Composite Structures 104 (2013) 196–214.

[58] J. G. Ren, Bending theory of laminated plate, Composites Science and Technology 27 (3) (1986) 225–248.

[59] M. Di Sciuva, An improved shear-deformation theory for moderately thick multilayered anisotropic shells and plates, Journal of Applied Mechanics 51 (1987) 745–752.

[60] M. Cho, R. Parmerter, An efficient higher-order plate theory for laminated composites, Composite Structures 20 (2) (1992) 113–123.

[61] A. Chakrabarti, H. Chalak, M. A. Iqbal, A. H. Sheikh, A new FE model based on higher order zigzag theory for the analysis of laminated sandwich beam with soft core, Composite Structures 93 (2) (2011) 271–279.

[62] S. Ambartsumian, On the theory of bending plates, Izv Otd Tech Nauk AN SSSR 5 (5) (1958) 69–77.

[63] V. Panc, Theories of elastic plates, Springer Science & Business Media 2 (1975).

[64] B. N. Pandya, T. Kant, Finite element analysis of laminated composite plates using a higher-order displacement model, Composites Science and Technology 32 (2) (1988) 137–155.

[65] R. Shimpi, H. Arya, N. Naik, A higher order displacement model for the plate analysis, Journal of Reinforced Plastics and Composites 22 (18) (2003) 1667–1688.

[66] M. Karama, K. Afaq, S. Mistou, Mechanical behaviour of laminated composite beam by the new multi-layered laminated composite structures model with transverse shear stress continuity, International Journal of Solids and Structures 40 (6) (2003) 1525–1546.

[67] N. EL Meiche, A. Tounsi, N. Ziane, I. Mechab, et al., A new hyperbolic shear deformation theory for buckling and vibration of functionally graded sandwich plate, International Journal of Mechanical Sciences 53 (4) (2011) 237–247.

[68] J. Mantari, A. Oktem, C. G. Soares, A new higher order shear deformation theory for sandwich and composite laminated plates, Composites Part B: Engineering 43 (3) (2012) 1489–1499.

[69] J. L. Mantari, A. S. Oktem, C. G. Soares, A new trigonometric shear deformation theory for isotropic, laminated composite and sandwich plates, International Journal of Solids and Structures 49 (1) (2012) 43–53.

[70] A. Neves, A. Ferreira, E. Carrera, M. Cinefra, C. Roque, R. Jorge, C. Soares, A quasi-3D hyperbolic shear deformation theory for the static and free vibration analysis of functionally graded plates, Composite Structures 94 (5) (2012) 1814–1825.

[71] C. H. Thai, L. V. Tran, D. T. Tran, T. Nguyen-Thoi, H. Nguyen-Xuan, Analysis of laminated composite plates using higher-order shear deformation plate theory and node-based smoothed discrete shear gap method, Applied Mathematical Modelling 36 (11) (2012) 5657–5677.

[72] H. T. Thai, T. P. Vo, A new sinusoidal shear deformation theory for bending, buckling, and vibration of functionally graded plates, Applied Mathematical Modelling 37 (5) (2013) 3269–3281.

[73] A. M. Zenkour, A simple four-unknown refined theory for bending analysis of functionally graded plates, Applied Mathematical Modelling 37 (20-21) (2013) 9041–9051.

[74] S. Timoshenko, S. Woinowsky-Krieger, Theory of plates and shells, Vol. 2, McGraw-hill New York, 1959.

[75] J. N. Reddy, A. A. Khdeir, L. Librescu, Levy type solutions for symmetrically laminated rectangular plates using first-order shear deformation theory, Journal of Applied Mechanics 54 (3) (1987) 740–742.

[76] T. Kant, S. Marur, G. Rao, Analytical solution to the dynamic analysis of laminated beams using higher order refined theory, Composite Structures 40 (1) (1997) 1–9.

[77] H. Matsunaga, Vibration and stability of cross-ply laminated composite plates according to a global higher-order plate theory, Composite Structures 48 (4) (2000) 231–244.

[78] H. Matsunaga, Vibration and stability of angle-ply laminated composite plates subjected to in-plane stresses, International Journal of Mechanical Sciences 43 (8) (2001) 1925–1944.

[79] S. S. Akavci, Buckling and free vibration analysis of symmetric and antisymmetric laminated composite plates on an elastic foundation, Journal of Reinforced Plastics and Composites 26 (2007) 1907–1919.

[80] M. Karama, K. S. Afaq, S. Mistou, A new theory for laminated composite plates, Proceedings of the Institution of Mechanical Engineers, Part L: Journal of Materials: Design and Applications 223 (2) (2009) 53–62.

[81] H. Matsunaga, Free vibration and stability of angle-ply laminated composite and sandwich plates under thermal loading, Composite Structures 77 (2) (2007) 249–262.

[82] S. S. Akavci, A. H. Tanrikulu, Buckling and free vibration analyses of laminated composite plates by using two new hyperbolic shear-deformation theories, Mechanics of Composite Materials 44 (2) (2008).

[83] Y. M. Ghugal, A. S. Sayyad, Free vibration of thick orthotropic plates using trigonometric shear deformation theory, Latin American Journal of Solids and Structures 8 (3) (2011) 229–243.

[84] J. L. Mantari, C. G. Soares, Analysis of isotropic and multilayered plates and shells by using a generalized higher-order shear deformation theory, Composite Structures 94 (8) (2012) 2640–2656.

[85] N. Grover, B. N. Singh, D. K. Maiti, Analytical and finite element modeling of laminated composite and sandwich plates: An assessment of a new shear deformation theory for free vibration response, International Journal of Mechanical Sciences 67 (2013) 89–99.

[86] Y. M. Ghugal, A. S. Sayyad, Stress analysis of thick laminated plates using trigonometric shear deformation theory, International Journal of Applied Mechanics 5 (01) (2013) 1350003.

[87] B. Adim, T. H. Daouadji, A. Rabahi, A simple higher order shear deformation theory for mechanical behavior of laminated composite plates, International Journal of Advanced Structural Engineering (IJASE) 8 (2) (2016) 103–117.

[88] K. Y. Lam, C. M. Wang, X. Q. He, Canonical exact solutions for Levy-plates on two-parameter foundation using green's functions, Engineering Structures 22 (4) (2000) 364–378.

[89] Y. Xiang, C. M. Wang, Exact buckling and vibration solutions for stepped rectangular plates, Journal of Sound and Vibration 250 (3) (2002) 503–517.

[90] Y. Xiang, Y. B. Zhao, G. W. Wei, Levy solutions for vibration of multi-span rectangular plates, International Journal of Mechanical Sciences 44 (6) (2002) 1195–1218.

[91] H. Hashemi, S. H. Taher, H. R. Damavandi, Free vibration of functionally graded rectangular plates using first-order shear deformation plate theory, Applied Mathematical Modelling 34 (5) (2010) 1276–1291.

[92] A. H. Baferani, A. R. Saidi, E. Jomehzadeh, An exact solution for free vibration of thin functionally graded rectangular plates, Proceedings of the Institution of Mechanical Engineers, Part C: Journal of Mechanical Engineering Science 225 (3) (2011) 526–536.

[93] M. A. Farsangi, A. R. Saidi, Levy type solution for free vibration analysis of functionally graded rectangular plates with piezoelectric layers, Smart Materials and Structures 21 (9) (2012) 094017.

[94] M. Bodaghi, A. R. Saidi, Levy-type solution for buckling analysis of thick functionally graded rectangular plates based on the higher-order shear deformation plate theory, Applied Mathematical Modelling 34 (11) (2010) 3659–3673.

[95] M. Mohammadi, A. R. Saidi, E. Jomehzadeh, Levy solution for buckling analysis of functionally graded rectangular plates, Applied Composite Materials 17 (2) (2010) 81–93.

[96] Y. Hu, M. Khezri, K. Rasmussen, Analytical buckling solutions for Levy-type plates with edge and interior point-support, Thin-Walled Structures 145 (2019) 106419.

[97] A. S. Oktem, R. A. Chaudhuri, Levy type analysis of cross-ply plates based on higher-order theory, Composite Structures 78 (2) (2007) 243–253.

[98] S. D. Singh, R. Sahoo, Static and free vibration analysis of functionally graded CNT reinforced composite plates using trigonometric shear deformation theory, Structures 28 (2020) 685–696.

[99] J. Kim, J. N. Reddy, Analytical solutions for bending, vibration, and buckling of FGM plates using a couple stress-based third-order theory, Composite Structures 103 (2013) 86–98.

[100] S. R. Atashipour, A. R. Saidi, E. Jomehzadeh, On the boundary layer phenomenon in bending of thick annular sector plates using third-order shear deformation theory, Acta Mechanica 211 (1) (2010) 89–99.

[101] A. M. Zenkour, M. H. Aljadani, Buckling response of functionally graded porous plates due to a quasi-3d refined theory, Mathematics 10 (4) (2022) 565.

[102] R. Li, X. Ni, G. Cheng, Symplectic superposition method for benchmark flexure solutions for rectangular thick plates, Journal of Engineering Mechanics 141 (2) (2015) 04014119.

[103] W. Ritz, On a new method for solving some variational problems in mathematical physics, Journal for Pure and Applied Mathematics 135 (1908) 1–61.

[104] J. N. Reddy, An introduction to the finite element method, Vol. 3, McGraw-Hill New York, 2013.

[105] Y. X. Zhang, C. H. Yang, Recent developments in finite element analysis for laminated composite plates, Composite Structures 88 (1) (2009) 147–157.

[106] C. P. Wu, K. H. Chiu, Y. M. Wang, A differential reproducing kernel particle method for the analysis of multilayered elastic and piezoelectric plates, CMES-Computer Modeling in Engineering and Sciences 27 (3) (2008) 163–186.

[107] T. Belytschko, Y. Y. Lu, L. Gu, Element-free galerkin methods, International Journal for Numerical Methods in Engineering 37 (2) (1994) 229–256.

[108] K. Liew, X. Chen, J. Reddy, Mesh-free radial basis function method for buckling analysis of non-uniformly loaded arbitrarily shaped shear deformable plates, Computer Methods in Applied Mechanics and Engineering 193 (3-5) (2004) 205–224.

[109] Z. Han, A. Rajendran, S. N. Atluri, Meshless local petrov-galerkin (MLPG) approaches for solving nonlinear problems with large deformations and rotations, Computer Modeling in Engineering and Sciences 10 (1) (2005) 1–12.

[110] J. J. Monaghan, Why particle methods work, SIAM Journal on Scientific and Statistical Computing 3 (4) (1982) 422–433.

[111] A. J. M. Ferreira, A formulation of the multiquadric radial basis function method for the analysis of laminated composite plates, Composite Structures 59 (2003) 385–392.

[112] R. Bellman, J. Casti, Differential quadrature and long-term integration, Journal of Mathematical Analysis and Applications 34 (2) (1971) 235–238.

[113] C. W. Bert, M. Malik, Differential quadrature method in computational mechanics: a review, Applied Mechanics Review 49 (1) (1996) 1–28.

[114] W. Chen, A. G. Striz, C. W. Bert, A new approach to the differential quadrature method for fourth-order equations, International Journal for Numerical Methods in Engineering 40 (11) (1997) 1941–1956.

[115] T. Wu, G. Liu, A differential quadrature as a numerical method to solve differential equations, Computational Mechanics 24 (3) (1999) 197–205.

[116] Q. Chen, Y. W. Chan, Integral finite element method for dynamical analysis of elastic–viscoelastic composite structures, Computers & Structures 74 (1) (2000) 51–64.

[117] P. Ribeiro, A hierarchical finite element for geometrically non-linear vibration of thick plates, Meccanica 38 (1) (2003) 117–132.

[118] X. X. Hu, T. Sakiyama, C. W. Lim, Y. Xiong, et al., Vibration of angle-ply laminated plates with twist by Rayleigh–Ritz procedure, Computer Methods in Applied Mechanics and Engineering 193 (9-11) (2004) 805–823.

[119] A. Chakrabarti, A. H. Sheikh, A new triangular element to model inter-laminar shear stress continuous plate theory, International journal for numerical methods in engineering 60 (7) (2004) 1237–1257.

[120] A. Chakrabarti, A. H. Sheikh, Vibration of laminate-faced sandwich plate by a new refined element, Journal of Aerospace Engineering 17 (3) (2004) 123–134.

[121] K. Liew, Y. Huang, J. Reddy, Vibration analysis of symmetrically laminated plates based on fsdt using the moving least squares differential quadrature method, Computer Methods in Applied Mechanics and Engineering 192 (19) (2003) 2203–2222.

[122] P. Malekzadeh, G. Karami, Vibration of non-uniform thick plates on elastic foundation by differential quadrature method, Engineering Structures 26 (10) (2004) 1473–1482.

[123] U. S. Gupta, A. H. Ansari, S. Sharma, Buckling and vibration of polar orthotropic circular plate resting on winkler foundation, Journal of Sound and Vibration 297 (3-5) (2006) 457–476.

[124] F. A. Fazzolari, E. Carrera, Advanced variable kinematics ritz and galerkin formulations for accurate buckling and vibration analysis of anisotropic laminated composite plates, Composite Structures 94 (1) (2011) 50–67.

[125] F. A. Fazzolari, E. Carrera, Accurate free vibration analysis of thermo-mechanically pre/post-buckled anisotropic multilayered plates based on a refined hierarchical trigonometric Ritz formulation, Composite Structures 95 (2013) 381–402.

[126] O. Vaseghi, H. R. Mirdamadi, D. Panahandeh-Shahraki, Non-linear stability analysis of laminated composite plates on one-sided foundation by hierarchical Rayleigh–Ritz and finite elements, International Journal of Non-Linear Mechanics 57 (2013) 65–74.

[127] O. O. Oyekoya, D. Mba, A. M. Zafrany, Buckling and vibration analysis of functionally graded composite structures using the finite element method, Composite Structures 89 (1) (2009) 134–142.

[128] A. J. M. Ferreira, L. M. Castro, S. Bertoluzza, A high order collocation method for the static and vibration analysis of composite plates using a first-order theory, Composite Structures 89 (3) (2009) 424–432.

[129] M. Talha, B. N. Singh, Static response and free vibration analysis of FGM plates using higher order shear deformation theory, Applied Mathematical Modelling 34 (12) (2010) 3991–4011.

[130] L. Castro, A. J. M. Ferreira, S. Bertoluzza, R. C. Batra, J. N. Reddy, A wavelet collocation method for the static analysis of sandwich plates using a layerwise theory, Composite Structures 92 (2010) 1786–1792.

[131] Y. Hao, W. Zhang, J. Yang, Nonlinear dynamics of a FGM plate with two clamped opposite edges and two free edges, Acta Mechanica Solida Sinica 27 (4) (2014) 394–406.

[132] B. Zhang, Y. He, D. Liu, Z. Gan, L. Shen, A non-classical mindlin plate finite element based on a modified couple stress theory, European Journal of Mechanics-A/Solids 42 (2013) 63–80.

[133] J. L. Mantari, C. G. Soares, Generalized layerwise hsdt and finite element formulation for symmetric laminated and sandwich composite plates, Composite Structures 105 (2013) 319–331.

[134] A. Chakrabarti, H. D. Chalak, M. Iqbal, A. H. Sheikh, Buckling analysis of laminated sandwich beam with soft core, Latin American Journal of Solids and Structures 9 (3) (2012) 1–15.

[135] H. D. Chalak, A. Chakrabarti, A. H. Sheikh, M. A. Iqbal, C0 FE model based on hozt for the analysis of laminated soft core skew sandwich plates: Bending and vibration, Applied Mathematical Modelling 38 (4) (2014) 1211–1223.

[136] S. Pandey, S. Pradyumna, A new c0 higher-order layerwise finite element formulation for the analysis of laminated and sandwich plates, Composite Structures 131 (2015) 1–16.

[137] A. J. M. Ferreira, E. Carrera, M. Cinefra, E. Viola, F. Tornabene, N. Fantuzzi, A. M. Zenkour, Analysis of thick isotropic and cross-ply laminated plates by generalized differential quadrature method and a unified formulation, Composites Part B: Engineering 58 (2014) 544–552.

[138] B. Liu, A. J. M. Ferreira, Y. F. Xing, A. M. A. Neves, Analysis of composite plates using a layerwise theory and a differential quadrature finite element method, Composite Structures 156 (2016) 393–398.

[139] R. Ansari, J. Torabi, M. F. Shojaei, Buckling and vibration analysis of embedded functionally graded carbon nanotube-reinforced composite annular sector plates under thermal loading, Composites Part B: Engineering 109 (2017) 197–213.

[140] T. Belytschko, Y. Krongauz, D. Organ, M. Fleming, P. Krysl, Meshless methods: An overview and recent developments, Computer Methods in Applied Mechanics and Engineering 139 (1) (1996) 3–47.

[141] G. R. Liu, X. L. Chen, A mesh-free method for static and free vibration analyses of thin plates of complicated shape, Journal of Sound and Vibration 241 (5) (2001) 839–855.

[142] A. J. M. Ferreira, C. M. C. Roque, R. M. N. Jorge, Free vibration analysis of symmetric laminated composite plates by FSDT and radial basis functions, Computer Methods in Applied Mechanics and Engineering 194 (39-41) (2005) 4265–4278.

[143] A. J. M. Ferreira, C. M. C. Roque, R. M. N. Jorge, E. J. Kansa, Static deformations and vibration analysis of composite and sandwich plates using a layerwise theory and multiquadrics discretizations, Engineering Analysis with Boundary Elements 29 (12) (2005) 1104–1114.

[144] R. Vaghefi, G. H. Baradaran, H. Koohkan, Three-dimensional static analysis of thick functionally graded plates by using meshless Local Petrov-Galerkin MLPG method, Engineering Analysis with Boundary Elements 34 (6) (2010) 564–573.

[145] T. Q. Bui, M. N. Nguyen, C. Zhang, An efficient meshfree method for vibration analysis of laminated composite plates, Computational Mechanics 48 (2011) 175–193.

[146] J. D. Rodrigues, C. C. Roque, A. J. M. Ferreira, M. Cinefra, E. Carrera, Radial basis functions-differential quadrature collocation and a unified formulation for bending, vibration and buckling analysis of laminated plates, according to Murakami's zig-zag theory, Computers & Structures 90 (2012) 107–115.

[147] J. J. Monaghan, An introduction to SPH, Computer Physics Communications 48 (1) (1988) 89–96.

[148] N. Jafari, M. Azhari, Buckling of moderately thick arbitrarily shaped plates with intermediate point supports using a simple hp-cloud method, Applied Mathematics and Computation 313 (2017) 196–208.

[149] J. Belinha, A. L. Araújo, A. J. M. Ferreira, L. M. J. S. Dinis, et al., The analysis of laminated plates using distinct advanced discretization meshless techniques, Composite Structures 143 (2016) 165–179.

[150] L. Sator, V. Sladek, J. Sladek, Coupling effects in elastic analysis of FGM composite plates by mesh-free methods, Composite Structures 115 (2014) 100–110.

[151] V. N. Van Do, C. H. Lee, Nonlinear analyses of FGM plates in bending by using a modified radial point interpolation mesh-free method, Applied Mathematical Modelling 57 (2018) 1–20.

[152] V. N. Van Do, C. H. Lee, Mesh-free thermal buckling analysis of multilayered composite plates based on an nth-order shear deformation theory, Composite Structures 224 (2019) 111042.

[153] J. Huang, N. Nguyen-Thanh, J. Gao, Z. Fan, K. Zhou, Static, free vibration, and buckling analyses of laminated composite plates via an isogeometric meshfree collocation approach, Composite Structures 285 (2022) 115011.

[154] H. Chaabani, S. Mesmoudi, L. Boutahar, K. El Bikri, A high-order finite element continuation for buckling analysis of porous FGM plates, Engineering Structures 279 (2023) 115597.

[155] F. Mouaici, S. Benyoucef, H. A. Atmane, A. Tounsi, Effect of porosity on vibrational characteristics of non-homogeneous plates using hyperbolic shear deformation theory, Wind & Structures 22 (4) (2016) 429–454.

[156] E. l. Meiche, T. Noureddine, Z. Abdelouahed, I. Mechab, A new hyperbolic shear deformation theory for buckling and vibration of functionally graded sandwich plate, International Journal of Mechanical Sciences 53 (4) (2011) 237–247.

[157] Y. S. Joshan, N. Grover, B. N. Singh, Analytical modelling for thermo-mechanical analysis of cross-ply and angle-ply laminated composite plates, Aerospace Science and Technology 70 (2017) 137–151.

[158] L. L. Ke, J. Yang, S. Kitipornchai, M. A. Bradford, Bending, buckling and vibration of size-dependent functionally graded annular microplates, Composite Structures 94 (11) (2012) 3250–3257.

[159] A. Rezaei, A. Saidi, M. Abrishamdari, M. P. Mohammadi, Natural frequencies of functionally graded plates with porosities via a simple four variable plate theory: an analytical approach, Thin-Walled Structures 120 (2017) 366–377.

[160] N. Grover, D. Maiti, B. Singh, An efficient c0 finite element modeling of an inverse hyperbolic shear deformation theory for the flexural and stability analysis of laminated composite and sandwich plates, Finite Elements in Analysis and Design 80 (2014) 11–22.

[161] T. Kant, K. Swaminathan, Estimation of transverse/interlaminar stresses in laminated composites–a selective review and survey of current developments, Composite Structures 49 (1) (2000) 65–75.

[162] K. Swaminathan, D. Ragounadin, Analytical solutions using a higher-order refined theory for the static analysis of antisymmetric angle-ply composite and sandwich plates, Composite Structures 64 (3-4) (2004) 405–417.

[163] M. Aydogdu, Comparison of various shear deformation theories for bending, buckling, and vibration of rectangular symmetric cross-ply plate with simply supported edges, Journal of Composite Materials 40 (23) (2006) 2143–2155.

[164] S. S. Akavci, A. H. Tanrikulu, Buckling and free vibration analyses of laminated composite plates by using two new hyperbolic shear-deformation theories, Mechanics of Composite Materials 44 (2) (2008) 145.

[165] M. Karama, K. Afaq, S. Mistou, A new theory for laminated composite plates, Proceedings of the Institution of Mechanical Engineers, Part L: Journal of Materials: Design and Applications 223 (2) (2009) 53–62.

[166] J. L. Mantari, A. S. Oktem, C. G. Soares, Static and dynamic analysis of laminated composite and sandwich plates and shells by using a new higher-order shear deformation theory, Composite Structures 94 (1) (2011) 37–49.

[167] V. Piskunov, V. Verijenko, S. Adali, P. Tabakov, V. Prisyazhnyouk, S. Buryhin, Rational transverse shear deformation higher-order theory of anisotropic laminated plates and shells, International Journal of Solids and Structures 38 (36-37) (2001) 6491–6523.

[168] M. Dhuria, N. Grover, K. Goyal, Influence of porosity distribution on static and buckling responses of porous functionally graded plates, Structures 34 (2021) 1458–1474.

[169] T. Yu, S. Yin, T. Q. Bui, S. Xia, S. Tanaka, S. Hirose, NURBS-based isogeometric analysis of buckling and free vibration problems for laminated composites plates with complicated cutouts using a new simple FSDT theory and level set method, Thin-Walled Structures 101 (2016) 141–156.

[170] C. H. Thai, H. Nguyen-Xuan, N. Nguyen-Thanh, T. H. Le, T. Nguyen Thoi, T. Rabczuk, Static, free vibration, and buckling analysis of laminated composite reissner–mindlin plates using nurbs-based isogeometric approach, International Journal for Numerical Methods in Engineering 91 (6) (2012) 571–603.

[171] S. Merdaci, A. Tounsi, A. Bakora, A novel four variable refined plate theory for laminated composite plates, Steel and Composite Structure 22 (4) (2016) 713–732.

[172] J. N. Reddy, Mechanics of laminated composite plates and shells: theory and analysis, CRC press, 1997.

[173] N. S. Putcha, J. N. Reddy, Stability and natural vibration analysis of laminated plates by using a mixed element based on a refined plate theory, Journal of Sound and Vibration 104 (2) (1986) 285–300.

[174] A. J. M. Ferreira, L. M. Castro, C. Roque, J. N. Reddy, S. Bertoluzza, Buckling analysis of laminated plates by wavelets, Computers & Structures 89 (7-8) (2011) 626–630.

[175] L. Liu, L. Chua, D. Ghista, Mesh-free radial basis function method for static, free vibration and buckling analysis of shear deformable composite laminates, Composite Structures 78 (1) (2007) 58–69.

[176] A. K. Noor, Stability of multilayered composite plates, Fibre Science and Technology 8 (2) (1975) 81–89.

[177] J. Ren, Bending, vibration, and buckling, Handbook of Ceramics and Composites: Synthesis and Properties 1 (1990) 413.

[178] S. Suresh, A. Mortensen, Fundamentals of functionally graded materials, The Institute of Materials, 1998.

[179] M. Arefi, M. Kiani, A. M. Zenkour, Size-dependent free vibration analysis of a three-layered exponentially graded nano-/micro-plate with piezomagnetic face sheets resting on pasternak's foundation via mcst, Journal of Sandwich Structures & Materials 22 (1) (2020) 55–86.

[180] W. Y. Jung, W. T. Park, S. C. Han, Bending and vibration analysis of S-FGM microplates embedded in pasternak elastic medium using the modified couple stress theory, International Journal of Mechanical Sciences 87 (2014) 150–162.

[181] N. Wattanasakulpong, B. G. Prusty, D. W. Kelly, M. Hoffman, Free vibration analysis of layered functionally graded beams with experimental validation, Materials & Design 36 (2012) 182–190.

[182] K. Magnucki, P. Stasiewicz, Elastic buckling of a porous beam, Journal of Theoretical and Applied Mechanics 42 (4) (2004) 859–868.

[183] D. Chen, J. Yang, S. Kitipornchai, Elastic buckling and static bending of shear deformable functionally graded porous beam, Composite Structures 133 (2015) 54–61.

[184] D. Chen, S. Kitipornchai, J. Yang, Nonlinear free vibration of shear deformable sandwich beam with a functionally graded porous core, Thin-Walled Structures 107 (2016) 39–48.

[185] M. Jabbari, A. Mojahedin, A. Khorshidvand, M. Eslami, Buckling analysis of a functionally graded thin circular plate made of saturated porous materials, Journal of Engineering Mechanics 140 (2) (2014) 287–295.

[186] A. Mojahedin, E. F. Joubaneh, M. Jabbari, Thermal and mechanical stability of a circular porous plate with piezoelectric actuators, Acta Mechanica 225 (12) (2014) 3437–3452.

[187] T. Yu, T. Q. Bui, S. Yin, D. H. Doan, C. Wu, T. Van Do, S. Tanaka, On the thermal buckling analysis of functionally graded plates with internal defects using extended isogeometric analysis, Composite Structures 136 (2016) 684–695.

[188] Y. Q. Wang, Y. H. Wan, Y. F. Zhang, Vibrations of longitudinally traveling functionally graded material plates with porosities, European Journal of Mechanics-A/Solids 66 (2017) 55–68.

[189] M. Kamranfard, A. Saidi, A. Naderi, Analytical solution for vibration and buckling of annular sectorial porous plates under in-plane uniform compressive loading, Proceedings of the Institution of Mechanical Engineers, Part C: Journal of Mechanical Engineering Science 232 (12) (2018) 2211–2228.

[190] P. A. Demirhan, V. Taskin, Bending and free vibration analysis of Levy-type porous functionally graded plate using state space approach, Composites Part B: Engineering 160 (2019) 661–676.

[191] S. Trabelsi, A. Frikha, S. Zghal, F. Dammak, A modified FSDT-based four nodes finite shell element for thermal buckling analysis of functionally graded plates and cylindrical shells, Engineering Structures 178 (2019) 444–459.

[192] S. Trabelsi, S. Zghal, F. Dammak, Thermo-elastic buckling and post-buckling analysis of functionally graded thin plate and shell structures, Journal of the Brazilian Society of Mechanical Sciences and Engineering 42 (5) (2020) 1–22.

[193] M. Guellil, H. Saidi, F. Bourada, A. A. Bousahla, A. Tounsi, M. M. Al-Zahrani, M. Hussain, S. Mahmoud, Influences of porosity distributions and boundary conditions on mechanical bending response of functionally graded plates resting on pasternak foundation, Steel and Composite Structures 38 (1) (2021) 1–15.

[194] F. Y. Addou, M. Meradjah, A. A. Bousahla, A. Benachour, F. Bourada, A. Tounsi, S. Mahmoud, Influences of porosity on dynamic response of FG plates resting on Winkler/Pasternak/Kerr foundation using quasi 3D HSDT, Computers and Concrete 24 (4) (2019) 347–367.

[195] M. Medani, A. Benahmed, M. Zidour, H. Heireche, A. Tounsi, A. A. Bousahla, A. Tounsi, S. Mahmoud, Static and dynamic behavior of FG-CNT reinforced porous sandwich plate using energy principle, Steel and Composite Structures 32 (5) (2019) 595–610.

[196] J. Kim, K. K. Żur, J. N. Reddy, Bending, free vibration, and buckling of modified couples stress-based functionally graded porous micro-plates, Composite Structures 209 (2019) 879–888.

[197] M. Kaddari, A. Kaci, A. A. Bousahla, A. Tounsi, F. Bourada, A. Tounsi, E. Bedia, M. A. Al Osta, A study on the structural behaviour of functionally graded porous plates on elastic foundation using a new quasi-3D model: bending and free vibration analysis, Computers and Concrete 25 (1) (2020) 37–57.

[198] V. Kumar, S. Singh, V. Saran, S. Harsha, Vibration characteristics of porous FGM plate with variable thickness resting on pasternak's foundation, European Journal of Mechanics-A/Solids 85 (2021) 104124.

[199] N. V. Nguyen, H. Nguyen Xuan, D. Lee, J. Lee, A novel computational approach to functionally graded porous plates with graphene platelets reinforcement, Thin-Walled Structures 150 (2020) 106684.

[200] Y. S. Al Rjoub, J. A. Alshatnawi, Free vibration of functionally-graded porous cracked plates, Structures 28 (2020) 2392–2403.

[201] T. T. Tran, Q. H. Pham, T. Nguyen-Thoi, Static and free vibration analyses of functionally graded porous variable-thickness plates using an edge-based smoothed finite element method, Defence Technology 17 (2021) 971–986.

[202] K. Xie, Y. Wang, H. Niu, H. Chen, Large-amplitude nonlinear free vibrations of functionally graded plates with porous imperfection: A novel approach based on energy balance method, Composite Structures 246 (2020) 112367.

[203] E. Reissner, Y. Stavsky, Bending and stretching of certain types of heterogeneous aeolotropic elastic plates, Journal of Applied Mechanics 28 (3) (1961) 402–408.

[204] Z. Hashin, Analysis of Composite Materials -A Survey, Journal of Applied Mechanics 50 (3) (1983) 481–505.

[205] J. N. Reddy, J. Berry, Nonlinear theories of axisymmetric bending of functionally graded circular plates with modified couple stress, Composite Structures 94 (12) (2012) 3664–3668.

[206] E. Arshid, A. R. Khorshidvand, Free vibration analysis of saturated porous FG circular plates integrated with piezoelectric actuators via differential quadrature method, Thin-Walled Structures 125 (2018) 220–233.

[207] L. Della Croce, P. Venini, Finite elements for functionally graded Reissner–Mindlin plates, Computer Methods in Applied Mechanics and Engineering 193 (9-11) (2004) 705–725.

[208] K. Mercan, A. K. Baltacıoglu, O. Civalek, Free vibration of laminated and FGM/CNT composites annular thick plates with shear deformation by discrete singular convolution method, Composite Structures 186 (2018) 139–153.

[209] S. Zghal, A. Frikha, F. Dammak, Large deflection response-based geometrical nonlinearity of nanocomposite structures reinforced with carbon nanotubes, Applied Mathematics and Mechanics 41 (8) (2020) 1227–1250.

[210] T. V. Vu, A. Khosravifard, M. Hematiyan, T. Q. Bui, A new refined simple TSDT-based effective meshfree method for analysis of through-thickness FG plates, Applied Mathematical Modelling 57 (2018) 514–534.

[211] A. Frikha, S. Zghal, F. Dammak, Dynamic analysis of functionally graded carbon nanotubes-reinforced plate and shell structures using a double directors finite shell element, Aerospace Science and Technology 78 (2018) 438–451.

[212] J. L. Mantari, C. G. Soares, A novel higher-order shear deformation theory with stretching effect for functionally graded plates, Composites Part B: Engineering 45 (1) (2013) 268–281.

[213] S. Zghal, A. Frikha, F. Dammak, Static analysis of functionally graded carbon nanotube-reinforced plate and shell structures, Composite Structures 176 (2017) 1107–1123.

[214] S. Singh, I. V. Singh, B. Mishra, G. Bhardwaj, Analysis of cracked functionally graded material plates using xiga based on generalized higher-order shear deformation theory, Composite Structures 225 (2019) 111038.

[215] T. H. L. Bekkaye, B. Fahsi, A. A. Bousahla, F. Bourada, A. Tounsi, K. H. Benrahou, A. Tounsi, M. M. Al-Zahrani, Porosity-dependent mechanical behaviors of FG plate using refined trigonometric shear deformation theory, Computers and Concrete 26 (5) (2020) 439–450.

[216] A. Zine, A. A. Bousahla, F. Bourada, K. H. Benrahou, A. Tounsi, E. Adda Bedia, S. Mahmoud, A. Tounsi, Bending analysis of functionally graded porous plates via a refined shear deformation theory, Computers and Concrete 26 (1) (2020) 63–74.

[217] H. Bellifa, M. M. Selim, A. Chikh, A. A. Bousahla, F. Bourada, A. Tounsi, K. H. Benrahou, M. M. Al-Zahrani, A. Tounsi, Influence of porosity on thermal buckling behavior of functionally graded beams, Smart Structures and Systems 27 (4) (2021) 719.

[218] E. Arshid, M. Khorasani, Z. Soleimani-Javid, S. Amir, A. Tounsi, Porosity-dependent vibration analysis of FG microplates embedded by polymeric nanocomposite patches considering hygrothermal effect via an innovative plate theory, Engineering with Computers (2021) 1–22.

[219] H. Berghouti, E. A. Bedia, A. Benkhedda, A. Tounsi, Vibration analysis of nonlocal porous nanobeams made of functionally graded material, Advances in Nano Research 7 (5) (2019) 351–364.

[220] V. Birman, L. W. Byrd, Modeling and analysis of functionally graded materials and structures, Applied Mechanics Review 60 (2007) 195–216.

[221] D. Jha, T. Kant, R. Singh, A critical review of recent research on functionally graded plates, Composite Structures 96 (2013) 833–849.

[222] A. Gupta, M. Talha, Recent development in modeling and analysis of functionally graded materials and structures, Progress in Aerospace Sciences 79 (2015) 1–14.

[223] S. Zghal, D. Ataoui, F. Dammak, Static bending analysis of beams made of functionally graded porous materials, Mechanics Based Design of Structures and Machines (2020) 1–18.

[224] Z. Jin, R. Batra, Stress intensity relaxation at the tip of an edge crack in a functionally graded material subjected to a thermal shock, Journal of Thermal Stresses 19 (4) (1996) 317–339.

[225] Y. L. Chung, S. H. Chi, The residual stress of functionally graded materials, Journal of the Chinese Institute of Civil and Hydraulic Engineering 13 (2001) 1–9.

[226] W. Lee, S. Han, W. Park, A refined higher order shear and normal deformation theory for E-, P-, and S-FGM plates on pasternak elastic foundation, Composite Structures 122 (2015) 330–342.

[227] S. H. Chi, Y. L. Chung, Mechanical behavior of functionally graded material plates under transverse load-Part II: Numerical results, International Journal of Solids and Structures 43 (13) (2006) 3675–3691.

[228] N. D. Duc, P. H. Cong, Nonlinear dynamic response of imperfect symmetric thin S-igmoid-functionally graded material plate with metal-ceramic-metal layers on elastic foundation, Journal of Vibration and Control 21 (4) (2015) 637–646.

[229] F. A. Fazzolari, Modal characteristics of P-and S-FGM plates with temperature-dependent materials in thermal environment, Journal of Thermal Stresses 39 (7) (2016) 854–873.

[230] P. Gu, R. Asaro, Crack deflection in functionally graded materials, International Journal of Solids and Structures 34 (24) (1997) 3085–3098.

[231] F. Erdogan, B. Wu, Crack problems in FGM layers under thermal stresses, Journal of Thermal Stresses 19 (3) (1996) 237–265.

[232] X. Zhao, Y. Lee, K. M. Liew, Free vibration analysis of functionally graded plates using the element-free Kp-Ritz method, Journal of Sound and Vibration 319 (3-5) (2009) 918–939.

[233] B. Uymaz, M. Aydogdu, S. Filiz, Vibration analyses of FGM plates with in-plane material inhomogeneity by Ritz method, Composite Structures 94 (4) (2012) 1398–1405.

[234] G. Bhardwaj, I. V. Singh, B. K. Mishra, T. Q. Bui, Numerical simulation of functionally graded cracked plates using nurbs based xiga under different loads and boundary conditions, Composite Structures 126 (2015) 347–359.

[235] N. D. Duc, P. H. Cong, Nonlinear postbuckling of symmetric S-FGM plates resting on elastic foundations using higher order shear deformation plate theory in thermal environments, Composite Structures 100 (2013) 566–574.

[236] S. Singh, S. P. Harsha, Exact solution for free vibration and buckling of sandwich S-FGM plates on pasternak elastic foundation with various boundary conditions, International Journal of Structural Stability and Dynamics 19 (03) (2019) 1950028.

[237] W. Y. Jung, S. C. Han, W. T. Park, Four-variable refined plate theory for forced-vibration analysis of sigmoid functionally graded plates on elastic foundation, International Journal of Mechanical Sciences 111 (2016) 73–87.

[238] P. Thang, T. Nguyen Thoi, J. Lee, Closed-form expression for nonlinear analysis of imperfect sigmoid-FGM plates with variable thickness resting on elastic medium, Composite Structures 143 (2016) 143–150.

[239] K. Mehar, S. K. Panda, B. K. Patle, Stress, deflection, and frequency analysis of CNT reinforced graded sandwich plate under uniform and linear thermal environment: A finite element approach, Polymer Composites 39 (10) (2018) 3792–3809.

[240] W. Y. Jung, S. C. Han, Analysis of sigmoid functionally graded material S-FGM nanoscale plates using the nonlocal elasticity theory, Mathematical Problems in Engineering (2013).

[241] M. I. Ali, M. Azam, V. Ranjan, J. Banerjee, Free vibration of sigmoid functionally graded plates using the Dynamic Stiffness method and the Wittrick-Williams algorithm, Computers & Structures 244 (2021) 106424.

[242] S. A. Kulkarni, K. M. Bajoria, Finite element modeling of smart plates/shells using higher order shear deformation theory, Composite Structures 62 (1) (2003) 41–50.

[243] S. Udagiri, R. Kumar, A. Srivastava, S. Jain, Finite element modelling of smart curved beam, in: Proceedings of All India Seminar on Advances in Product Development (APD-2006), New Age International, 2006.

[244] R. Kumar, B. Mishra, S. Jain, Static and dynamic analysis of smart cylindrical shell, Finite Elements in Analysis and Design 45 (1) (2008) 13–24.

[245] A. Sofiyev, The stability of functionally graded truncated conical shells subjected to a periodic impulsive loading, International Journal of Solids and Structures 41 (13) (2004) 3411–3424.

[246] A. Sofiyev, The buckling of functionally graded truncated conical shells under dynamic axial loading, Journal of Sound and Vibration 305 (4-5) (2007) 808–826.

[247] H. S. Shen, Functionally graded materials: nonlinear analysis of plates and shells, CRC press (Taylor & Francis group), 2016.

[248] M. Darabi, M. Darvizeh, A. Darvizeh, Nonlinear analysis of dynamic stability for functionally graded cylindrical shells under periodic axial loading, Composite Structures 83 (2) (2008) 201–211.

[249] H. Ait Atmane, A. Tounsi, F. Bernard, Effect of thickness stretching and porosity on mechanical response of a functionally graded beams resting on elastic foundations, International Journal of Mechanics and Materials in Design 13 (1) (2017) 71–84.

[250] S. Han, G. R. Lomboy, K. Kim, Mechanical vibration and buckling analysis of FGM plates and shells using a four-node quasi-conforming shell element, International Journal of Structural Stability and Dynamics 8 (02) (2008) 203–229.

[251] B. O. Sallai, A. Tounsi, I. Mechab, B. B. Mohamed, M. Mustapha, A. B. El Abbas, A theoretical analysis of flexional bending of Al/Al2O3 S-FGM thick beams, Computational Materials Science 44 (4) (2009) 1344–1350.

[252] T. Q. Bui, A. Khosravifard, C. Zhang, M. Hematiyan, M. Golub, Dynamic analysis of sandwich beams with functionally graded core using a truly meshfree radial point interpolation method, Engineering Structures 47 (2013) 90–104.

[253] P. M. Ramteke, S. K. Panda, Nonlinear thermomechanical static and dynamic responses of bidirectional porous functionally graded shell panels and experimental verifications, Journal of Pressure Vessel Technology 145 (4) (2023) 041301.

[254] W. Y. Jung, S. C. Han, Static and eigenvalue problems of sigmoid functionally graded materials S-FGM micro-scale plates using the modified couple stress theory, Applied Mathematical Modelling 39 (12) (2015) 3506–3524.

[255] H. T. Thai, D. H. Choi, Size-dependent functionally graded kirchhoff and mindlin plate models based on a modified couple stress theory, Composite Structures 95 (2013) 142–153.

[256] E. Carrera, S. Brischetto, M. Cinefra, M. Soave, Effects of thickness stretching in functionally graded plates and shells, Composites Part B: Engineering 42 (2) (2011) 123–133.

[257] A. Neves, A. J. M. Ferreira, E. Carrera, M. Cinefra, C. M. C. Roque, R. Jorge, C. M. Soares, Static, free vibration and buckling analysis of isotropic and sandwich functionally graded plates using a quasi-3d higher-order shear deformation theory and a Meshless technique, Composites Part B: Engineering 44 (1) (2013) 657–674.

[258] N. V. Nguyen, H. X. Nguyen, S. Lee, H. Nguyen, Geometrically nonlinear polygonal finite element analysis of functionally graded porous plates, Advances in Engineering Software 126 (2018) 110–126.